Università degli Studi di Ferrara

DOTTORATO DI RICERCA IN FISICA

CICLO XXV

COORDINATORE Prof. Vincenzo Guidi

Devices and techniques for the characterization of inverse Compton sources

Settore Scientifico Disciplinare FIS/07

Dottorando

Dott. Paolo Cardarelli

Tutore

Prof. Mauro Gambaccini

Anni 2010/2012

Contents

Introduction

Novel intense monochromatic x/γ-ray sources are of great interest in the scientific community. A large number of applications, in basic and applied physics research, as well as in different science fields, require an intense, (quasi-)monochromatic, tunable radiation source. Synchrotron radiation is optimal for low energy applications (<100 keV) but the size and cost of synchrotron facilities prevent a large-scale spread of this kind of source, fundamental for such applications as routine clinical diagnostic. Moreover, synchrotron light is not suitable in the case of high energy applications (>1 MeV), such as those for nuclear physics experiments, due to the limitation on the maximum energy obtainable for monochromatic beams with synchrotron light. Alternative sources that can overcome such limitations are those based on inverse Compton interaction, which could be compact and cost-effective for low energy applications and provide monochromatic collimated beam in the high energy range.

Compton scattering is the process in which a free electron and a photon interact, it is usually implicit that the photon releases part of its energy to the electron and then it is scattered with a lower frequency. In the case of inverse Compton scattering this energy exchange is reversed, this occurs when the interacting electrons are in motion at a relativistic speed and the photon increases its energy in the scattering process. This process can be used to produce hard x/γ-rays by the collision of low energy laser photons and a relativistic electron beam. A radiation source based on this interaction is usually called an inverse Compton source, alternatively it can be called Thomson source when the energies involved allow a classical description of the process as in the case Thomson scattering.

The work described in this dissertation concerns the devices and techniques developed to perform the characterization of inverse Compton sources. In particular, the work is focused on two major projects: BEATS2 experiment and ELI-NP-GBS proposal of E-Gammas collaboration.

BEATS2 is an experiment funded by Istituto Nazionale di Fisica Nucleare (INFN) aimed to study medical applications, in particular to mammographic imaging, of the SL-Thomson source of SPARC-LAB at the INFN-LNF that will be commissioned in the first half of 2013. A summary of the characteristics of the x-ray beam provided by this source is reported in Table 1.

E-Gammas is an international collaboration composed by several Universities and Institutions including: INFN and Università di Roma La Sapienza, in Italy, Universitè de Paris Sud and IN2P3/CNRS, in France, and ASTeC of STFC, in UK. The collaboration is aimed to the preparation of a Technical Design Report for the ELI-NP gamma beam system (ELI-NP-GBS) to be commissioned by the end of 2016. This gamma beam system will be a high energy inverse Compton source, included in the Extreme Light Infrastructure - Nuclear physics (ELI-NP), an European project dedicated to

Table 1: Summary of the radiation characteristics expected for ELI-NP-GBS and SL-Thomson.

Source	SL-Thomson	ELI-NP-GBS
Energy	20 - 500 keV	0.2 - 20 MeV
Energy bandwidth $\Delta E/E$	< 0.2	$< 5\times10^{-3}$
Photons per pulse	$\sim 10^9$	$\sim 10^5$
Pulse duration	5 - 15 ps	0.7-1.5 ps
Repetition rate	1 - 10 Hz	100 Hz [a]
Source rms size	10 - 15 μm	10 - 30 μm
Divergence	< 9.33 mrad	25 - 250 μrad

[a] 100 Hz macropulse, each macropulse is made of 32 pulses with a time separation of 16 ns correponding to 62.5 MHz

the development of laser beams and the generation of high intensity gamma beams for frontier research in nuclear physics. ELI-NP is hosted by the Horia Hulubei National Institute of Physics and Nuclear Engineering (IFIN-HH) in Magurele, Bucharest, Romania. The main expected characteristics of the beam produced by ELI-NP-GBS facility are also listed in Table 1.

As it is possible to notice from the values reported in Table 1, these two sources have very different energy range of operation but show similar characteristics regarding their time structure. They are both pulsed and ultra-fast sources, with a pulse duration of 1-10 ps, a relatively slow repetition-rate and high instantaneous flux. This peculiar time structure and the high instantaneous flux imply that traditional techniques, such as single-photon counting spectroscopic detectors, are not directly usable for a precise measurement of the photons yield and the energy distribution. In order to perform a thorough characterization of these sources suitable detectors and techniques must be designed and implemented, taking into account the specific characteristics expected.

In the case of BEATS2 experiment, in order to evaluate the possible performances of SL-Thomson source for the various diagnostic imaging applications of the beam, a crucial step is a full characterization including the evaluation of the total photon yield, the energy distribution, the spatial distribution of the radiation produced and the size of the emitting area (focal spot). The main tasks of the Ferrara research unit have concerned the design and realization of an x-ray flux on-line monitoring system and a device for an absolute x-ray flux measurement. The devices have been realized, tested and calibrated with traditional x-ray tubes and (quasi-)monochromatic sources and finally installed on the SL-Thomson beamline in Frascati. Furthermore, a K-edge subtraction technique for the evaluation of the energy distribution was developed and experimentally tested.

Regarding the proposal for ELI-NP-GBS of the E-Gammas collabora-

tion, the research unit of Ferrara section of INFN has been involved in the design of the collimation, characterization and monitoring system of the gamma beam. In particular, the activity have concerned the realization of the preliminary design and the evaluation of the expected performance of two flux monitor devices. The first based on a silicon detector for fast signal production and acquisition, to provide information on the pulsed temporal structure of the photon beam. The second is a slower device based on scintillator crystal for a more accurate evaluation and monitoring of the source photon yield. Moreover, the design and the evaluation of the expected performances of an imaging system for the high-energy gamma beam was carried out. This detector will provide a diagnostic tool for the beam profile shape, position, collimation and alignment.

This dissertation is organized as follows. In Chapter 1, after a brief introduction, the basic physics of inverse Compton interaction is described to allow to illustrate the basilar properties of inverse Compton - Thomson sources.

In Chapter 2 SL-Thomson beamline at SPARC-LAB facility is described, with special focus on the x-ray beam for BEATS2 experiment.

A brief overview of the European Project ELI and its pillar ELI-NP is given in Chapter 3, followed by the description of the main characteristics of ELI-NP Gamma Beam System proposal of E-Gammas collaboration.

A detailed description of the devices and detectors realized for BEATS2 experiment, as well as the results obtained for the tests and calibration carried out is given in Chapter 4. In the same chapter is also discussed the theory at the basis of the K-edge subtraction technique developed for the energy distribution evaluation of BEATS2 x-ray beam and the results of the experimental test performed.

At last, the devices designed for ELI-NP-GBS proposal and their expected performances are described in Chapter 5.

1 Inverse Compton and Thomson backscattering sources

1.1 Introduction

The search for novel intense monochromatic x/γ-ray sources is of great interest in the scientific community. A large number of experiments, both in basic and applied physics research, require an intense radiation source with the following characteristics:

- monochromatic, or quasi-monochromatic energy distribution;
- tunable average energy of the photon beam produced;
- small focal spot size;
- high flux, high brilliance;
- collimation;
- polarization.

Depending on the application, the requirements on some these parameters can be more or less demanding, but the main source that satisfy completely these requirements is synchrotron radiation, at least for what it concern the generation photon beams with energies ranging from few eV up to hundreds of keV (UV to hard x-rays). Applications of synchrotron light in this energy range cover several different fields such as solid state physics and cristallography [1], chemistry and applied chemistry [2, 3], earth science and environmental science [4, 5], life science [6], non destructive testing and medical physics [7, 8]. Nowadays, there are over 50 synchrotron light sources operating worldwide which can be broadly classified into three categories, or generations [9]. Each generation differs from the previous one by technological innovation and, at least, by the improvement of one order of magnitude in performance, usually quantified by the flux and the brilliance of the source. In chronological order, these are as follows:

– *1st generation* synchrotron radiation light sources, which were born essentially as parasitic applications of storage ring for high energy physics. Examples include the Synchrotron Ultraviolet Radiation Facility (SURF), in Maryland, USA and the 6 GeV Deutsches Elektronen-Synchrotron (DESY) in Hamburg, Germany;

– *2nd generation* synchrotron radiation light sources, which were dedicated synchrotron radiation facilities but not designed for low emittance or with many straight sections for insertion devices such as undulators and wigglers, as the Daresbury SRS in the UK and HASYLAB at DESY;

– *the current 3rd generation* synchrotron radiation light sources are dedicated synchrotron radiation facilities designed for low emittance and with many straight sections for incorporating several insertion devices allowing the simultaneous use of various beamlines for different applications. Examples include the ESRF and Soleil in France, the ALS in the USA, BESSY II in Germany and Diamond in the UK and ELETTRA in Italy.

The candidate for a 4th-generation source is the hard x-ray (<10 keV) free-electron laser (FEL) based on a very long undulator in a high-energy electron linear accelerator. Such a device can have a peak brightness many orders of magnitude beyond that of the third-generation sources, as well as pulse lengths of 100 fs or shorter, and a beam fully coherent. Example of this kind of facilities are, the Linac Coherent Light Source in the United States, that uses 15-GeV electrons from the SLAC linac as the source for a FEL with energies up to about 10 keV; in Europe, the European project XFEL in Hamburg, that is expected to produce photon with energies up to 24 keV, and the Italian FERMI (Trieste) a FEL user-facility covering the wavelength range from 100 nm (12 eV) to 10 nm (124 eV).

The unique properties of synchrotron radiation can be summarized as:

– high brightness and high intensity, many orders of magnitude than with X-rays produced in conventional X-ray tubes (see Fig. 1.1);

– high level of polarization (linear or elliptical);

– low emittance and high collimation, *i.e.*, small angular divergence of the beam and small focal spot;

– wide tunability in energy by monochromatization (from sub-eV up to hundreds of keV) with typical energy bandwidth $\Delta E/E \sim 10^{-3}$–10^{-4});

– pulsed light emission with durations of 1 ns or less.

As already mentioned these characteristics are optimal for a wide range of applications, but in particular, considering medical physics, a tunable monochromatic or quasi-monochromatic beam have significant advantages compared to traditional x-ray tubes sources both for planar and three-dimensional imaging, as also for the implementation of advanced imaging techniques [7, 8, 10]. Monochromatic x-ray beams can have significant advantages, for example, in mammography [11–14] and coronary angiography [15]. The optimal energy of the incident photons can be adjusted in order to optimize the trade-off between the maximum diagnostic power and the radiation dose imparted. The absorption properties of contrast media can be optimally used in K-edge imaging, both in planar and three-dimensional imaging and this could lead to improved diagnostic techniques and new types of therapy. Tomographic x-ray imaging would benefit from the use of quasi-monochromatic spectra avoiding beam hardening issues and allowing to perform multi-energy image acquisitions. A bright source of x-rays with a small spot sizes permits phase-contrast imaging, both in planar and three-dimensional configurations, with its advantages in medical imaging [14, 16, 17].The major limitation to a large-scale clinical application of synchrotron light are the costs of realization and operation, as well as the size, of synchrotron facility, implying that a routine clinical use and the spread on a large scale of this kind of sources it is not feasible. This infrastructures in fact are usually large facilities, as result of national or international collaborations providing many radiation beamlines to satisfy a large base of users. A compact alternative source featuring the same characteristics of synchrotron radiation would permit a broad range of applications, as those previously described for medical physics, but also including for example non-destructive testing, material science, life science and protein crystallography.

Different applications of monochromatic radiation with the characteristics previously mentioned require beams in the energy range going from 1 to hundreds of MeV. Such a source allows to perform fundamental studies in nuclear physics dealing with the nucleus structure and the role of giant dipole resonances, of great relevance also for astrophysics topics, as well as for applications in material science, life science and nuclear materials management [19, 20]. In this case synchrotron radiation is not usable, the maximum energies obtainable at synchrotron facilities are limited to hundreds of keV and can not reach such a high energy range. This is due to limitations to the critical frequency of synchrotron radiation, requiring high electron energies and high magnetic fields, and also to difficulties in the monochromatization of beam with high energy, where a traditional double-crystal configuration is not effective. A plot of the brightness typical emission as a function of the photon energies for various radiation source is plotted in Fig. 1.1. As it is possible to notice, the brightness drops significantly for energies higher than 100 keV for typical synchrotron radiation sources (wiggler and bending

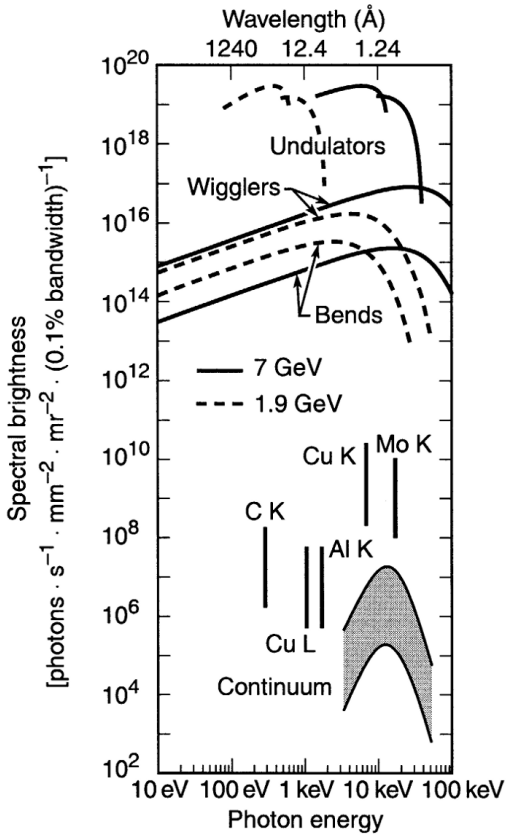

Figure 1.1: Spectral brightness for several synchrotron radiation sources and conventional x-ray sources. The data for conventional x-ray tubes should be taken as rough estimates only, since brightness depends strongly on such parameters as operating voltage and take-off angle. The indicated two-order-of-magnitude ranges show the approximate variation that can be expected among stationary-anode tubes (lower end of range), rotating-anode tubes (middle), and rotating-anode tubes with microfocusing (upper end of range) [18].

magnets). In fact, typical values of high-energy beamlines for some of the major synchrotron facilities worldwide are: 30 - 500 keV at the beamline ID15 for high energy radiation of ESRF (Grenoble) [21, 22], 100-300 keV for BL08W beamline at SPring-8 (Japan) [23] and 50-150 keV at I12-JEEP beamline at Diamond (UK) [24]. Also FEL sources are more focused on low energy applications and as previously described the maximum energy currently obtainable is lower than 100 keV.

Since the 1980s to nowadays, the main gamma source for nuclear physics applications has been based on the inverse Compton interaction of a laser beam and an accelerated electron beam.

The Compton effect was discovered in the early 1920s via the scattering of x-rays from electrons in metals,but only four decades later this effect was recognized as a useful mechanism to convert low energy photons to very high energy x/γ-ray. In 1963, Milburn [25], and Arutyunian and Tumanian [26], independently proposed a method for the production of very high energy γ-rays using Compton backscattering of photons by high-energy electrons produced in charged particle accelerators.

In the following years several experimental demonstrations of high energy γ radiation production using inverse Compton scattering were carried out in various laboratories worldwide [27–29]. In 1978 the first inverse Compton light source facility for nuclear physics research, the Ladon project, started to be operational in INFN-LNF Frascati (Italy) [30–32] using the electron beam of ADONE storage ring. This facility could provide polarized gamma beams with energy up to 80 MeV with a flux up to 5×10^5 ph/s for nuclear experiments. Following the success of the Ladon facility at Frascati, several new Compton light source facilities were brought into operation, including LEGS and HIγS in the US, Graal in France ROKK-1/ROKK-2/ROKK-1M in Russia, and LEPS in Japan.

Currently there are several ongoing project worldwide for the development of new Compton sources to improve the performances on spectral density and monocromaticity of the gamma beam, some examples are SLEGSS at SSR (Shangai), LBSF at MAX-IV laboratory (Sweden), MEGa-Rays at Lawrence Livermore National Laboratory (US) and, in particular, ELI-NP-GBS in Bucharest, Romania that will be described in Sec. 3.2. Inverse Compton, or Thomson backscattering, can be used to produce also radiation in a lower energy range, compatible to medical applications. The recent technological progress in charged particles acceleration techniques, high-power laser systems and light re-circulator would currently permit to build compact and relatively low-cost x-ray sources with beam characteristics and photon yield compatible with a wide range of applications [33, 34]. In the last few years Inverse Compton (or relativistic Thomson back-scattering) has been considered also for the production of (quasi-)monochromatic x-rays in the lower energy range (1-500 keV) by many laboratories around the world such as BNL-ATF in the US, ELSA (France), AIST (Japan), COBALD at Dares-

bury Laboratories (UK) [35–41]. For the aim of this work, the SL-Thomson beamline of SPARC-LAB facility has a particular relevance and will be described in detail in Chapter 2. In the next sections a description of the basic physics of inverse Compton scattering is given and the main characteristics of the radiation emitted by a source based on this interaction are described.

1.2 Inverse Compton and Thomson backscattering sources

The process in which a free electron and a photon interact is called Compton scattering. It is usually implicit that the photon releases part of its energy to the electron and then it is scattered with a lower frequency. When this energy exchange is reversed it is the case of inverse Compton scattering, occurring when the interacting electrons are in motion at a relativistic speed and the photon increases its energy in the scattering process. This process can be used to produce hard x/γ-rays by the interaction of low energy laser photons and a relativistic electron beam. An overview of the physics involved in the production of an x/γ-ray beam via inverse Compton, and in the Thomson limit, will be given in this chapter in order to illustrate the basic properties of this kind of x-ray sources.

1.2.1 Compton scattering

The interaction between a free electron at rest and a photon, resulting in the scattering of the photon, is called Compton scattering. In this process the photon transfers part of its energy to the electron. This is a well-known phenomenon and the kinematics can be fully described as a relativistic elastic collision of a photon and an electron. Figure 1.2 shows the collision configuration, in which a photon of energy $E = h\nu$ collides with a stationary electron, having no initial kinetic energy or momentum. After the collision the electron recoils at an angle φ with kinetic energy T and momentum p, while the photon is scattered with an energy $E' = h\nu'$ at an angle θ.

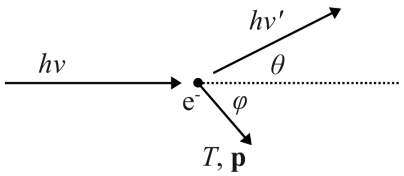

Figure 1.2: Compton scattering typical configuration.

A complete solution of the kinematics of Compton interaction can be obtained considering the conservation of both energy and momentum, resulting in:

$$h\nu' = \frac{h\nu}{1 + \frac{h\nu}{m_e}(1 - \cos\theta)} \tag{1.1}$$

$$T = h\nu - h\nu' \tag{1.2}$$

$$\cot\varphi = \left(1 + \frac{h\nu}{m_e}\right)\tan(\theta/2) \tag{1.3}$$

where m_e is the mass at rest of the electron equal to 511 keV. The cross section of the process is described by the Klein-Nishina formula

$$\frac{d\sigma}{d\Omega_\theta} = \frac{r_0^2}{2}\left(\frac{h\nu'}{h\nu}\right)^2\left(\frac{h\nu}{h\nu'} + \frac{h\nu'}{h\nu} - \sin^2\theta\right) \tag{1.4}$$

The classical limit of Compton scattering, occurring when the energy of the incident photon is small compared to the electron mass at rest, is the Thomson scattering. In this case the energy of the scattered photon is not changed and the cross section is:

$$\frac{d\sigma}{d\Omega_\theta} = \frac{r_0^2}{2}\left(2 - \sin^2\theta\right) = \frac{r_0^2}{2}\left(1 + \cos^2\theta\right) \tag{1.5}$$

where r_0 is the classical electron radius $r_0 = e^2/m_e = 2.818 \times 10^{-15}$ m. In the case of Thomson scattering the photon energy is unchanged and the cross-section is independent from the energy.

1.2.2 Inverse Compton and Thomson backscattering

Inverse Compton refers to the case in which the scatter of the photon occurs in a reference frame where the electron is not at rest but has a relativistic speed and an energy higher than the one of the interacting photon. In this process it is possible that the photon gains energy in the interaction and for this reason it is usually called *inverse Compton scattering* [42].

Consider an interaction as depicted in Fig. 1.3 where an electron is moving with an energy E_e and a photon of initial energy $h\nu$, that propagates toward the electron at an angle θ_i, after the interaction is scattered at angle θ_f with an energy $h\nu'$. In the rest frame of the electron the process can be described as a Compton scattering for a photon that has undergone an energy up-shift due to the relativistic Doppler effect. Considering the electron having a Lorentz factor γ, the up-shifted energy $h\nu*$ will be $h\nu* = 2\gamma h\nu_i$. Thus, in this reference frame a Compton interaction will occur with the photon with the energy $h\nu*$, but in order to obtain the description of the process in the laboratory frame of reference a Lorentz transformation from the electron rest frame must be performed.

Assuming the collision geometry sketched in Fig. 1.3, where $E_e, \mathbf{p}$ and $E'_e, \mathbf{p}'$ are the energy and the momentum of the electron before and after

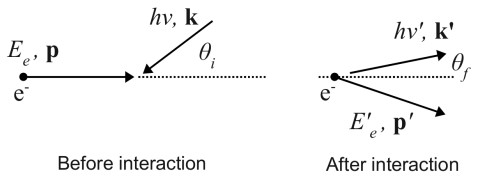

Figure 1.3: Inverse Compton scattering configuration.

the collision, while $E_\gamma = h\nu, \mathbf{k}$ and $E'_\gamma = h\nu', \mathbf{k'}$ denote the energy and the wave vector of the photon before and after the collision, using conservation of four-momentum it is possible to write E'_γ as [43]:

$$E'_\gamma = h\nu' = E_\gamma \frac{E(1 - \beta\cos\theta_i)}{1 - \beta\cos\theta_f + \frac{E}{\gamma m_e}(1 - \cos\theta_p)} \tag{1.6}$$

where γ is the Lorentz factor of the relativistic electron and m_e is it mass at rest (511 keV); θ_i and θ_f are the angles between the momentum of the incident and scattered photon with respect to the direction of motion of the electron ($\cos\theta_i = \mathbf{p}\cdot\mathbf{k}$ and $\cos\theta_f = \mathbf{p}\cdot\mathbf{k'}$), and θ_p is the angle between the two photons ($\cos\theta_p = \mathbf{k}\cdot\mathbf{k'}$).

Considering an head-on collision ($\theta_i = \pi$), denoting with θ the angle of the scattered photon, it is possible to rewrite eq. (1.6) as:

$$E'_\gamma = h\nu' = E_\gamma \frac{E(1 + \beta)}{1 - \beta\cos\theta + \frac{E}{\gamma m_e}(1 - \cos\theta)} \tag{1.7}$$

In the case of a collision of a relativistic electron and a photon having an up-shifted energy $h\nu*$ that is negligible compared to the electron rest mass m_e, it possible to consider that the interaction in the electron frame of reference is basically a classical Thomson scattering. This means that the electron does not recoil and the photon is re-emitted with unchanged frequency corresponding to the original one Doppler up-shifted. In this case the result in the laboratory frame of reference is a Lorentz boosted Thomson emission, where the scattered photons are peaked along the direction of motion of the electron in a cone with aperture proportional to $1/\gamma$ due to the effect of the Lorentz transformation. When this approximation is valid the process is described as Thomson backscattering and the energy of the photon scattered at small angles θ can be expressed with good approximation when $\gamma \gg 1$, as [44]:

$$E'_\gamma = h\nu' \simeq E_\gamma \frac{4\gamma^2}{1+\gamma^2\theta^2}. \tag{1.8}$$

It is possible to notice that in eq. (1.8) the maximum energy E_γ^{max} is obtained for $\theta = 0$ and it is equal to $E_\gamma^{max} \simeq 4h\nu\gamma^2$. In this case it is worth noting that the final energy boost factor comes from two consequent relativistic Doppler up-shift between the laboratory and the electron reference frame, each of those gives a boost of a factor $\gamma(1+\beta) \simeq 2\gamma$ for $\beta \sim 1$.

In the practical case of a photon having an initial energy $h\nu = 1.5$ eV, the backscattering with an electron having a $\gamma = 60$, corresponding to an energy $E_e \sim 30$ MeV, would result in an energy $h\nu' = 4E_\gamma\gamma^2 = 21.6$ keV; otherwise, for a photon having an initial energy $h\nu = 2.4$ eV if the electron $\gamma = 1440$ ($E_e \sim 720$ MeV) the resulting energy $h\nu'$ is equal to 19.9 MeV[1]. It is worth noting that it is possible to obtain a maximum energy of the backscattered radiation ranging from 20 keV to 20 MeV, using a visible light photon and just varying the electron beam energy. The scaling of the backscattered energy with γ^2 makes possible to reach high values with electron beam having energies that are easily obtainable at the state of the art of particle accelerator technology.

When the energy of the electron or of the incident photon increase such as the Thomson approximation is no more valid ($2\gamma h\nu \ll m_e$) and the electron recoil must be taken into account for the determination of the backscattered photon energy, it is possible to correct the equation (1.8) adding a correction parameter Δ for Compton recoil as [44, 45]

$$E_\gamma^{Compton'} = E_\gamma^{Thomson'}(1-\Delta), \tag{1.9}$$

where

$$\Delta = \frac{\frac{4\gamma h\nu}{m_e}}{1+2\gamma\frac{h\nu}{m_e}}. \tag{1.10}$$

As expected this correction factor Δ is negligible when the electron mass is bigger than $2\gamma h\nu$, that is the energy of the incident photon as seen by the electron in its rest frame. This is exactly the condition for the Thomson interaction as classical limit of the quantum Compton scattering.

Considering the two practical scenarios previously mentioned, namely: $h\nu = 1.5$ eV, $\gamma = 60$ and $h\nu = 2.4$ eV, $\gamma = 1440$; the ratio $2\gamma h\nu/m_e$ is equal to 3.5×10^{-4} and 1.35×10^{-2}, respectively. These correspond to a Compton correction factor Δ 7×10^{-4} in the first case and 2.7×10^{-2} in the second. As it is possible to notice also for the higher energy case the

[1]This particular values were taken as representative of the typical one for the two sources described in this work, see Sec.3.2 and Sec.2.

Thomson approximation is quite good, even if, for an accurate calculation of the energy, the Compton correction should be taken into account.

Combining eq. (1.9) with eq. (1.8) it is possible to obtain the expression for the scattered energy at small angles corrected by Compton recoil:

$$E'_\gamma = h\nu' \simeq E_\gamma \frac{4\gamma^2}{1+\gamma^2\theta^2}\left[1+\frac{\frac{4\gamma h\nu}{m_e}}{1+2\gamma\frac{h\nu}{m_e}}\right] \tag{1.11}$$

The energy distribution of the scattered radiation as a function of the scattering angle is shown in Fig. 1.4 for the two different cases: $h\nu = 1.5$ eV, electron $\gamma = 60$ and $h\nu = 2.4$ eV, electron $\gamma = 1440$.

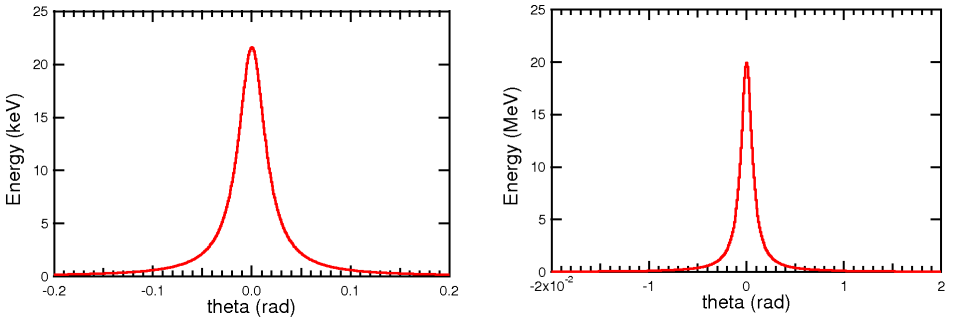

Figure 1.4: Plot of the energy distribution of the scattered radiation as a function of the scattering angle for the two different cases: $h\nu$= 1.5 eV, electron $\gamma = 60$ (*on the left*) and $h\nu$= 2.4 eV, electron $\gamma = 1440$ (*on the right*)

.

It is possible to notice that as the electron energy increases, the more the energy distribution is peaked along the backward direction. This strong correlation between the angle and the photon energy permits to obtain beams with an energy bandwidth simply adjustable by varying the collimation. The more the beam is collimated, thus decreasing the angular acceptance, the more the bandwidth will decrease. Moreover, the spatial distribution of the scattered photon is peaked in a cone corresponding to an angular divergence of $1/\gamma$, a complete and detailed description regarding the cross-section of the interaction can be found in [42, 44, 46], while a description of the radiation spatial distribution of the sources considered in this work will be given is Sec. 3.3 and Sec. 2.2.

This discussion, so far, has been made considering a simplified interaction of a single photon on a single electron. The description of the elastic Thomson scattering between a laser light photon and a relativistic electron counter-propagating can be also made as spontaneous synchrotron radiation emitted by the relativistic electron wiggling in the e.m. field of the interacting light (assumed as a plane wave, with no diffraction). In the actual case

of a Thomson-inverse Compton source, the interaction is between an intense laser beam and an electron beam, if the light considered has a long wavelength and high intensity this can result in a red-shift of the peak energy and the formation of harmonics [46,47]. The parameter used to quantify the relevance of those effects is the dimensionless amplitude of the vector potential associated to the laser e.m. field a_0, often called the *laser parameter*. This can be expressed as a function of the laser intensity I as [46]:

$$a_0 = \frac{eE\lambda_L}{2\pi m_e c} = 0.85 \times 10^{-9} \lambda_l[\mu m] I^{1/2}[W/cm^2] \tag{1.12}$$

This parameter allow to distinguish between two different regimes: the linear Thomson scattering, if $a_0 \ll 1$, and non-linear Thomson scattering when $a_0 \gtrsim 1$. It is possible to take account for small non-linear effects on the electron transverse motion and eq. (1.8) is modified as:

$$E'_\gamma = h\nu' \simeq E_\gamma \frac{4\gamma^2}{1 + \gamma^2\theta^2 + a_0^2/2}. \tag{1.13}$$

As it is possible to notice this non-linear effect is responsible for a small decrease of the energy of the scattered photon, as well as for the generation of higher harmonics (not showed here).

To obtain a complete prediction of the radiation produced by the interaction of a laser beam scattered by a relativistic electron beam it is necessary to consider a complex process in which are taken into account quantum effects, effects of size, shape, focusing and energy spread of both the electron and laser beam, polarization and non-linear effect that is beyond the scope of this overview. A more extensive discussion of the characteristics of the beams and the radiation produced for the sources considered in this work will be given is Sec. 3.3 and Sec. 2.2 and relative bibliography.

Concluding, from the previous discussion, it is possible to summarize the characteristics of a radiation source obtained by an inverse Compton interaction (Thomson backscattering) of laser light with a relativistic electron beam, as:

- *monochromaticity*, the emission is peaked in a cone with an aperture proportional to $1/2\gamma$. The maximum energy is obtained in the backward direction and the energy decrease by increasing the angle, this implies that varying the angular acceptance by collimating the beam it is possible to adjust the energy bandwidth of the source;

- *energy tunability*, the maximum energy is proportional to $4\gamma^2$ and incident the laser wavelength, assuming to keep the laser wavelength constant it is possible to tune continuously the maximum energy of the radiation produced by adjusting the electron beam energy;

– *small focal spot*, the radiation emitting area size are determined by the electron beam cross-section and the laser focusing, typical values are of the order of 10-100 $/mu$m;

– *flux*, the number of photon produced roughly scale as [48]:

$$N_p h = \frac{N_L N e}{r_L^2 + r_e^2} \tag{1.14}$$

so it is possible to increase the number of photon produced increasing the number of laser photons and electrons interacting and decreasing the beam sizes, as long as unwanted effects of nonlinearity do not affect the source performance;

– *temporal structure*, the duration of the radiation pulse emitted is directly related to the duration of the pulses of the laser beam and the electron bunches interacting. Thus it is possible to obatin very intense ultrashort radiation pulses ($<$ 1 ps) as well as less intense pulses with a high repetition-rate.

– *polarization*, the polarization of the backscattered radiation if fully controllable by acting on the laser polarization.

2

SL-Thomson source and BEATS2

2.1 SPARC-LAB

SPARC-LAB (Sources for Plasma Accelerators and Radiation Compton with Lasers and Beams) is an interdisciplinary laboratory dedicated to the study of new acceleration techniques of particles (electrons, protons, ions) and to the development and application of advanced radiation sources resulting from merging the potentialities of the former INFN projects SPARC and PLASMONX. The facility is located at the Laboratori Nazionali di Frascati (LNF) of the Istituto Nazionale di Fisica Nucleare (INFN), near Rome, Italy [49, 50].

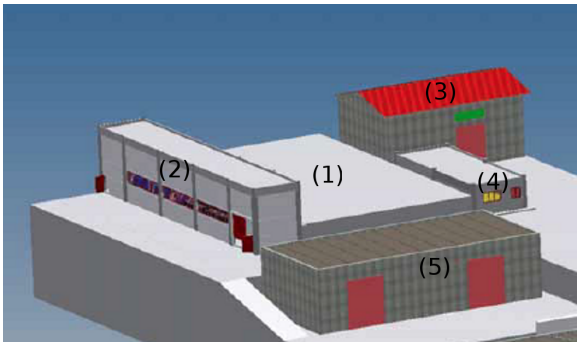

Figure 2.1: A drawing of the buildings of SPARC-LAB facility.

SPARC-LAB hosts a 150 MeV high brightness electron beam injector: SPARC [51, 52], able to operate also in the velocity bunching configuration, and a high intensity laser beam: FLAME [53], a Ti-sapphire laser that can deliver pulses with energy up to 6 J.

In Fig. 2.1 a view of SPARC-LAB infrastructure is shown, the different buildings, labeled with numbers in the figure, are respectively:

1. the SPARC building, hosting the electron beam injector and the various experimental beamlines;

2. the SPARC klystron and power suppliers building;

3. the FLAME laser facility;

4. the main control room;

5. a user facility that will be possibly implemented in the future (not available at the moment).

In Fig. 2.2 the layout of the SPARC building is shown. At the bottom of the picture it is possible to see the terminal section of the electron beam injector that feeds four different beamlines, corresponding to four different applications:

1. The first is a 12 meters long undulator for free electron laser (FEL) production. Observations of FEL radiation in the SASE [5], Seeded [6] and HHG [7] modes have been performed with tunable wavelength from 500 nm down to 40 nm;

2. a second beam line has been currently installed and it is hosting a narrow band THz radiation source [8];

3. the third beamline, using the interaction with FLAME laser that will be linked to the linac, will explore laser-matter interaction, in particular with regard to laser-plasma acceleration of electrons [9] (and protons) in the self injection and external injection modes;

4. the fourth beamline is aimed to the realization of a monochromatic and tunable X-ray source (*SL-Thomson*) in the 20 - 500 keV range, based upon Thomson backscattering of FLAME laser pulses by the relativistic electron beam.

For the purpose of this thesis, the main interest is for the BEATS2 experiment that is aimed to study medical applications of SL-Thomson source in diagnostic imaging. For this reason after a brief description of FLAME laser and SPARC electron beam injector (in Sec. 2.1.1), SL-Thomson beamline will be described in detail in Sec 2.2, as well as BEATS2 experiment in Sec. 2.3.

2.1.1 FLAME and SPARC

The SPARC-LAB high power laser system, named FLAME, has been fully commissioned in 2012. FLAME is based upon a Ti:Sa, chirped pulse amplification (CPA) laser able to deliver up to 220 TW laser pulses, 25 fs long, with a 10 Hz repetition rate at a fundamental wavelength of 800 nm, see Fig. 2.3. The system features a high contrast ratio ($>10^{10}$) and has a fully remotely controlled operation mode. It includes a front-end with pulse contrast enhancement, bandwidth control and regenerative amplifier and yields

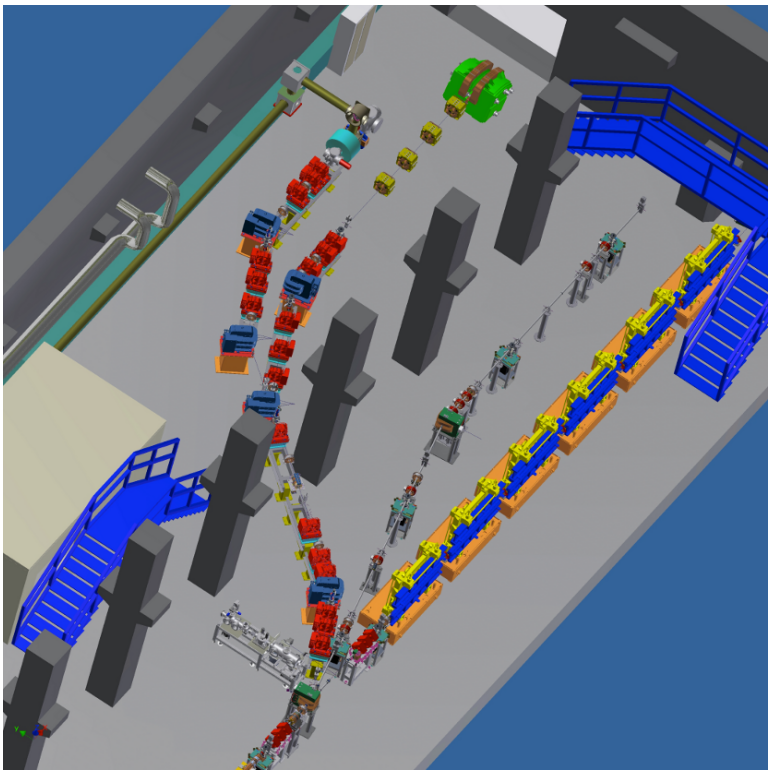

Figure 2.2: Layout of the experimental beamlines inside SPARC-LAB building.

Table 2.1: FLAME laser specifications.

Repetition Rate	10 Hz
Energy (after compression)	up to 6 J (typ. exp. 5.6 J)
Wavelength	800 nm
Pulse duration	down to 20 fs (typ.23 fs)
Peak power	up to 300 TW
ASE contrast <	10^{10}
Pre-pulse contrast	$< 10^{-8}$

pulses with 0.7 mJ in 80 nm bandwidth. These pulses are then further amplified by the first amplifier up to 25 mJ while the second amplifier brings the energy up to the 600 mJ. The third cryogenic amplifier is based on a 50 mm Ti:Sa crystal pumped by 10 frequency doubled Nd:YAG laser pulses, reaching an energy up to 20 J at 532 nm. The extraction energy is as high as 35%, leading to a final energy in the stretched pulses in excess of 7 J. The pulse then can be compressed to a minimum pulse duration smaller than 30 fs.

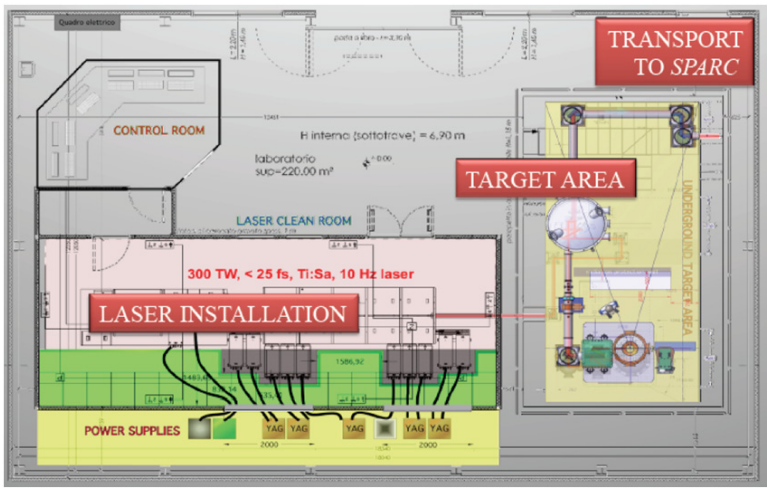

Figure 2.3: Flame laser laboratory [54].

Once compressed, the pulse is transported under vacuum to the target area via remotely controlled beam steering mirrors. A summary of the specifications of FLAME is reported in Table 2.1. Among the different uses of FLAME, the scientific plan includes self-injection and external injection [12] experiments and the realization of the SL-Thomson source as previously described; to this purpose, a careful characterization of FLAME performances, with particular reference to the transverse beam quality was carried out during the commissioning.

The SPARC electron beam injector consists of: a 1.6 cell RF gun operated at S-band (2.856 GHz, of the BNL/UCLA/SLAC type) and high peak

Table 2.2: SPARC electron beam characteristics [54].

Electron Beam Energy (MeV)	155
Bunch charge (nC)	1.1
Repetition rate (Hz)	1-10
Cathode peak field (MV/m)	120
Peak solenoid field @ 0.19 m (T)	0.273
Photocathode spot size (mm, hard edge radius)	1.13
Central RF launch phase (RF deg)	33
Laser pulse duration, flat top (ps)	10
Laser pulse rise time (ps)	1
Bunch energy @ gun exit (MeV)	5.6
Bunch peak current @ linac exit (A) (0.5 beam fraction)	100
Rms normalized transverse emittance @ linac exit (mm-mrad)	<2
Rms slice norm. emittance (300 um slice)	<1
Rms longitudinal emittance (deg.keV)	1000
Rms total correlated energy spread (percent)	0.2
Rms uncorrelated energy spread (percent)	0.06
Rms beam spot size @ linac exit (mm)	0.4
Rms bunch length @ linac exit (mm)	1

field on the cathode ($\geq$ 120 MV/m) with incorporated metallic photo-cathode (Copper or Mg), generating a $\geq$ 5.6 MeV beam which is properly focused and matched into 3 accelerating sections of the SLAC type (S-band, travelling wave) which accelerate the bunch up to 150-200 MeV.

The production of highest brightness electron beams in the photo-injector requires that a temporally-flat, picosecond laser source to be used to drive the photo-cathode. The laser system driving the photocathode employed is a high bandwidth Ti:Sa technologies with the oscillator pulse train locked to the RF [55].

In Fig. 2.4 a schematic layout of the electron beam injector is shown. A summary of the characteristics of SPARC electron beam is reported in Table 2.2.

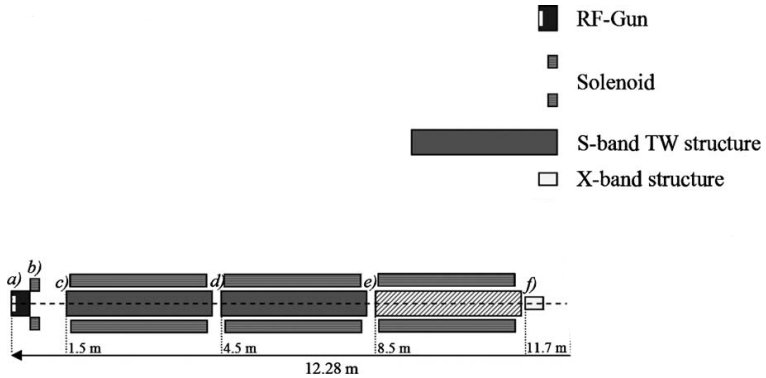

Figure 2.4: Schematic layout of SPARC electron beam injector [56].

2.2 SL-Thomson

The SPARC-LAB Thomson backscattering source (SL-Thomson) is based on the interaction of the high brightness electron beam (SPARC) and the high intensity FLAME laser beam; the source will be able to provide a high flux (up to $10^{10}\gamma/s$) of quasi-monochromatic photons with average energy variable from 20 keV to 500 keV by adjusting the electron beam energy. The source will be commisioned and characterized by the end of 2013.

The Thomson back-scattering (TS) X-ray source is foreseen to work in three different operating modes: the high-flux moderate-monochromaticity mode (HFM2), suitable for medical imaging (see Sec. 2.3), the moderate-flux monochromatic mode (MFM) suitable to improve the detection/dose performance [57] and the short and monochromatic mode (SM), useful for pump-and-probe experiments, *e.g.* in physical-chemistry when tens of femtosecond long monochromatic pulses are needed.

The SL-Thomson beamline consists of the vacuum lines for the transport both of the electron beam and the laser beam to the interaction area. The general layout is showed in Figure 2.2, where the electron transfer line departs from a three way vacuum chamber inside the first dipole downstream the RF deflector that is used for the six-dimensional phase space analysis of the electron beam. This dipole is also part of the 14 degrees dogleg that brings the electron beam up to the SPARC THz source. The electron beamline consists in a 30 m double dogleg starting, as mentioned, downstream the SPARC photoinjector; at the end of this section a two branch beam delivery line provides two separate interaction regions with the possibility to host two different experiments at the same time: the Thomson source and the external injection in a plasma accelerator experiment. In this configuration the electron beam energy can range from 28 MeV up to 150 MeV, and the electron beam transport is meant to preserve the high brightness coming from the linac and to ensure a very high focusing and a longitudinal phase space optimization in the whole energy range. The laser beam transfer line to the interaction region is composed by a series of high reflectivity mirrors inserted in a vacuum pipe (10^{-6} Torr) 50 m long that transfer the laser from FLAME building to the interaction chamber of SL-Thomson beamline in the SPARC bunker.

The layout of SL-Thomson interaction region is showed in Fig. 2.5, in which:

- the electron beam enters from the left, is focused by the solenoid (1), then interacts with the laser (3) and it is dumped on the floor using a magnet (4) to split its trajectory from the x-ray beam direction;

- the laser beam enters from top, as represented by the red arrow, then is reflected and focused by a parabolic mirror (5) to reach the interaction

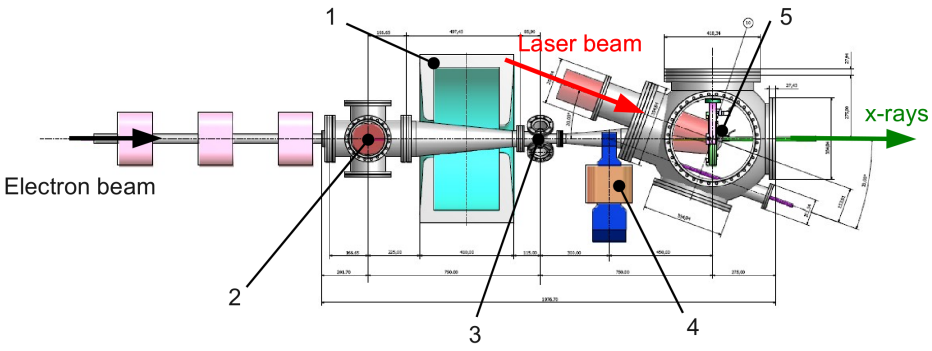

Figure 2.5: Drawing of the layout of SL-Thomson beamline interaction region.

point (3), after the interaction the laser is extracted by means of a 45 degrees mirror (2);

– the x-ray beam produced in the interaction point propagates toward the right through a hole provided in the parabolic mirror to avoid attenuation and x-ray scattering. The exit window of the chamber for the x-ray beam is made of 2 mm of beryllium that ensure vacuum tightness and a negligible x-ray absorption.

After the exit window the x-ray beam propagates in air in the experimental area.

The Thomson scattering experiment needs an extremely precise synchronization between electron bunch and laser pulse. The relative time of arrival jitter of the two beams is fundamental to obtain a repeatable and efficient interaction. The electrons and photons have to be synchronized with a relative jitter < 500 fs. This can be obtained with a standard electrical distribution of the reference signal. Anyway an optical distribution is preferable to obtain precise time of arrival measurement resolution (equal or less than 5 fs) and to obtain better synchronization between the two beams, a necessary requirement for the external injection in the plasma accelerator experiments [58]. This can be achieved by means of an optical cross- correlation between short laser pulses (100-200 fs). In particular the electrical (or optical) master oscillator will serve two laser oscillator clients: the photo injector laser for the production of electrons and the FLAME laser. The RF system phase will be also locked to the master oscillator using low noise phase detection; al last the phase feedback loops will be also implemented.

2.3 BEATS2 Experiment

The Thomson scattering x-ray sources show relevant features for several applications due to the capability of producing intense, quasi-monochromatic, tunable x-ray beams, maintaining still reasonably small size apparatus. Applications to medical physics are straightforward, in particular in mammography where dose control in screening programs is the main relevant issue. Theoretical and experimental studies on the mammographic imaging suggest that the optimal x-ray source for mammography should provide a beam with a narrow energy band and a tunable average energy ranging from 17 to 24 keV [11–14, 59]. The obtainable fluence rate is not as high as those typically achievable by synchrotron sources, but still compatible with the requirements of x-ray imaging applications, and considering compactness and smaller costs, Thomson sources represent a promising alternative to conventional x-ray tubes.
The BEATS2 experiment is aimed to study applications of Thomson radiation to mammographic imaging, using the SL-Thomson source of SPARC-LAB at the INFN-LNF that will be commissioned in the first half of 2013.

For this reason BEATS2 experiment will study imaging applications and performances of an x-ray beam produced by SL-Thomson with an average energy of 20 keV and an energy spread of about 10%. In particular, the activities will be focused on image quality and dosimetric evaluation of images produced by traditional absorption radiography, phase contrast with free propagation and phase contrast with interference gratings.

In order to provide a beam with the aforementioned characteristics, the electron beam generation system will produce and transport electron bunches of energy $E_{e-} = 30.28$ MeV, (corresponding to a Lorentz factor $\gamma \approx 60$), reaching the focal spot with a transverse size comparable with the laser focal spot size ($\sigma_x, y \approx 8 - 10\mu$m) and minimizing the hourglass effect [60], in order to allow the optimization of the geometrical overlapping with the laser pulse on the whole interaction duration.

These considerations imply severe constraints on the longitudinal energy spread and on the transverse emittance of the electron beam at the interaction point. First, the electron beam system is meant to produce high brightness electron beam able to accomplish to the experiment requirements. Second, the electron beam transfer line should provide the beam transport from the photoinjector up to the interaction point. The 6D-phase space characteristics have to be preserved up to that point to provide the required final strong focusing for the interaction with the laser pulse. In Fig. 2.6 the transverse beam rms size evolution is reported for the reference working point setup starting from the photoinjector down to the interaction point as obtained from the simulations performed with the Tstep code tracking 15 kparticles, for a beam energy of 30 MeV, and a quite high value for the starting normalized emittance $\epsilon_{nx,y} \approx 2.7\mu m$ [58]. The reference average

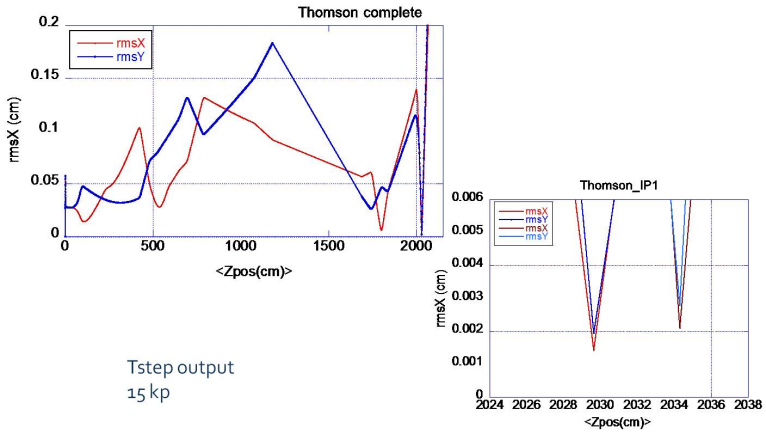

Figure 2.6: Rms beams sizes evolution along the transfer line (left), and detail of longitudinal "tunability" of the beam waist at the interaction point [58].

Table 2.3: Main average characteristics of the reference electron beam for the BEATS2 experiment.

Energy (MeV)	30.28
Envelope r.m.s (μm)	9.9
Emitt. (mm mrad)	0.8
En. spread	5×10^{-4}
Length r.m.s. (mm)	2
Charge (nC)	1

characteristics for the electron beam are summarized in Table 2.3.

The laser used in this experiment is the FLAME laser that is a Ti-sapphire laser able to deliver pulses with energy up to 6J, whose duration can vary from a few ps down to 20 fs, with a maximum repetition rate of 10 Hz. For the BEATS2 experiment, in order to fit the electron bunch length, the laser pulse will be only partially compressed to attain about 10 ps of duration. The optimal laser pulse is meant to produce the highest possible x-ray flux while keeping the relative energy spread of the radiation below 20% FWHM for the fundamental harmonic. Furthermore high order harmonics should be as low as possible in order to prevent their enhancement after filtration.
As result of the optimization process described in detail in [56] a laser pulse of waist size $w_0 = 15\mu m$, duration $T = 6$ ps , intensity $I = 2.3\times10^{17}$ W/cm^2 and amplitude $a_0 = 0.33$ has been chosen to collide with the electron bunch. With these parameters the harmonic contamination is less than 2% for the second harmonic and 10^{-4} for the third one.

2.3.1 Expected beam

The expected x-ray beam that will be produced for the BEATS2 experiment has been evaluated performing a complete simulation of the source [56] including electron beam transport on the dogleg, laser beam, and Thomson interaction. The optimization of the electron beam was performed by using the multi-particle code Astra in series with a genetic algorithm developed for solving problems in beam dynamics [61]. The Thomson interaction was simulated using *Thomson scattering simulation tool* ($(TS)^2$) code developed by P. Tomassini *et al.* [47]. The result of the simulations and parameters optimization are that each x-ray pulse of 5-10 ps of duration will contain 3.46×10^9 photons with a repetition rate variable from 1 to 10 Hz, adjusting the repetition rate of laser. The size of the region emitting photon will be about 10 μm of diameter.

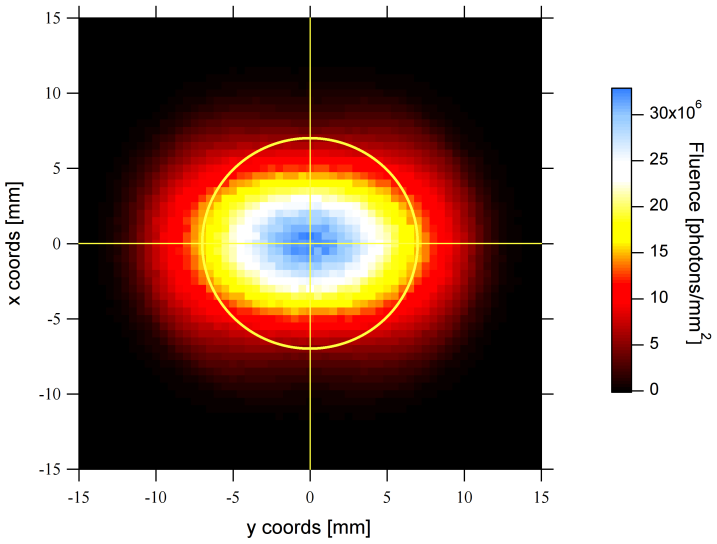

Figure 2.7: Expected spatial distribution of photon flux of SL-Thomson source for BEATS2 experiment, on a plane distant 75 cm from the interaction point.

The spatial distribution of the number of photons produced is showed in Fig. 2.7, where the fluence (ph/mm^2) is plotted as a function of the position on a plane distant 75 cm from the interaction point. This distance corresponds to the distance of the parabolic mirror for laser focusing from the interaction point, and the yellow circle in the figure represent the extraction hole for the x-ray beam, that sets the boundary for the maximum geometric angular semi-acceptance equal to 9.33 mrad. The spatial distribution of the

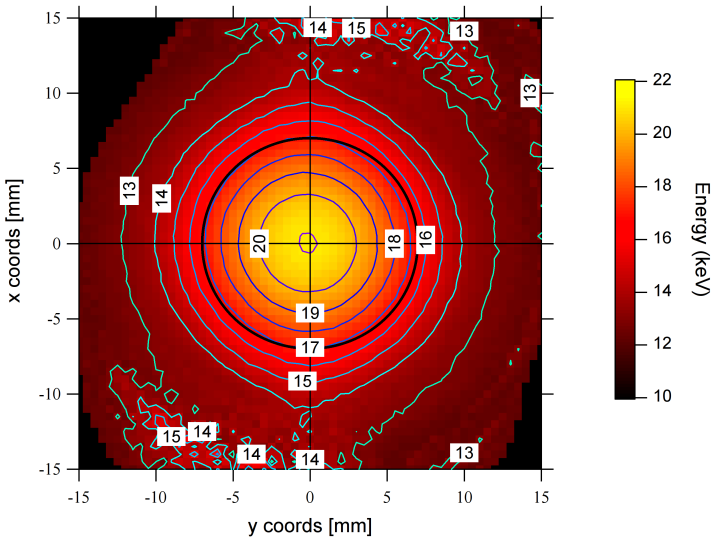

Figure 2.8: Expected spatial distribution of photon energies of SL-Thomson source for BEATS2 experiment, on a plane distant 75 cm from the interaction point.

photon energies is showed in Fig. 2.8: also in this case the energy is plotted as a function of the position on a plane distant 75 cm from the interaction point. As it can be noticed in Fig. 2.7 and Fig. 2.8, this distributions reflect the physics of the Thomson backscattering interaction considering that both the energy and the number of photons decrease as the angle increase from the backscattering direction. In particular this imply that the energy distribution depends on the angular acceptance considered, in the case of 6.0 mrad the average energy is 20 keV and the FWHM bandwidth is about the 10 %. A plot of the energy distribution for various angular acceptances is shown in Fig. 2.9. As it can be seen, the energy band ranges from 14 - 21 keV, considering an acceptance of 12.0 mrad, to 20.5 - 21 keV considering 0.67 mrad. The geometrical setup of the apparatus is such that the x-ray beam extraction system has a maximum intrinsic collimation of about 18.66 mrad that can be decreased using the collimation system of the beamline apparatus.

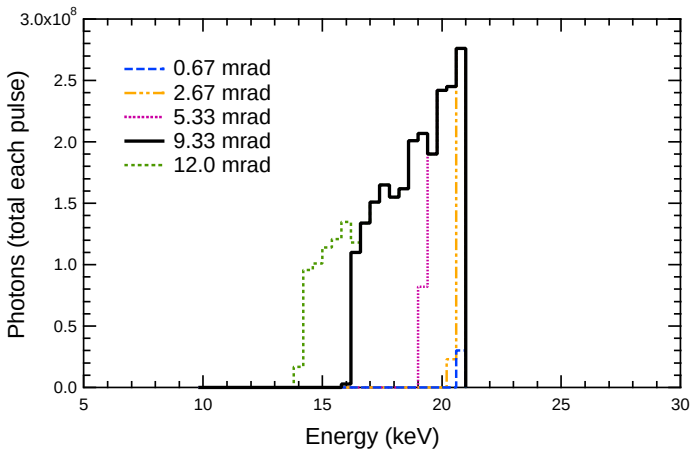

Figure 2.9: Expected energy distribution of photons of SL-Thomson for BEATS2 experiment.

3

ELI-NP Gamma beam system

3.1 Extreme Light Infrastructure

Extreme Light Infrastructure (*ELI*) is an European Project, involving nearly forty research and academic institutions from thirteen Countries members of European Union, forming a pan-European facility for scientific research in laser field, dedicated to the investigation and applications of laser-matter interaction at the highest intensity level (more than 6 orders of magnitude higher than current state of art laser intensity). The facility will be the first large scale infrastructure based on four sites on the eastern European Community [62]. The first three sites will be situated in Prague (Czech Republic), Szeged (Hungary) and Magurele (Romania) and should be operational in 2015. The fourth site has not yet been selected and is scheduled for commissioning in 2017.

In particular the ELI project will comprise three branches:

- *ELI-Nuclear Physics (Magurele, Romania)*: dedicated to the development of laser beams and the production of high intensity gamma beams for frontier research in nuclear physics.

- *ELI-Beamlines (Prague, Czech Republic)*: dedicated to providing ultrashort energetic particle (10 GeV) and x/γ-beams (up to few MeV) produced from compact laser plasma accelerators for a wide range of user's applications;

- *ELI-Attosecond (Szeged, Hungary)*: dedicated to extremely fast dynamics by taking snap-shots in the attosecond scale of the electron dynamics in atoms, molecules, plasmas and solids. It will also pursue research in ultrahigh intensity laser

- *ELI-Ultra High Field Facility*: the highest intensity pillar location has not yet been selected. The laser power will reach the 200 PW. It will depend, among other things, on the laser technology development and validation. It could be built on one of the existing three sites or in a new country. With the possibility of going into the ultra-relativistic

regime, ELI-UHF will allow new investigations in particle physics, nuclear physics, gravitational physics, nonlinear field theory, ultrahigh-pressure physics, astrophysics and cosmology (generating intensities exceeding 10^{23} W/cm^2).

(a) (b) (c)

Figure 3.1: View of artistic rendition of ELI pillars infrastructure buildings: (a) ELI-Nuclear Physics, (b) ELI-Attosecond, (c) ELI-Beamlines.

3.2 ELI Nuclear Physics Gamma Beam Source

ELI Nuclear physics, the pillar of the project dedicated to the development of laser beams and the generation of high intensity gamma beams for frontier research in nuclear physics, will be hosted by the Horia Hulubei National Institute of Physics and Nuclear Engineering (IFIN-HH) in Magurele, Bucharest, Romania [63].

ELI-NP will be a very complex facility based mostly on two machines of extreme performances:

- *Multi-Petawatt Laser System (MPLS)*, a very high intensity laser, where the beams of two 10 PW lasers are coherently added to get intensities of the order of 10^{23} - 10^{24} W/cm^2 and electrical fields of 10^{15} V/m;

- *Gamma Beam System (GBS)*, a very intense and brilliant gamma beam obtained by inverse Compton scattering of a laser light by an accelerated electron beam ($E_e > 700$ MeV) produced by a warm linac.

These machine will permit the creation of a new European laboratory to consistently investigate a very broad range of science domains, from new fields of fundamental studies in nuclear physics dealing with the nucleus structure and the role of giant dipole resonances, of great relevance also for astrophysics topics, to applications in material science, life science and nuclear materials management.

A report describing the whole range of possible experimental applications with lasers and gamma beams having the characteristics expected to be

realized at ELI-NP, has been prepared from contributions by many scientists from various laboratories throughout the world. Their contributions have been merged by a group of editors in the White Book of ELI-NP [19].

In particular, nuclear structure physics with gamma-ray beams is an emerging field of research with a high discovery potential involving also high social-impact applications such as nuclear energy, national security and medicine. Inverse Compton sources, providing gamma beams with high spectral density, will play a crucial role in advancing to new generation sources to explore the nuclear photonics field. ELI-NP will become a major facility in this field providing: energy-tunable, high-flux, high-resolution, ps-long, polarized gamma-ray beam from the gamma beam system, counting on a large international user community.

The source will produce a very intense and brilliant gamma beam, obtained by inverse Compton scattering of laser light with a very brilliant and intense electron beam. The envisioned experiments that could be performed using the ELI-NP gamma source suggest that the optimal parameters of the gamma beam should be:

- energy continuously tunable in the range from 0.2 to 19.5 MeV,
- r.m.s bandwidth equal or smaller than 5×10^3,
- time-average spectral density at peak energy 5×10^3 photons/sec eV,
- peak brilliance higher than 10^{19} photons/mm^2 /mrad^2 /s/(0.1% BW),
- focal spot smaller than 100 μm,
- polarization larger than 95 %.

The driving force behind the development of light sources is the optimization of their brilliance (or spectral brightness), which is the figure of merit of many experiments. Brilliance is defined as a function of frequency given by the number of photons emitted by the source in unit time in a unit solid angle, per unit surface of the source, and in a unit bandwidth of frequencies around the given one. The units in which it is usually expressed are photons/s/mm^2 /mrad^2 /0.1%BW. As it is possible to notice from the definition, brilliance depends both on the photon flux (photons per second in a given bandwidth) and on the phase-space density of the photons. High brilliance means a source with a high flux and with the radiation emitted from a small area and with high directional collimation, for this reason, especially when a radiation beam is used to investigate low cross-section interaction in a target, this is one of the principal parameter to maximize in order to increase the detectability of the phenomenon. In Table 3.1 a list of the parameters of the major gamma source facilities worldwide is shown. As it is possible to see the parameters required for the ELI-NP-GBS are

Table 3.1: Parameters of major Compton gamma source facilities worldwide [20].

Project	LADON	LEGS	ROKK-1M	GRAAL	LEPS	HIγS
Location	Frascati, Italy	Brookhaven, US	Novosibirsk, Russia	Grenoble, France	Harima, Japan	Durham, US
Stor. ring	Adone	NSLS	VEPP-4M	ESRF	SPring-8	Duke-SR
Energy (MeV)	5-80	110-450	100-1600	550-1500	1500-2400	1-200
Energy resolution (%)	5	1.1	1-3	1.1	1.25	0.8-10
Max. flux	5×10^5	5×10^6	10^6	3×10^6	10^4	5×10^8
Years of operation	1978-1993	1987-2006	1993-	1995-2008	1998-	1996-

very demanding being 1-2 orders of magnitude better than those at state of the art of similar gamma sources, in particular considering the HIγS facility, located on the campus of Duke University and operated by Triangle Universities Nuclear Laboratory (North Carolina, US) that currently is the world's most intense polarized gamma-ray source operating [64].

In order to realize the source with these cutting edge specifications, Horia Hulubei National Institute of Physics and Nuclear Engineering made a call for tender for the public procurement contract for the realization of a high intensity Gamma Beam System (GBS) for the ELI-NP (Extreme Light Infrastructure Nuclear Physics) research infrastructure [65].

To meet these challenging specifications, an European collaboration named E-Gammas was set up to prepare a Technical Design Report for a machine capable to deliver by the end of 2016 the gamma beam to users in the ELI-NP research infrastructure. This international collaboration is composed by several Universities and Institutions: Istituto Nazionale di Fisica Nucleare and Università di Roma La Sapienza, in Italy, Universitè de Paris Sud and IN2P3/CNRS, in France, and ASTeC of STFC, in UK [66].

Within this collaboration, the research unit of Ferrara section of INFN is involved in the design and realization of the collimation and characterization and monitoring system of the gamma beam. In the next section (3.3) a brief description of the characteristics of ELI-NP Gamma Beam System of the E-Gammas proposal will be given, as well as the characteristics of the expected gamma beam produced. A more detailed description of the characterization system, with particular attention to the detectors studied by the INFN Ferrara research unit will be given in Chapter 5.

3.3 E-Gammas proposal for ELI-NP-GBS

In the following a summary of the characteristics of the gamma beam system proposed by the E-Gammas collaboration will be given. A detailed description of the apparatus can be find on the *Technical Design Report of the E-Gammas proposal for the ELI-NP Gamma beam system* by L. Serafini *et al.* [45]. As previously mentioned, the gamma beam system envisioned will be obtained by the head-on collimation of an accelerated electron beam with a high power pulsed laser.

In particular, the gamma beam system will be composed by two parallel beamline. The first will allow the interaction the laser pulse (wavelength 2.4 eV, pulse energy 0.5 J) with the electron beam having an energy up to 360 MeV. This interaction will provide gamma beams with energy up to 5 MeV and it is called the *low energy* line. The second line will extract the electron beam from the former and further accelerate it to provide electron energies up to 720 MeV, to generate gamma beam with energies ranging from 5 to 19.5 MeV, thus the low and high energy lines combined will cover the whole energy range required by the tender specifications (0.2 - 19.5 MeV). The duration of a laser pulse is 1.5 ps with a repetition rate of 100 Hz. Each laser pulse will undergo a recirculation system that permits to reiterate the interaction of the same pulse 32 times (16+16 with slightly different angles of incidence) with the same number of different electron bunches. The time separation between each recirculation is 16 ns and the electron bunches will be synchronized with this time structure. This will result in the time structure of the gamma beam represented in Fig. 3.2, as it is possible to notice it will be composed by macro-pulses with a time separation of 10 ms (100 Hz), where each of these macro-pulses is made of 32 pulses 1.5 ps-long separated by 16 ns.

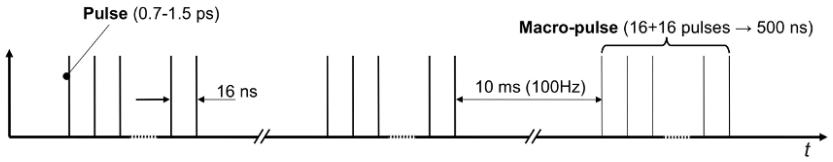

Figure 3.2: ELI-NP gamma beam temporal structure.

A summary of the expected characteristics for the ELI-NP gamma beam system beam are reported in Table 3.2 for three selected energies.

Table 3.2: Gamma beam characteristics summary for three selected collision examples (from start-to-end simulations) [45].

Photon energy (MeV)	4.60	9.72	18.50
Spectral Density (ph/sec eV)	4.5×10^{4}	2.4×10^{4}	1.1×10^{4}
Bandwidth (rms %)	0.3	0.3	0.3
photons per shot within FWHM bw	2.1×10^{5}	2.3×10^{5}	1.9×10^{5}
photons/sec within FWHM bw	6.7×10^{8}	7.4×10^{8}	6.1×10^{8}
Source rms size μm	21	18	18
Source rms divergence μrad	48	36	24
Peak Brilliance (ph/sec mm^2 mrad^2 0.1%)	7.6×10^{22}	2.0×10^{23}	3.8×10^{23}
Average Brilliance (ph/sec mm^2 mrad^2 0.1%)	2.2×10^{14}	5.9×10^{14}	1.1×10^{15}
Radiation pulse length (rms, psec)	0.91	0.95	0.90
Linear Polarization	99.8%	99.8%	99.8%
Macro-pulse rep. rate (Hz)	100	100	100
Pulses per macro-pulse	16+16	16+16	16+16
Pulse-to-pulse separation (ns)	16	16	16

3.3.1 Gamma beam collimation system

The gamma energy bandwidth is one of the most challenging parameter to be achieved. Defined as the ratio of the r.m.s. to the maximum of the beam energy spectrum, the energy bandwidth required by the tender specifications is to be smaller than 0.5 %. The value considered for the calculations of the collimation is 0.3 % for the entire energy range.

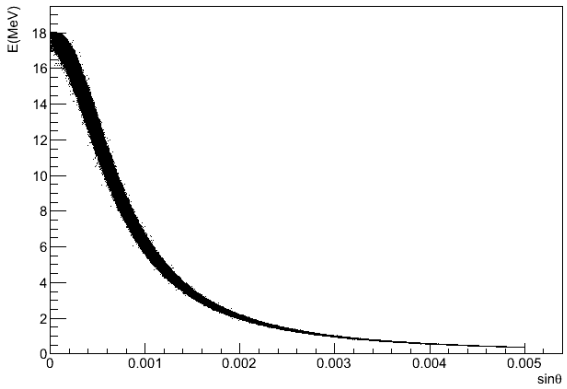

Figure 3.3: Plot of the angular dependence of the gamma energy in the case of gamma beam maximum energy equal to 18 MeV (Courtesy of O. Dadoun, Universitè de Paris Sud).

Figure 3.3 shows a typical energy distribution as a function of the angular divergence for the gamma emerging from the interaction point in the case of a maximum photon energy of 18 MeV. As it is possible to notice, the wider is angular acceptance considered, the lower is the energy of the photons included, implying a lower average energy and the broadening of the energy distribution bandwidth. In order to obtain a monochromatic spectrum, the

Table 3.3: Collimation parameters for selected gamma beam energies.

Energy (MeV)	1.0	4.60	9.72	18.50
Source rms divergence (μrad)	250	48	36	24
Collimator aperture at 10 m from IP (μm)	5×10^3	960	720	480

photons with a lower energy, emitted at larger angles, can be taken away using an appropriate absorber collimation system. In this way high energies are then selected and the bandwidth requirements can be achieved. Two different gamma beam extraction systems are considered, corresponding to the two different incident electron drive beam energies. In the case of the low energy (electron drive beam at 360 MeV) the maximum mean energy of the gammas is about 2.4 MeV, and goes up to 9.0 MeV in the case of the high energy line (electron drive beam at 720 MeV). At those energy only a thick material with a high atomic number is able to stop the gammas.

In Table 3.3 a summary of the r.m.s divergences needed to obtained the 0.3 % bandwidth is shown for four typical values of gamma beam energy. Also, the corresponding diameters of collimation aperture, for a collimator placed at 10 m from the interaction point, are listed.

The main requirements for the collimation systems are:

1. a low transmission of gamma photons (high density and high atomic number material);

2. continuously adjustable aperture, in order to reach the correct energy bandwidth in the whole energy range;

3. to avoid contamination of the primary beam and experimental area downstream with production of secondary radiation (electromagnetic, neutrons *etc.*).

Various types of collimators and materials solutions have been studied. The final choice is a dual slit collimator analogous to the one designed and assembled at INFN-Ferrara for the DARMA experiment [67]. This consists of an aluminum framework supporting two 20 mm-thick tungsten edges, that can be translated to adjust the slit aperture width. By staking several slit collimators with a rotation around the central axis, it is possible to create a pin-hole like collimator with a small enough angular acceptance and a significant thickness. In particular for the two lines, low and high energy, of the ELI-NP gamma beam system, the collimator setup will be:

– Low energy (1-5 MeV): 12 tungsten slits with a relative rotation of 30 degrees each.

– High energy (5-20 MeV): 14 tungsten slits with a relative rotation of 25.7 degrees each.

The position of the collimation system along the beam-line will be at about 10 m of distance from the interaction point (free to range from 5 to 15 m to fit building constraints) and each slit aperture will be adjustable from 0 to 20 mm. A schematic drawing of the low energy collimation configuration, with a total of 12 slits, is shown in Fig. 3.4, in which it is possible to notice the relative rotation displacement of the various slits, each one connected with a remote controlled movement stage for the aperture size adjusting.

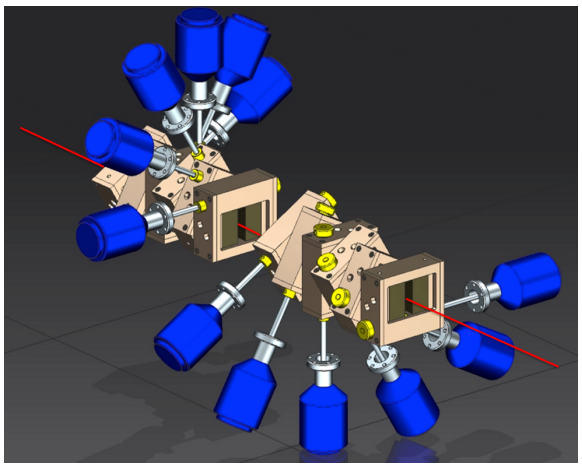

Figure 3.4: Drawing of the configuration of low energy collimator made up of 12 tungsten adjustable slits with a relative 30 degrees rotation each.

Concrete block for scatter removal

In order to avoid that the scattered radiation produced by the interaction of the primary gamma beam with the collimation system interferes with the downstream detectors, a concrete block will be placed after the collimators exit. This block will be shaped as a cylinder of concrete material 100 cm-long and with a radius of 100 cm. To evaluate the efficiency of this block in absorbing scatter radiation, being photons, electron, positrons and neutrons, a Monte Carlo simulation using FLUKA [68] was performed. The gamma beam considered has an energy of 20 MeV, a beam radius at source equal to 0.5 mm and a divergence of 200 μrad. After propagating in vacuum for 10 m, the beam impinges on a cylindrical tungsten collimator (length = 28 cm, inner radius 0.024 cm, outer radius 0.5 cm). At a distance of 30 cm from the collimator exit is placed the parallelepiped concrete shielding 1 m long, with a square transverse section of 60×60 cm^2 and an aperture radius of 1.45 cm. The simulation of 10^5 photons, comparable to the number of photons per each pulse, results in the collection of 1 electron, 2 positrons and 20 photons on a collecting screen: inner radius 1 cm, outer radius 20 cm. The plots in Fig. 3.5 show the fluence of electrons, positrons photons

and neutrons with and without the concrete shielding.

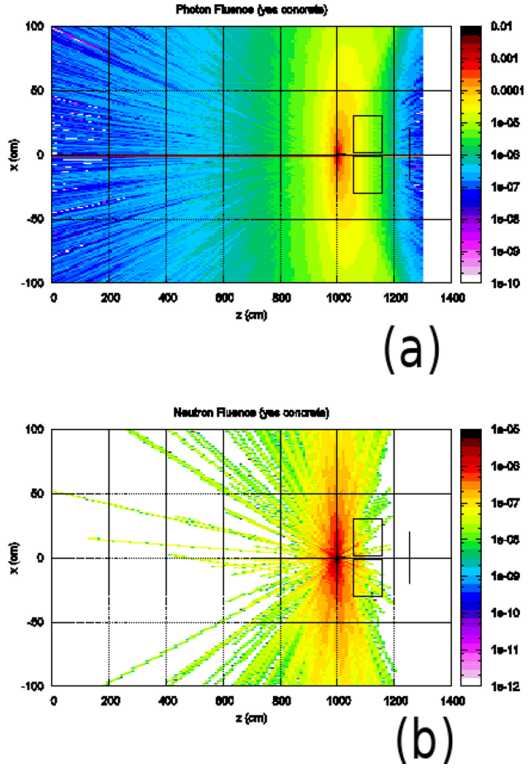

Figure 3.5: Plot of result of Monte Carlo simulations for the removal of radiation produced by collimator interaction using a concrete block (Courtesy of F. Broggi, INFN-Mi).

4

BEATS2 x-ray beam characterization apparatus

The BEATS experiment is aimed to study applications of Thomson backscattering radiation to mammographic imaging, using the SL-Thomson source of SPARC-LAB at the INFN-LNF that will be commissioned in the first months of 2013, as described in Section 2.3. The collaboration involves INFN sections of Pisa, Cagliari, Roma, Bari, Milano, Laboratori Nazionali di Frascati and Ferrara as the coordination unit of the experiment.

The first task of this project is the full characterization of the beam produced by the Thomson source, in order to verify the theoretical model used to simulate the Thomson backscattering process and to evaluate the possible performances in the various applications of the beam. The characterization of an x-ray source includes the evaluation of the total photon yield, the energy distribution, the spatial distribution and the size of the emitting area (*i.e.* focal spot). Once the x-ray beam is fully characterized it will possible to evaluate the performances of this beam for medical imaging applications. In particular, in addition to quasi-monochromatic absorption mammography it will be possible to study advanced imaging techniques such as propagation-based phase contrast [17, 69–71], gratings-based phase contrast [72,73], phase retrieval techniques [74] and (quasi-)monochromatic CT or micro-CT applications [75, 76] .

The main tasks of the Ferrara research unit in the first stage of BEATS2 experiment include the realization of the hardware for the operation of the x-ray beamline and the realization of devices and techniques for the characterization of the x-ray beam, in particular:

- design and realization of the collimation and filtering system for the x-ray beamline;
- design and realization of an x-ray flux on-line monitoring system;
- design and realization of a device for flux measurement;
- implementation of a technique for the evaluation of the x-rays energy

distribution (in collaboration with the research units of Pisa and Sassari).

In the following sections each of the system components designed and realized will be described in detail. The results of various experimental tests performed on the devices will be also illustrated.

In Figure 4.1 it is shown a picture of the x-ray beamline apparatus that will be installed and integrated with the SL-Thomson beamline at SPARC-LAB in the first months of 2013. This devices will be installed after the x-ray exit window of the vacuum interaction chamber. The x-ray beam propagates in air for the whole length of the beamline.

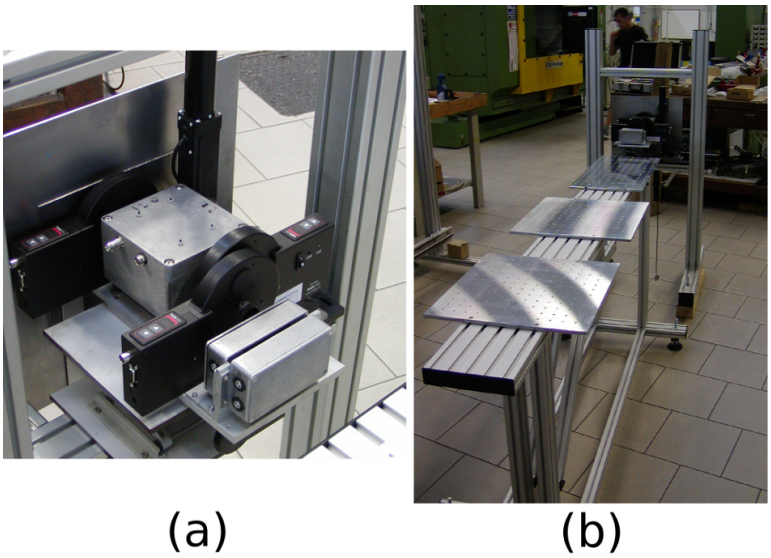

Figure 4.1: X-ray beamline for BEATS2 experiment, (a) detail of the apparatus for collimation, monitoring and characterization; (b) a view of the complete x-ray beamline.

The first stage of the x-ray beamline is for x-rays monitoring and characterization, in particular this system consists of:

- first collimation and lead shutter for beam stopping;
- a rotating collimator holder that allows to reduce the angular divergence of the beam, equipped with six different collimator corresponding to angular acceptance varying from about 9 mrad to 1 mrad;
- a free-air ionization chamber, used as a x-ray beam on-line monitoring;
- two additional filter/collimator holders with six available position each, for beam filtration or further collimation;

Table 4.1: Values of angular divergence obtainable with the collimation system.

Collimator number	Semi-divergence (mrad)
1	none (9.33)
2	8.00
3	6.66
4	4.66
5	3.34
6	2.00

– a removable device based on a silicon PIN diode for X-ray flux measurement.

In Fig. 4.1 it is also shown the 2.5 m-long table that will provide the support for samples and imaging detectors. An additional table will be placed downstream the beam, at a distance of approximatively 10 m from the interaction point, to permit the study of imaging techniques, such as free-propagation phase-contrast, that require longer x-rays propagation distances.

4.1 Beam collimation and filtering

The collimation system consists of a first wide circular collimation placed at the exit window of the vacuum interaction chamber that limit the angular acceptance of the x-ray beam to 12 mrad. This collimation does not intercept the primary beam but it is aimed to absorb possible off-axis scattering at low energies. In the same position is also placed a remote controlled beam shutter made of 3 mm of lead for a complete attenuation of the beam.

At a distance of 136.3 cm from the interaction point it is placed a six-position filter-wheel containing 5 lead rings 2 mm-thick with decreasing internal radius that permit the collimation of the x-ray beam at various angular divergences, as listed in Table 4.1. In order to test the absorption of the lead rings mounted on the filter-wheel and the correct alignment and repeatability of the movement, a series of radiographic images using a W-anode x-ray tube at 36 kVp was performed. A montage of the radiographic images obtained is shown in Fig. 4.2, where it is possible to notice that there are no x-ray leakages and the edge profiles are sharp.

4.2 X-ray beam monitoring

The task of this device is the evaluation of the x-ray yield produced. This measurement is needed to check the repeatability of the source and to monitor the delivered x-ray flux during experiments. It is also important to

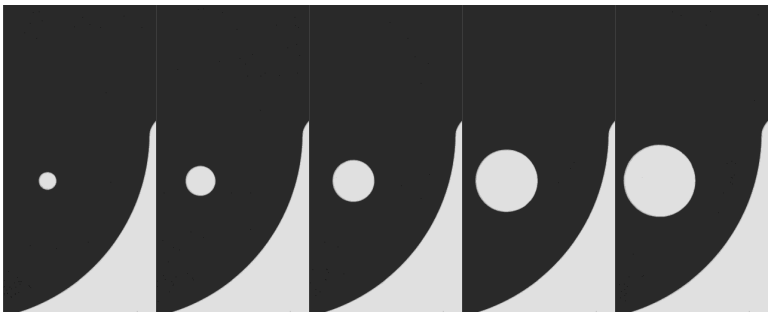

Figure 4.2: Montage of the radiographic images of the changeable collimators of BEATS2 beamline.

provide a real-time check of the apparatus proper operation that is fundamental in the commissioning phase of the source, but in particular during routine use.

This device is intended as an on-line monitor of the flux: assuming that the energy distribution does not change, the signal in the detector will be proportional to the flux of photons emitted by the source. In order to perform an absolute measurement of x-beam flux, the efficiency of the detector and the incident beam energy distribution must be known very accurately. As it will be discussed later, the task of this detector is just the monitoring of the photon yield, in order to perform an accurate absolute measurement of the photon flux other dedicated devices have been realized and tested. The required features for this x-ray monitor are:

- *stability*, the stability of the detector response must be good enough to permit the verification of the repeatability of the source over the time of a measurement session (at least a few weeks);
- *radiation hardness*, the radiation hardness of the device should be compatible with a routine utilization, in order to guarantee an adequate lifetime of the monitoring system;
- *time resolution*, the detector signal elaboration should operate at a frequency of 10 Hz in order to obtain an integral information of a single pulse; otherwise, if the information needed is on signal time structure, the sampling frequency should be higher, according to the time resolution needed;
- *signal to background ratio*, the signal produce by the detection of the primary beam must be recognizable from the possible background present in the SPARC-LAB bunker, due to electromagnetic noise and/or ionizing radiation, related to particles acceleration, particles scattering, residual bremsstrahlung, etc;

– *no contamination of x-ray beam*, the interaction of the x-ray beam with the monitor should not produce secondary radiation along the primary beam direction to avoid interfering with downstream applications.

Considering that the x-ray beam propagates in air along the experimental beamline, to realize a monitor device the simplest solution is to collect and measure the charge produced by the air ionization along the beam path. An ionization chamber naturally satisfies the requirement for radiation hardness and no contamination of the primary beam. Moreover, this kind of detector shows a very stable response, admitted the environmental conditions such as temperature and humidity do not vary much, as it is the case in the SPARC-LAB bunker. A free-air parallel plate ionization chamber was designed, realized and tested; the device and the result of tests carried out is described in the following sections.

4.2.1 Ionization chamber description

A free-air parallel plate ionization chamber was designed and realized. The chamber is composed by two gold-plated copper rectangular electrodes, placed on parallel planes at a relative distance of 25 mm by mean of plastic spacers. The x-ray beam is mean to pass through the chamber in the direction parallel to the electrode in order to avoid absorption and scatter from the interaction with any material. In figure 4.3 the size of the plates are shown, as it is possible to notice a guard-electrode was obtained in both plates in order to avoid the collection of parasite currents from the plastic spacers and supports and to avoid border distortion of the collecting electric field.

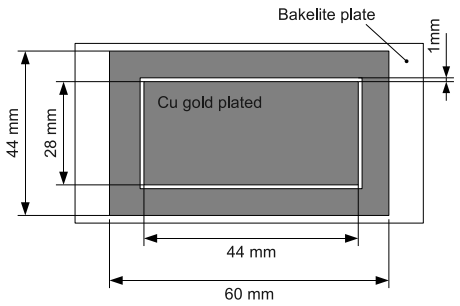

Figure 4.3: Drawing of the ionization chamber plates with sizes.

The plates are installed in an aluminum box, provided with a hole (25.0 mm of diameter) to allow x-ray beam crossing and with two connectors for high voltage supply and signal extraction (see Fig. 4.6). A negative high

voltage is applied to the electrode of the chamber keeping one of the two connected to ground. The signal is collected from this ground electrode in order to avoid eventual damages to the acquiring circuitry in case of short-circuit or high-voltage issues.

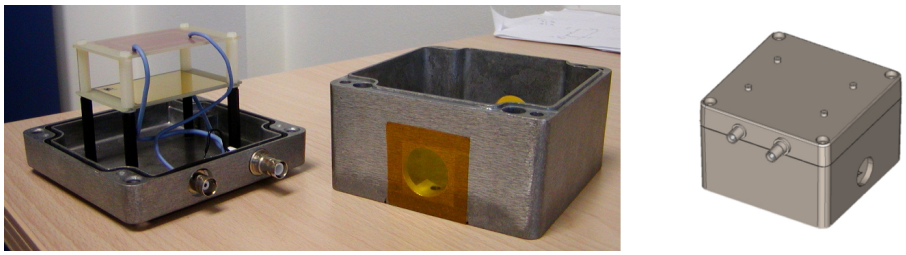

Figure 4.4: Picture of the ionization chamber realized for BEATS2 experiment opened (*left*); drawing in the closed, final configuration (*right*).

The signal of ionization chamber is acquired using an electrometer Keithley mod. 6517B (Keithley, US). This device has a reading rates of up to 425 readings/sec and can work in autoranging mode over the full span of ranges on different measurements: current (1 fA - 20 mA), resistance (50 MΩ-10 Ω), voltage (10 μV - 200 V) and charge (10 fC- 2 μC).

This electrometer is also equipped with an HV supplier (1-100/100-1000 V) and can be remote controlled using RS-232 connection with a PC serial port or GPIB connection via a dedicated Labview application. For this reason a Labview software was implemented and a screen-shot is shown in Fig. 4.5. The software permits to control the voltage applied to the ionization camera and to perform acquisitions of current or charge, that can be written in a log text file with a sampling frequency adjustable by the user. Moreover, various other reading parameters are controllable through this software, such as the acquisition range and NLPC for measurement accuracy.

4.2.2 Ionization chamber testing

The correct operational HV applied to the chamber is a key parameter that ensures to work in the so called *ionization chamber regime*, that is when all the charges produced by the ionizing radiation in air without multiplication are collected. In order to find the correct HV an analysis of the signal variation with respect to the voltage applied has been carried out. The optimal HV value was found to be -700 V, as it is possible to notice in Fig. 4.6, the signal saturation plateau is centered on this value.

To check the background signal various tests in different environmental conditions were performed at the Larix laboratories at Physics Department of Ferrara University. The chamber was connected and HV applied for long time intervals (hours-days) in various location and conditions showing an

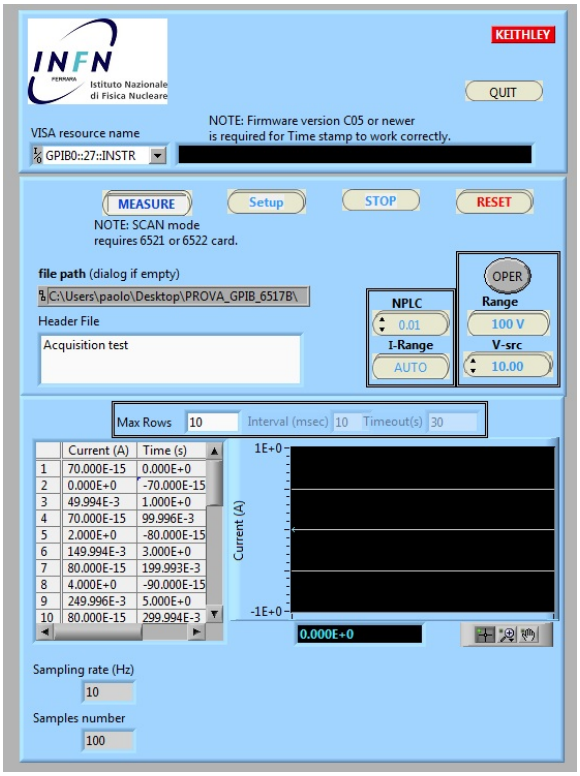

Figure 4.5: Screen-shot of the LabView software for Keithley electrometer mod. 6517B data acquisition.

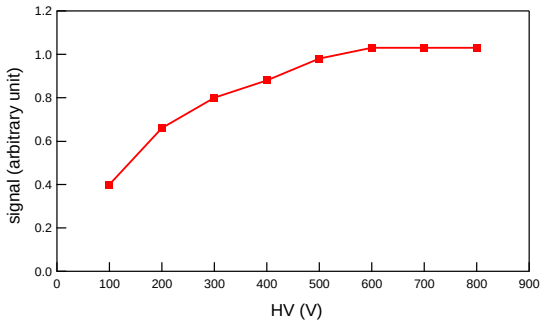

Figure 4.6: Plot of signal with respect to the HV applied for BEATS2 monitor chamber.

average background signal always smaller than 10 pA with slow oscillations of a few picoamperes at maximum. Furthermore the chamber was tested for background in SPARC-LAB bunker at LNF. At the time of this test the dogleg for the electrons transport and the interaction region for the SL-Thomson source was not installed yet, but the chamber was placed in a position close to the electron principal beamline were it was supposed to be more subject to scattered radiation and electromagnetic noise than in its final place at the SL-Thomson beamline. The result of these preliminary tests showed that the current acquired could exceed 50 pA during electron beam parameters adjustments, but stabilized around 25 pA or less during steady electron beam transport. These values are slightly higher than what was measured in radiation-free environments, but they are still compatible with source monitoring, considering the signal-to-background ratio for the expected signal. A complete check of the background signal in the final experimental configuration will be made in March 2013 during the commissioning of the electron transport beamline preceding the electron-laser collisions.

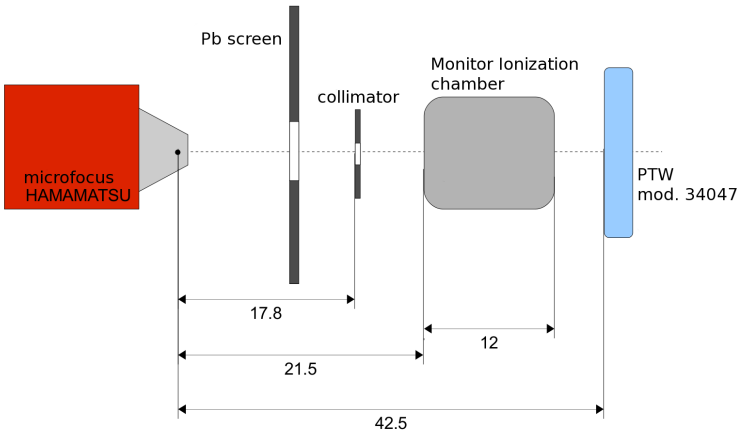

Figure 4.7: Experimental setup for the monitor chamber testing at Pisa Laboratories (reported quotes in cm).

In order to check the proper operation of the chamber and its linearity, the response of the free air ionization chamber, irradiated with a conventional x-ray tube, was compared to the response of a commercial reference soft x-ray chamber PTW mod.34047 (PTW - Freiburg, Germany). This test was performed at the medical physics laboratory of Pisa University, in collaboration with Pisa research unit. The experimental setup is shown in Fig. 4.7 where it is possible to notice that both the chambers, the monitor one and the PTW mod. 34047 were irradiated simultaneously using an Hamamatsu microfocus x-ray tube (Hamamatsu, Japan) with a tungsten anode

Table 4.2: Results of monitor ionization chamber testing at Pisa laboratories.

Anodic current (μA)	Monitor chamber signal (pA)	PTW air-dose (Gy)
200	28.0	8.45×10^{-5}
100	14.1	4.25×10^{-5}
50	7.1	2.12×10^{-5}
25	3.6	1.07×10^{-5}
12	1.7	5.16×10^{-6}
6	0.9	2.68×10^{-6}

and a 150 μm-thick beryllium exit window. In order to obtain an energy distribution comparable to the one expected for BEATS2 experiment, the x-ray beam produced by the microfocus tube at 30 kVp was filtered with 1 mm of aluminum, providing a beam with an average energy of about 21 keV, reported in Fig. 4.8.

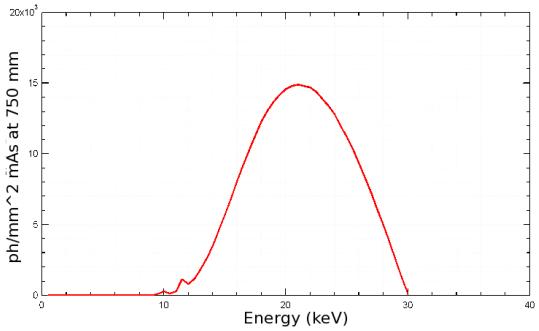

Figure 4.8: Plot of the energy spectrum of a W-anode x-ray tube at 30 kVp, with 1 mm Al of additional filtration.

Various acquisitions have been done, changing the anodic current in the tube from 2 to 200 μA. The results of the currents collected in the monitor chamber and the air-dose obtained with the PTW chamber are reported in Table 4.2. The same data are plotted in Fig. 4.9 together with a linear fit. As it is possible to notice, in this regime of continuous irradiation the response of the monitor chamber realized is linear and in good agreement with the result obtained with a calibrated commercial chamber. Moreover, the values of current produced were compared to those expected for the charge production in air for this x-ray beam with this flux, showing good agreement.

Considering the results of these tests, together with the result of the signal produced in the chamber irradiated with monochromatic synchrotron light (see Sec. 4.3.2), it is possible to conclude that the ionization chamber in continuous irradiation regime showed a stable and linear response over a wide range of fluxes (from 10^7 ph/s up to $> 10^{10}$ ps).

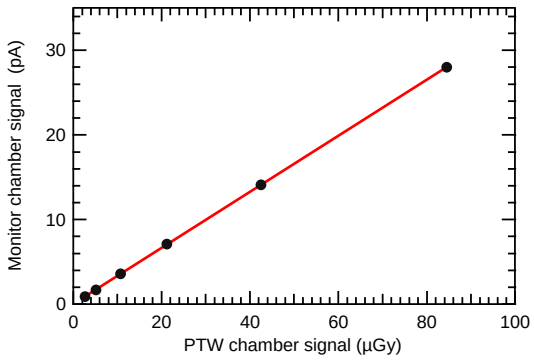

Figure 4.9: Plot of the signal obtained with the monitor chamber as a function of the PTW chamber signal, obtained irradiating with the energy distribution of Fig. 4.8 and anodic current varying from 2 to 200 μA.

4.2.3 Expected signal

Considering the application of the monitor chamber to the BEATS2 experiment and the expected x-ray beam described in Sec. 2.3.1, *i.e.* pulses 10 ps long with 3.46 $\times 10^9$ photons each and with an average energy of 19.5 keV, it is possible to calculate the energy released and then the charge produced in the active volume of the ionization chamber.

The energy absorbed by air was evaluated using the mass energy-absorption coefficient μ_{en} of dry air (see [77, 78]) and 33.73 eV as the mean energy required to produce a ion pair in air [79]. The charge produced by each radiation pulse is expected to be 2.3 nC in a volume of 21.6 cm^3. An important parameter to describe an ionization chamber is the collection efficiency, that is the fraction of collected charge with respect to the total charge produced. In optimal conditions this efficiency is equal to one, but in the case of high intensity pulses, producing high charge-density in the air, it is possible that the recombination of ion-electron couples becomes a relevant effect, thus resulting in a partial collection of the charge produced. A simple model to evaluate the entity of the recombination have been described by J. W. Boag [79, 80]. This model works whether the pulse length is short enough to be negligible with respect to the collection time of charges and when the repetition rate is low enough to consider that before the next pulse the whole charge has been collected on the chamber electrodes. Considered that the typical collection time is on the order of few milliseconds, both the conditions are satisfied in our case. Thus, using Boag model, the fraction f_p of the charge collected in a parallel electrodes ionization chamber can be calculated as:

$$f_p = p \ln\left(1 + \frac{1}{p}\right) \tag{4.1}$$

where

$$p = \frac{e}{\alpha}(k_+ + k_-)\frac{V}{Q_0 d^2} = \mu' \frac{V}{Q_0 d^2} \tag{4.2}$$

and e is the elementary electric charge, α is the ion concentration in the gas, k_+ and k_- are the ions mobilities, Q_0 is the charge density produced by a pulse and d is the electron spacing. Using the value suggested by Boag for air, the dimensionless variable p becomes:

$$p = 0.306 \times 10^{-12} \frac{V}{Q_0 d^2} \tag{4.3}$$

where V is in volts, d is in cm and Q_0 in coulombs per cm^3 per pulse in air. Therefore, in pulsed operation the efficiency of charge collection depends on the amount of charge produced. In Fig. 4.10 a plot of the collection efficiency and the collected charge as a function of the charge produced by a single x-ray pulse is shown for the parameters related to our monitor chamber, namely $V = 700$ V, $d = 0.25$ cm and $Q_0 = (\text{Coulomb})/(21.6\ \text{cm}^3)$.

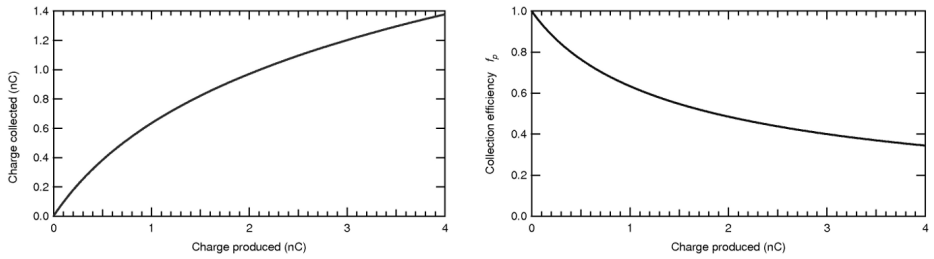

Figure 4.10: *(left)* Plot of the charge collected by the ionization chamber as a function of the charge produced; *(right)* Plot of collection efficiency as a function of the charge produced.

As it is possible to notice, the relation between the charge produced and the charge collected ceases to be linear for values larger than about 0.3 nC, and the collection efficiency is about 0.5 for the expected value of charge produced by each pulse of 2.3 nC. It must be underlined that these evaluations are based on an approximate and simplified model. For these reasons the use of the ionization chamber is intended to be aimed to a relative monitoring of the x-ray yield, in order to check the shot-to-shot repeatability of the source more than an absolute flux measurement. Nonetheless, if the collected charge variations from shot-to-shot are reasonably small, allowing to consider a linear approximation of the response function, then the values resulting from monitor results can also be used to rescale experimental results. In order to perform an absolute measurement of the photon number on each pulse (or the photon flux) an appropriate device should be used. In the next section (see Sec. 4.3) the description of those devices, as the tests and calibration performed, will be described in detail.

4.3 Flux measurement

In order to perform an evaluation of the photon flux of the x-ray beam a device showing the following characteristics is needed:

- High dynamic range, allowing the measurement of low flux level for the commissioning of the source as well as of high instantaneous flux for a full characterization after the commissioning;
- linear response;
- efficiency;
- accuracy.

This device would be fundamental both in the full characterization of the x-ray beam and also during the collision alignment, synchronization and source commissioning. The use of traditional photon counting (spectroscopic) techniques based on the detection of single photons, both using scintillator-photomultiplier systems or solid-state devices, is not feasible due to the ultrashort duration of the each x-ray pulse (about 10 ps). In fact, detectors able to operate with sub-picosecond time for signal generation and acquisition are not available at the current state of art. Therefore a way to measure the number of photons for each x-ray pulse is to measure an integral quantity, as the energy released in a medium per pulse, and extract the photon number using the knowledge of the energy distribution. A simple and reliable device that can be used for this task is a silicon PIN diode. This devices show optimal features in terms of linearity, high dynamic range and accuracy, are compact and do not require high voltage suppliers. In the next sections the basic principles of this technique will be described (Sec. 4.3) as well as the tests and calibration performed (Sec. 4.3.1 and 4.3.2). In Sec. 4.3.3 are described the possible issues that may occur when the instantaneous flux is extremely high as in the case of SL-Thomson source, as well as the test of this device with pulsed sources to evaluate these effects. To overcome this issue, an alternative detector suitable for high intensity pulsed radiation was realized and tested, as described in Sec. 4.3.4.

Measurement of x-ray flux using a silicon PIN diode

When an ionizing radiation impinges on a silicon diode based on a p-n junction the number of electron-hole couples is proportional to the energy released by the incident radiation in the active area, corresponding to the depletion area of the junction. The detector efficiency, that is the probability p of interaction of radiation with a certain energy in the silicon, depends on the thickness of the depletion region t as $p \propto e^{-\mu t}$. In order to increase the efficiency and to prevent rapid recombination of the electronhole pairs, two

methods are generally considered: the application of a reverse bias voltage to the diode, which has the effect of increasing the thickness of the depletion region in the junction, or the use of a PIN diode. A PIN diode is made of a large intrinsic silicon i layer, containing no added impurities, placed between the p and n regions (see Fig. 4.11). Any charge carrier formed in this region moves across the junction, resulting in a photocurrent. This device can be seen as a traditional $p-n$ junction in which the depletion layer is extended on the whole intrinsic silicon layer. In this intrinsic layer direct recombination of electron-hole pairs is a forbidden process in indirect band-gap semiconductors such as silicon, and it must be assisted by a lattice vibration to conserve momentum. Actually, the fastest way for electrons and holes to recombine is at defect sites in the silicon crystal lattice. Thus, a high-quality silicon PIN diode should exhibit a small, or ideally zero, charge carrier recombination [81].

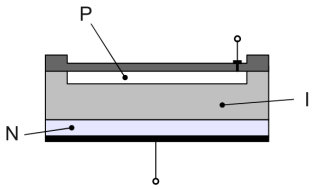

Figure 4.11: Drawing of a PIN diode configuration.

The current produced in a PIN diode by an x-ray beam is proportional to the rate of energy released in the diode active area by the radiation. The rate of energy released in a silicon slab depends on the incident photon energies and the flux. Owen *et al.* [82, 83] demonstrate that it is possible to evaluate the flux of a monochromatic x-ray beam impinging on a silicon PIN diode by measuring the photon induced current, that can be calculated using a simple model for energy deposition. In the case of monochromatic radiation with energy $E = h\nu$, provided that diode has a linear response, the ratio R of incident photon flux φ (ph/s) to the photocurrent i (Ampere) will be a constant and can be calculated considering a simple model of energy absorbed by silicon as [82]:

$$R = \frac{\varphi}{i} = \frac{\epsilon}{eE\left(1 - e^{-\mu_{ph} t_{Si} \rho_{Si}}\right)} \tag{4.4}$$

where ϵ is the average energy required for the production of a electron-hole pair in silicon (equal to 3.66 eV [81]), e is the electron charge, μ_{Si} is the photoelectric cross section of silicon for x-ray with an energy E, t_{Si} and ρ_{Si} are the thickness and the density of the silicon layer. Thus, by knowing the energy of the incident photon beam is possible to obtain the flux multiplying the current produced by a calibration coefficient R that can be

calculated from a theoretical model of energy absorption in the silicon layer or, alternatively, measured with a calibration monochromatic source with known flux and energy. As suggested by M. Krumrey [83], a more accurate way to calculate the energy absorption by the silicon interacting with the radiation would have been to use the energy absorption coefficient μ_{en} instead of the total deposition of photon energy weighted by the probability of a photoelectric interaction as made in eq. (4.4). However a calculation using both methods was done and the ratio between the result obtained with Owen approximation and with energy absorption coefficient μ_{en} is shown in Fig. 4.12 as a function of the incident photon energy.

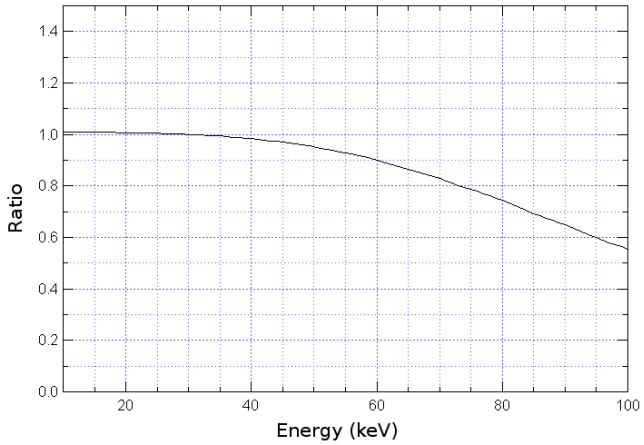

Figure 4.12: Ratio between the diode signal calculated considering energy deposition as proposed by Owen *et.al* [82] and using energy absorption coefficient μ_{en} as proposed by Krumrey [83].

It is possible to notice that in the energy range of interest, namely from 15 to 25 keV, the discrepancy is smaller than 1 %. Thus, Owen *et al.* approximation can be considered valid, provided that photon energy is not too high.

4.3.1 PIN diode device characterization and test

The PIN diode used is an Hamamatsu mod. S3584-09 silicon PIN diode. The active area surface is 28 x 28 cm^3, the depletion area thickness is 0.3 mm and the maximum reverse voltage applicable is 100 V (70 V recommended) [84].

The diode has been mounted in a metallic box provided with an entrance window made of an aluminum-coated polymide film to avoid photocurrent production by visible light. The x-ray absorption of this window is negligible in the energy range of interest. All the applications tested and described in the following sections were made operating in photovoltaic mode (*i.e.* without applying a reverse polarization). The connectors installed in the

metallic box have been designed to allow the polarization of diode and an additional box, that can be connected with the principal one, was realized to permit the insertion of a capacitor for voltage stabilization and a resistor to avoid short-circuit breakdown damages, in case of need when applying a polarization. Figure 4.13 shows a picture of the diode box and its cover (on the left) and the additional box for polarization circuitry.

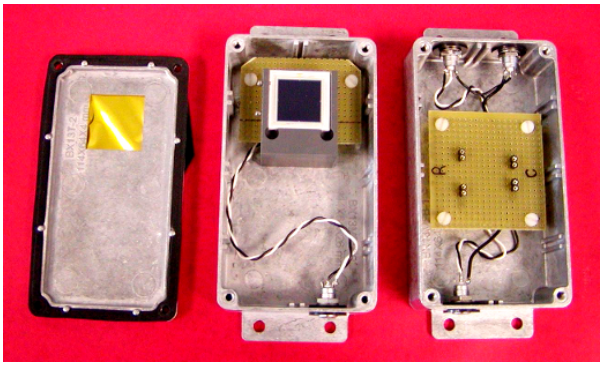

Figure 4.13: Picture of the PIN diode device. PIN diode box and cover, center and left respectively and additional circuitry for polarization box in the right.

The signal produced during the exposure (charge or current) was measured by an electrometer Keithley mod. 6517B (Keithley Instruments Inc., Ohio, US). This electrometer, as well as the acquisition software, are the same used for the monitor ionization chamber, described in Section 4.2.1.

Figure 4.14 shows a simplified model of a diode during an irradiation, it can be modeled as a current generator with a internal resistance in series R_S and a shunt resistance R_{Sh} connected in parallel. The shunt resistance implies that the current produced is split between the shunt branch and the load branch of the circuit, *i.e* the one connected to the electrometer in this case.

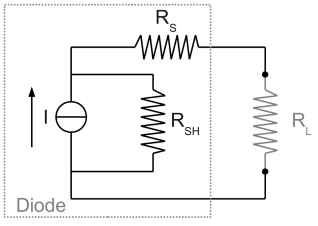

Figure 4.14: Simplified equivalent circuit of an irradiated diode.

For this reason, in order to avoid an underestimation of the current acquired, it is necessary that R_L is much smaller than R_{SH}. Shunt resistance was calculated applying a reverse voltage of 10 mV and measuring the inverse

current, resulting in $R_{SH} = 55$ MΩ. The inverse current with no polarization applied, as in the case of our application, is always smaller than 1 ps. A plot of the variations of inverse current with respect to the voltage applied is shown in Fig. 4.15.

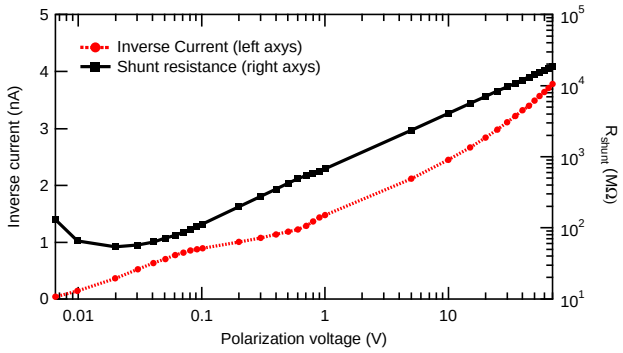

Figure 4.15: Plot of measurement of inverse current (*left axis*) and relative shunt resistance of PIN diode (*right axis*), as a function of the inverse polarization applied.

Following the evaluation of the diode shunt resistance, an evaluation of the input resistance of the electrometer was performed. In order to carry out this measurement the experimental apparatus used is sketched in Fig. 4.16.

With this configuration a fixed voltage was applied to a 500 MΩ resistor linked in series with a resistor R_L and the input of electrometer with its characteristic resistance R_K. The voltages applied were 20 mV and 5.0 V, in order to investigate two different current ranges (20 pA and 20 nA max), for each voltage a measurement was made with $R_L = \infty$ and $R_L = 10M\Omega$. The results of the current measured in the different configurations are reported in Table 4.3. As it is possible to notice, in the first case (lower current), the current is underestimated of about the 3%, while in the case of 20 nA maximum-range the current is accurate at least at the 0.1 %. Considering that the actual shunt resistance is bigger than 50 MΩ it is

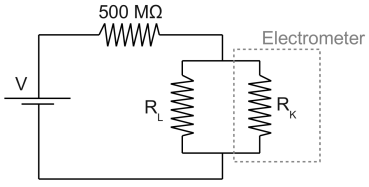

Figure 4.16: Sketch of the experimental setup to measure electrometer internal resistance effect resulting in a possible current underestimation.

Table 4.3: Results of current measurements for the evaluation of a possible underestimation due to internal resistance of the electrometer.

Range 20 pA (V = 20 mV)	
R_L (MΩ)	Measured current (pA)
∞	23.7
10	31.8
Range 20 nA (V = 5.0 V)	
R_L (MΩ)	Measured current (nA)
∞	10.025
10	10.025

possible to conclude that the underestimation of the acquired currents due to this effect will be negligible ($< 1\%$) in this application.

4.3.2 PIN diode calibration with monochromatic x-rays

The ratio R of the current produced in the PIN diode and the incident flux of monochromatic photons can be calculated using the theoretical model of energy deposition as previously described, see Eq. (4.4). This evaluation requires an accurate knowledge of the depletion layer thickness and the photoelectric cross section. The effective thickness of the depletion layer has been measured as described in the following and the cross section can be found in established database such as *Xcom, photon cross section database* [85]. However, the theoretical model includes some assumptions on the released energy and the creation and collection of charge carriers, in addition to possible errors on the evaluation of thickness or cross section, that imply a necessary experimental verification of the calculated calibration coefficient. For these reasons the system was tested at the SYRMEP beamline [86] of ELETTRA synchrotron facility (Trieste, Italy), with monochromatic x-rays in the energy range between 16 and 24 keV. The diode response has been calibrated for monochromatic beams, by measuring simultaneously the photocurrent produced in diode and the incident x-ray flux evaluated using the air-dose value provided by two independent free-air ionization chambers: the monitor chamber realized for BEATS2 experiment and the in-house monitor chamber at SYRMEP beamline.

A sketch of the experimental setup is shown in Fig. 4.17. As it is possible to notice, the x-ray beam after a collimation pass through the two ionization chamber and impinges on the PIN diode system. The CCD camera imaging system was used in order to check the collimation and positioning of the beam and to measure the size of the irradiated area ($\phi = 5.0$ mm on diode surface).

In order to scan different values of photon flux, for each energy (16, 18, 20, 22 and 24 keV) the beam has been filtered with aluminum thickness

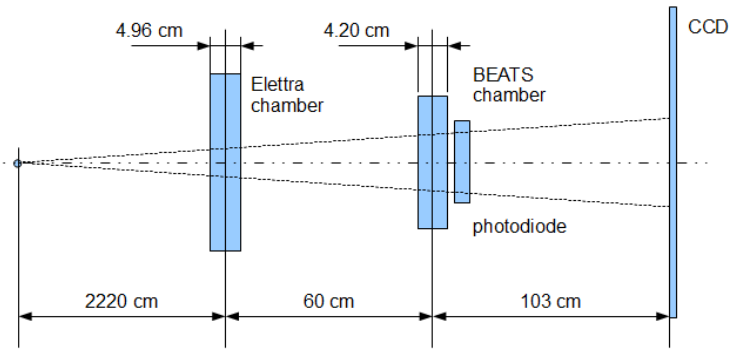

Figure 4.17: Sketch of the experimental setup for PIN diode system calibration at ELETTRA synchrotron facility.

varying from 0 to 6 mm. For each beam energy considered, the photon flux was calculated for the various values of aluminum filtration and plotted as a function of the diode current. A plot for the energy equal to 16 keV is shown in Fig. 4.18. A linear fit was then performed on these data sets, where the slope obtained represent the R calibration coefficient at that energy. The filtration thicknesses used and the dynamic range of the detectors allowed to scan a range of fluxes going approximatively from 10^7 to 10^9 ph/s, corresponding to diode current in the range from tens of picoamperes to hundreds of nanoampere.

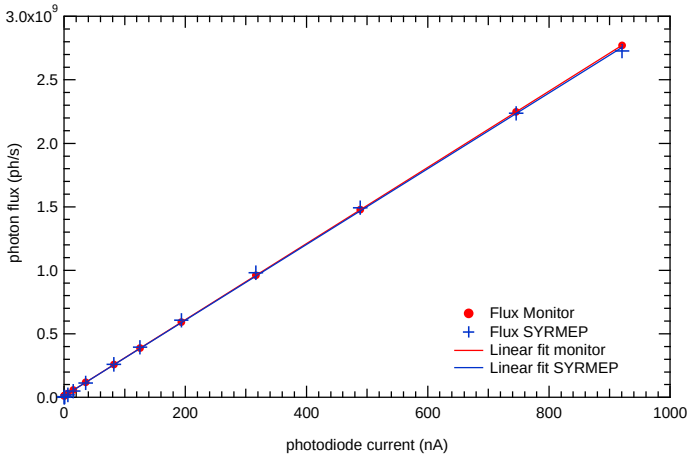

Figure 4.18: Plot of the flux calculated from SYRMEP chamber (*blue crosses*) and BEATS2 monitor chamber (*red dots*) as a function of diode current acquired. Solid lines are the result of linear fits.

As it is possible to see in Fig. 4.18, two different linear fit were made

Table 4.4: Results of diode calibration coefficients, measured at ELETTRA synchrotron facility R and evaluated from the theoretical model R_T, see Eq. (4.4).

E (keV)	R (ph/C)	R_T (ph/C)	Ratio (R_T/R)
16	$(2.99 \pm 0.09) \times 10^{15}$	3.04×10^{15}	1.02
18	$(3.43 \pm 0.10) \times 10^{15}$	3.56×10^{15}	1.04
20	$(4.14 \pm 0.12) \times 10^{15}$	4.18×10^{15}	1.01
22	$(4.79 \pm 0.14) \times 10^{15}$	4.91×10^{15}	1.03
24	$(5.50 \pm 0.16) \times 10^{15}$	5.73×10^{15}	1.04

with the two set of data obtained evaluating the flux with BEATS ionization chamber and with the SYRMEP one. Since the calibration coefficients obtained in the two cases differs of a few percents at maximum, a final value has been calculated as the average value of the two and the discrepancy was taken into account in the uncertainty evaluation. The final measured calibration coefficients R used to convert the current produced in the diode to the flux are shown in Table 4.4. In the same table are also reported the results predicted by the theoretical model R_T, see eq. (4.4), using a thickness of 0.33 mm and the values of μ_{ph} obtained from *Xcom, photon cross section database* [85].

As it possible to notice, the theoretical model is in good agreement with the measured values, allowing to use eq. (4.4) to interpolate these sets of experimental data for energies different from the measured ones. Moreover, this also permits to predict the diode response to any arbitrary photon energy distribution, and therefore also to measure the flux in the application to quasi-monochromatic source as the SL-Thomson, whether the radiation spectrum is known.

Diode active-layer thickness evaluation

The thickness of the active layer was obtained by measuring the current produced in the diode varying the angle θ made by the normal direction of the diode surface plan and the incident x-ray beam direction. In fact, in this way, it is possible to obtain the thickness t of the active area fitting with a function:

$$\frac{I(\theta)}{I(\phi)} = 1 - \exp\left[\frac{-\mu t}{cos(\theta + \phi)}\right] \tag{4.5}$$

which takes into account the change in the probability of interaction due to the increase of silicon thickness crossed by the beam, in which ϕ is the nominal angle corresponding to a perpendicular incidence and μ is the linear absorption coefficient of silicon at that energy. By carrying out a set

of measurements at various tilt angles and different energies it is the possible to obtain a value for the effective thickness.

Measurements of photocurrent were made varying the angle of the incident beam of about 100 degrees while irradiating the diode at two different beam energies: 16 and 22 keV. In figure 4.19 and 4.20 the results of the measurements and fit with (4.5) are shown for these two energies. In order to perform the fit, the value of linear absorption coefficient was taken from *Xmudat software* [87, 88] and the result for both the energies lead to the evaluation of an effective thickness $t = 0.33$ mm.

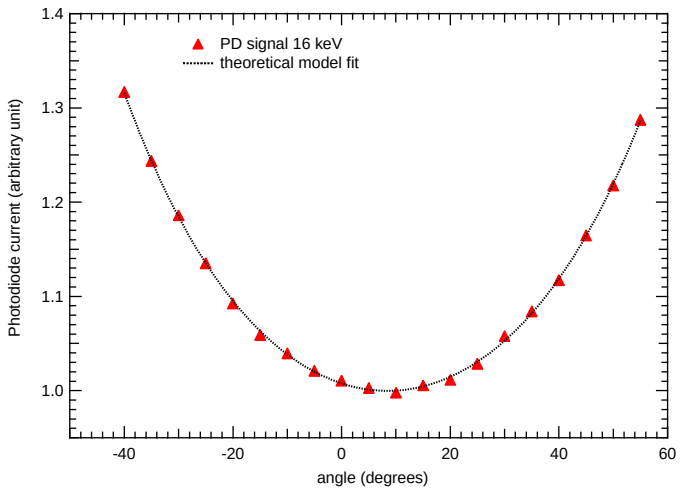

Figure 4.19: Plot of the signal produced in the PIN diode system as a function of the rotation angle of the incident beam with an energy of 16 keV.

4.3.3 Pulsed radiation issue

PIN diode have been proved to work properly as flux measurement detectors for fluxes up to 10^{12} ph/s in condition of continuous irradiation [82].

In the case of ultrashort pulsed source, such as SL-Thomson, high instantaneous fluxes, orders of magnitude larger than 10^{21} ph/s, could produce in the diode a charge density extremely high, leading to charge recombination and partial collection of charge, resulting in an underestimation of the real number of interacting photons.

In order to evaluate this effect an experimental study of diode response to ultrashort pulses was performed and the study of complementary techniques for flux measurements was carried out.

X-ray sources with energy distribution, instantaneous fluxes and temporal structure comparable to those of the SL-Thomson source were not available, for this reason the test has been made using a pulsed laser beam provided by Laboratories of the Istituto Nazionale di Ottica (INO)-CNR,

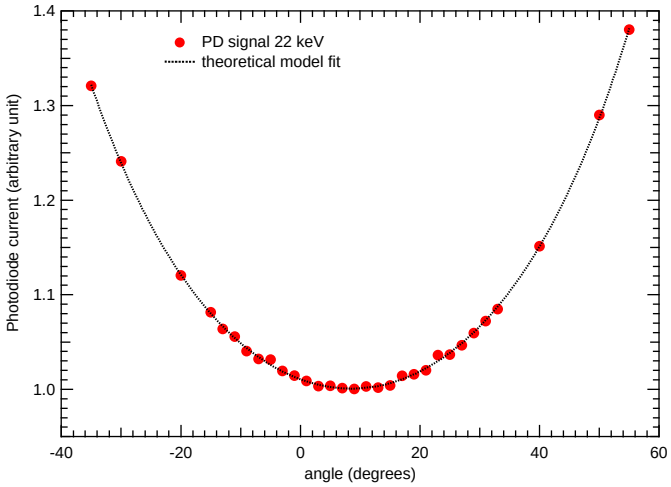

Figure 4.20: Plot of the signal produced in the PIN diode system as a function of the rotation angle of the incident beam with an energy of 22 keV.

(Pisa) [89]. This laser has a wavelength of 800 nm and a pulse duration that can be adjusted in the range from 45 fs to 30 ps. The silicon PIN diodes used for this study are the Hamamatsu mod. S3584-09 with an active area 28×28 mm^2 window-less, previously described in Sec. 4.3.1, and the Hamamatsu mod. S3204-08, that is identical to the former but with a smaller active area equal to 18×18 mm^2 (instead of 28×28 mm^2), and a epoxy resin window material.

The energy of the laser pulse was measured resulting in (0.26 ± 0.03) μJ. The cross-section area of the beam was about 20 x 10 mm^2, entirely included in the active region of the bigger diode (mod. S3584-09) and compatible with the size of the BEATS2 x-ray beam of 25 x 25 mm^2. In the case of smaller diode (mod. S3204-08) the laser was collimated to match the size of the sensitive area, resulting in an incident pulse energy of (0.14 ± 0.02) μJ.

Considering the nominal response of each diode for an incident wavelength equal to 800 nm, it has been possible to calculate the expected charge produced in the diodes using the measured pulse energy. In the case of the bigger PIN diode the nominal energy response is 0.58 A/W (or C/J) that results in a charge of (153 $\pm$19) nC produced for each pulse. In the case of the smaller diode the energy response is 0.56 A/W, due to the epoxy resin layer and the smaller area of active surface leads to a resulting charge expected of (82 $\pm$10) nC.

The expected charge produced by an x-ray pulse of BEATS2 experiment (about 3.5×10^9 photons with a mean energy of 20 keV) will be about 750 nC which is almost 5 times bigger. Nonetheless, what we need to consider is the spatial density of the charge produced instead of the total charge itself,

Table 4.5: Results of charge collected for different pulse durations, ranging from 45 fs to 30 ps.

Pulse duration (fs)	Average collected charge (nC)	Stand. deviation (nC)
45	8.80	0.95
120	8.32	0.89
525	9.14	0.98
900	9.22	0.99
30000	8.63	0.93

the interaction length in silicon is about 11 μm for photons at a wavelength of 800 nm and 960 μm in the case of 20 keV x-rays. For this reason it is possible to consider that in the case of laser the whole charge will be produced in the first 11 μm of the silicon layer, while in the case of x-rays the charge will be uniformly produced over the whole 330 μm of the active silicon layer (see Fig. 4.21). Thus, the spatial density of charge produced with the laser pulse described is expected to be about 6.7 times larger than the one produced by a BEATS2 x-ray pulse.

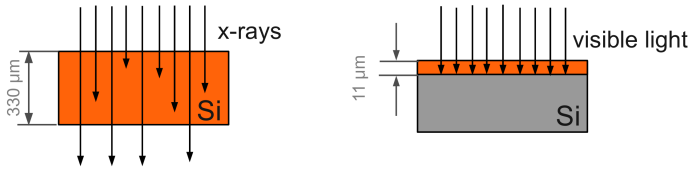

Figure 4.21: Thickness involved in signal production in the case of x-rays (20 keV) and in the case of light at 800 nm.

A first test was made in order to check a possible variation of the charge produced as a function of the time duration of pulses. For this reason the diode was irradiated with pulses of durations varying from 45 fs to 30 ps and the average charge produced was measured for 10 pulses at each time duration value. In Table 4.5 a summary of the results obtained irradiating the small diode (mod. S3204-08) is shown.

As expected there is not a noticeable correlation between the pulse duration and the charge collected in this interval of pulse durations. This is due to the fact that the time scale for charge collection in the diodes is on the order of hundreds of nanoseconds, therefore it is not sensitive to variations of the time of charge production in the femtoseconds/picoseconds time scale.

A signature of the fact that the diode device is not properly operating is that the average charge collected is 8.8 nC, about 1/10 of what is expected (82 nC), considering the pulse energy and wavelength and the diode efficiency. In addition to this, the shape of the signal acquired connecting the diode directly to an oscilloscope appears to be distorted compared to the response to a lower energy pulse, see Fig. 4.22 . As it possible to notice

Table 4.6: Values of filter transmission used to attenuate the laser pulse and corresponding pulse energies otained.

Transmission	Pulse energy (J)
1.00	2.64×10^{-7}
9.00×10^{-2}	2.38×10^{-8}
8.90×10^{-3}	2.35×10^{-9}
1.25×10^{-3}	3.30×10^{-10}

the signal does not show an exponential decay as expected (τ of about 300 ns for a negative exponential function fit) but the decrease is different and significantly slower, with a total duration longer than 4 μs.

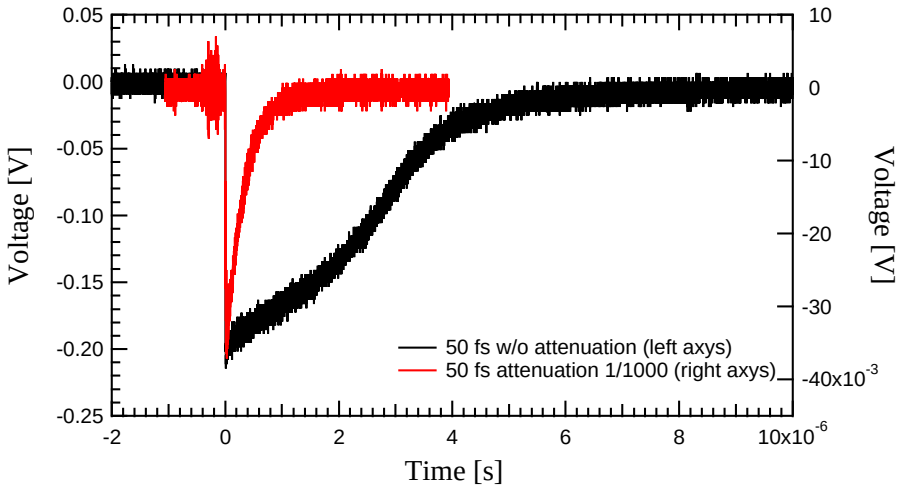

Figure 4.22: Comparison of signal shape in the case of a 50 fs light pulse with an energy of 0.26 μJ (*solid black line, left axis*) and in the case of an attenuation 1/1000 (*solid red line, right axis).*

After having verified that a *saturation* effect is present for pulses with energy of 0.26 μJ and 0.14 μJ for the 28×28 mm^2 and 18×18 mm^2 diode respectively, a test to analyze the response to decreasing energies of the pulses was made by filtering the laser beam with optical attenuators. The values of filter transmission used and the corresponding pulse energies are reported in Table 4.6.

For each value of transmission several measures of the charge produced in the diodes were performed, also varying the pulse duration. As previously shown, the time duration of pulse does not affect the collected charge, while the fraction of collected charge increases as the pulse energy decreases.

In figure 4.23 are shown two graphs representing the charge collected in the case of the 28×28 mm^2 diode for pulse duration of 30 ps and in the case

of 18×18 mm^2 for pulses 50 fs long. In the same graph it is also plotted the expected theoretical value of charge produced (*solid red line*), as it is possible to notice the collected charge corresponds to the charge that is expected to be produced only in the case of the transmission equal to 1.25×10^{-3}, *i.e.* for the lowest pulse energy measured. Unfortunately smaller values of transmission could not be obtained due to the slightly high background signal coming from inevitable light sources in the laser experimental room.

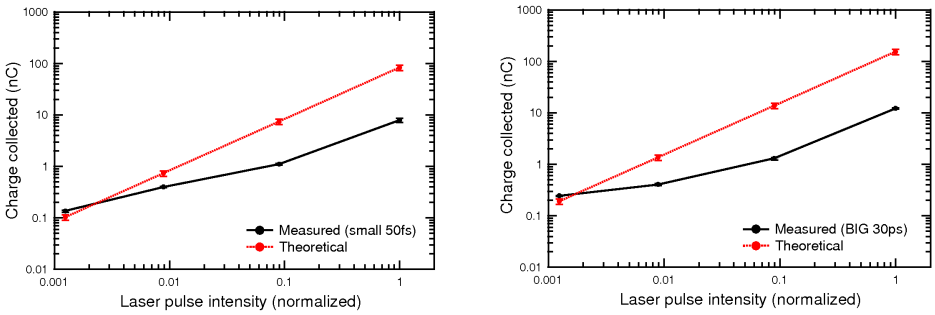

Figure 4.23: Plot of the collected charge as a function of the laser pulse energy. On the left the signal for the 18×18 mm^2 diode (*solid black line* and the expected theoretical one (*solid red line*).

Figure 4.24 represents an alternative way to see the previous results, where the fraction of collected charge is plotted as a function of the laser pulse energy, assuming that, for the maximum value of attenuation, this fraction was equal to one.

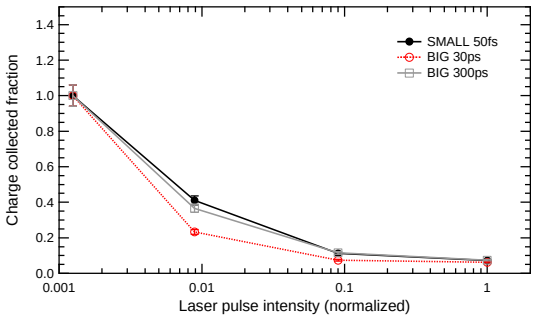

Figure 4.24: Fraction of charge collected with respect to the theoretical charge produced for the two different diodes and different pulse durations.

Even taking into account the differences between an irradiation of the diode with x-rays and the one using visible light, it is worth noting that for values of spatial and temporal charge density comparable to the one to be produced in BEATS2 experiment a partial collection effect will probably occur, thus leading to a flux underestimation. In order to verify at any moment the proper operation of the detector, it will be possible to filter the beam

with a set of known thicknesses of a selected material and then compare the trend of filtered signals with the expected one. A deviation from a linear response is the signal that a saturation effect is occurring. Furthermore a cross-check comparison can be made with the measures results from other detectors, as the monitor ionization chamber.

The result of this test showed that this PIN diode device could be not reliable for direct flux measurements on the commissioned SL-Thomson source. However, this device will permit to detect a very low number of photons per pulse, namely 10^3-10^4, and maintain a linear response up to 10^5-10^6 ph/pulse, so it will be useful during the source commissioning, especially for synchronization and collision alignment, where the presence and number of photon emitted is an important signature of correct operation.

In the following section an alternative system for the photon flux evaluation that will permit to avoid this saturation effect is described.

4.3.4 Crystal-diode system calibration

The reason for the loss of linearity of the diode detector described in previous section is the high temporal and spatial density of charge produced in the diode by each x-ray pulse. This high density leads to distortion of the collecting field and electron-hole recombination resulting in a underestimation of the signal and then a non-linear response. In order to avoid this effect, using the same silicon PIN diode detector, it would be enough to reduce suitably the temporal density of charge produced, *i.e.* increase the pulse length and consequently the charge production time.

The maximum repetition rate for SL-Thomson is 10 Hz, so there are not strict time constraint on the production and acquisition of signal, provided that the duration of this operation is less than 100 ms. Inorganic scintillator crystal like CsI:Tl with relatively slow scintillation decay (about 1 μs) and no evidence for linearity loss at high dose-rates, can be used to increase the duration of charge production in the silicon diode. Instead of using the direct interaction of radiation in the diode active layer, it is possible to make the x-rays interact in a slow scintillator crystal coupled to the diode that indirectly detects the light produced. For this reason a 2 mm-thick CsI:Tl crystal was optically coupled with the active surface of a silicon PIN diode Hamamatsu mod. S3204-08 (active area 18×18 mm^2, epoxy resin window). The transmission of this thickness of CsI is negligible for photons with energy in the range of interest (up to 30 keV), so it is possible to consider that no direct interactions will occur in diode active volume. In order to calibrate the response of the diode-crystal system its signal was compared to the one obtained with the PIN diode without the crystal previously calibrated at ELETTRA synchrotron facility as described above. Both the devices where irradiated simultaneously at Larix laboratories of Ferrara University using a quasi-monochromatic x-ray source. The signal from the direct interaction in

the silicon diode previously calibrated (see Sec. 4.3.2) was used to measure the flux and then inter-calibrate the response of diode-crystal system.

The quasi-monochromatic source used (see Fig. 4.25) is based on Bragg diffraction by mosaic crystal of the x-rays produced by a W-anode traditional tube and can provide x-ray beams with tunable average energy in the range between 15 and 30 keV with an energy spread Δ E/E = 10% [90].

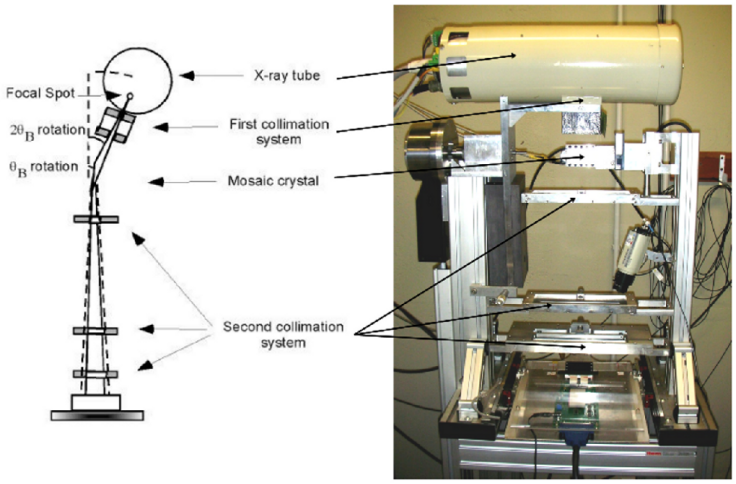

Figure 4.25: Sketch and picture of the quasi-monochromatic system operating at Larix-B, Ferrara University. The beam produced by a traditional W-anode x-ray tube is collimated and impinges on pyrolitic graphite mosaic crystal at an angle θ. Both the tube and the crystal are mounted on two co-axial remote controlled rotators in a θ-2θ geometry. The diffracted quasi-monochromatic beam is then further collimated resulting in a rectangular beam of size 15×240 mm^2.

The response of PIN diodes irradiated directly and coupled with a 2 mm-thick CsI(Tl) was measured for x-ray beams with an average energy in the range 16-24 keV, namely 16, 18, 20, 22 and 24.

In Fig. 4.26 a plot of the energy distribution of x-ray beams used for this measurement is reported. For each energy value various acquisition were performed changing the anodic current of the x-ray tube, that is changing the incident x-ray flux. This calibration permitted to evaluate the coefficients $R_{crystal}$ that relate the current produced in the diode-crystal system with the flux (or the charge produced with the number of photons) of the incident x-ray radiation. The results for the measured coefficient $R_{crystal}$ are shown in Table 4.7, compared to those obtained for the direct exposure of silicon PIN diode without scintillator crystal.

As it is possible to notice from the comparison to the direct diode detector, the values are almost the same at high energies, while the crystal-diode system is slightly less efficient at lower energies. Anyway, the values ob-

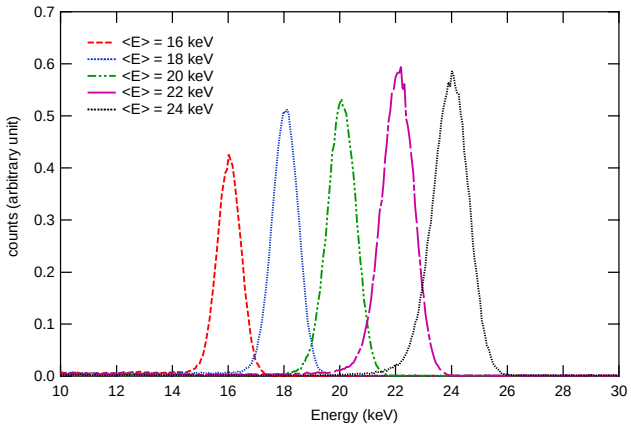

Figure 4.26: Measured spectra provided by the tunable, quasi-monochromatic source at Larix Laboratories, Ferrara University, measurements performed with a CZT solid state detector Amptek mod. XR-100T (Amptek, MA, USA).

Table 4.7: Diode calibration coefficients measured at synchrotron facility R, and diode-crystal system coefficients $R_{crystal}$ resulting from the inter-calibration with the former.

E (keV)	R (ph/C)	$R_{crystal}$ (ph/C)	Ratio
16	$2.99\pm0.09 \times 10^{15}$	$8.77\pm0.27 \times 10^{15}$	2.92
18	$3.43\pm0.10 \times 10^{15}$	$7.30\pm0.21 \times 10^{15}$	2.13
20	$4.14\pm0.12 \times 10^{15}$	$6.45\pm0.19 \times 10^{15}$	1.56
22	$4.79\pm0.14 \times 10^{15}$	$5.87\pm0.17 \times 10^{15}$	1.17
24	$5.50\pm0.16 \times 10^{15}$	$5.68\pm0.17 \times 10^{15}$	1.03

tained with this calibration showed that this system is compatible with the application on the BEATS2 experiment flux measurement.

4.4 Energy distribution evaluation

The knowledge of the energy distribution of the x-ray beam produced by SL-Thomson source is crucial for the study and development of its applications. Furthermore, the energy spectrum of emitted photons is also an important signature of the correct operation of apparatus, showing that the energy and focusing of the electron and laser beam are properly set, as well as the alignment of the collision.
The use of traditional spectroscopic techniques based on single-photon detection, made by either scintillator-photomultiplier combination or a solid state device, is very difficult because of the extremely high instantaneous flux produced by the source. Even if new developments both in the hardware and the software analysis may permit to reach very high photon counting-rates [91, 92], with this kind of detectors it is not feasible to operate with sub-picosecond data acquisition time. Therefore, a way to obtain information on the energy spectrum is to extract them from the measurement of an integral quantity, such as the total energy released in a medium by each pulse of photons produced by the source.
Several techniques have been proposed in order to retrieve the photon energy distribution from dose measurements of filtered beam with various absorbing materials and thicknesses. Usually this techniques imply transmission measurements and computational reconstruction of the incident spectra [93–95], or imaging of filtered beams for the evaluation of photon energy distribution correlated with position [35, 96]. The technique we proposed to use for BEATS2 x-ray beam, that will be described in the following, is somehow similar because filtration with x-ray absorbing materials is used; the difference lies in the fact that inverse-problem computation or reconstruction approach are not needed, but the information on photon energy is obtained using discontinuity in the attenuation coefficient due to photoelectric K-edge of the absorbing materials [97]. The proposed technique, described in detail in Sec. 4.4.1, has also been tested by evaluating the spectrum of a x-ray beam similar to the one expected to be produced at SPARC-LAB. A description of the experimental setup and methods will be given in Sec. 4.4.2, as well as the comparison of results obtained with this technique and using traditional spectroscopy detector (HPGe).

4.4.1 K-edge subtraction technique

Consider the energy spectrum $\varphi(E)$ of a photon beam as the distribution of the photon flux as a function of the photon energy.
The total photon flux φ, defined as $[photons/second]$ will be given by the

integration of spectrum over the whole energy range [E_{min},E_{max}] :

$$\varphi = \int_{E_{min}}^{E_{max}} \varphi(E)\mathrm{d}E$$

As previously mentioned, it is possible to obtain an evaluation of the energy spectrum of an x-ray beam by measuring x-ray fluxes transmitted by appropriate k-edge absorbing foils.
In particular, consider $\varphi(E)$ to be the energy distribution that needs to be evaluated.

If the photon beam is filtered with a material with no K-edge in the energy range of interest [E_{min},E_{max}], having an attenuation coefficient $\mu_f(E)$ and a thickness t, the transmitted photon flux φ_f will be:

$$\varphi_f = \int_{E_{min}}^{E_{max}} \varphi(E)e^{-\mu(E)_f t_f}\,\mathrm{d}E \tag{4.6}$$

Let us consider now a set of materials having photoelectric K-edge at energy E_{K_i} within the interval [E_{min},E_{max}] with attenuation coefficients $\mu_{K_i}(E)$ and thicknesses t_{K_i} chosen in such a way they satisfy the following conditions:

1. the thickness t_{k_i} of each k-edge filter has to be chosen in such a way that the absorption of all the filters have to be equal to the absorption of the filter without k-edge, up to the corresponding k-edge energy E_{k_i} of each filter:

$$\mu_f(E)t_f = \mu_{k_i}(E)t_{k_i} \text{ if } E_{min} \leq\ E \leq\ E_{k_i}\ ; \tag{4.7}$$

2. the k-edge filters transmission has to be negligible for photons having energies above the k-edge:

$$e^{-\mu_{k_i}(E)t_{k_i}} \approx 0 \text{ if } E > E_{k_i}\ . \tag{4.8}$$

When conditions (4.7) and (4.8) are satisfied, it is possible to demonstrate that the subtraction of total fluxes of two filtered x-ray beams φ_f and φ_{k_1} will be:

$$\varphi_f - \varphi_{k_1} = \int_{E_{k_1}}^{E_{max}} \varphi(E)e^{-\mu_f t_f} \tag{4.9}$$

This means that the difference of total fluxes is equal to the flux of photons with energies higher than E_{k_1} in the beam filtered with no k-edge. Lets now consider two k-edge filters with k-edge at energies $E_{k_1} < E_{k_2}$, both within the range [E_{min},E_{max}] and thicknesses t_1 and t_2, similarly to the previous case, if conditions (4.8) and (4.7) are satisfied, it is straightforward

to demonstrate that the subtraction of the total transmitted flux φ_{k_1} to φ_{k_2} is:

$$\varphi_{k_2} - \varphi_{k_1} \cong \int_{E_{k_1}}^{E_{k_2}} \varphi(E) e^{-\mu_f(E) t_f} \, \mathrm{d}E \tag{4.10}$$

Equation (4.10) shows that the difference between the total fluxes transmitted by two different k-edge absorbers is equal to the photon flux $\varphi_f(E_{k_2} : E_{k_1})$ transmitted from the filter with no k-edge in the range of energy between the two $k-$edge energies E_{k_1} and E_{k_2} (See Fig. 1). To obtain the unfiltered (and sought) $\varphi(E_{k_2} : E_{k_1})$ from $\varphi_f(E_{k_2} - E_{k_1})$ is sufficient to take into account the attenuation of the filter with no k-edge:

$$\varphi(E_{k_2} - E_{k_1}) = \varphi_f(E_{k_2} - E_{k_1}) / e^{-\mu_f t_f}. \tag{4.11}$$

By reiterating this procedure for several suitable couples of k-edge absorbers it is possible to obtain the photon flux in various energy band defined by the k-edge energies, allowing a complete investigation of the energy interval of interest. So, by measuring the photon flux transmitted by properly chosen k-edge materials with a suitable detector, such as a silicon PIN diode, using subtractions of the signal obtained, it is possible to perform an evaluation of the energy distribution with a resolution that depends on the energies of k-edges used.

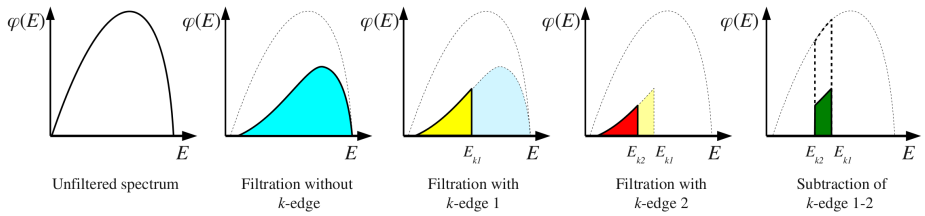

Figure 4.27: Schematic diagram of the k-edge subtraction technique.

4.4.2 K-edge subtraction technique experimental test

This technique has been developed in order to evaluate the spectrum of SL-Thomson source for BEATS2 experiment, previously described in Sec. 2.3.1, that in the case of the maximum angular acceptance is made by x-rays with energies ranging from 16 to 21 keV as shown in the expected spectrum reported in Fig. 4.28. In order to verify experimentally this technique an x-ray beam with an energy distribution comparable with the one expected is nedeed. To obtain this beam an x-ray tube with a tungsten anode (mod. GS 340 5, CGR, Paris, France) operating at 22 kVp with an added filtration

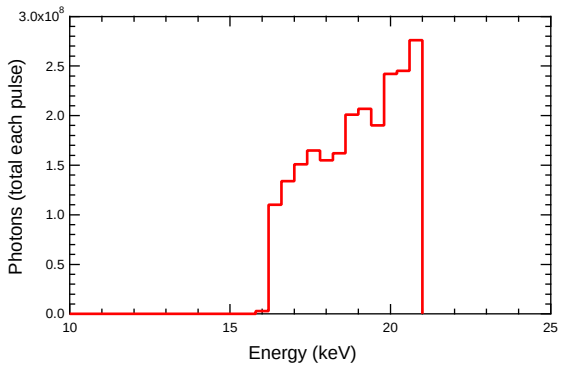

Figure 4.28: Simulated spectrum expected for BEATS2 experiment with SL-Thomson source. The energy distribution depends on the angular acceptance, solid black line refers to an angular semi-acceptance equal to 9.33 mrad.

of 3.10 mm of aluminum (Al) was used at Larix laboratories. A plot of the spectrum measured with an HPGe detector is shown in Fig. 4.31.

Choice of k-edge absorbers

In order to properly split the energy interval of interest, *i.e* from 16 to 22 keV, three k-edge absorber materials were chosen: molybdenum (Mo), niobium (Nb) and zirconium (Zr), having k-edge energies of 20, 19 and 18 keV, respectively. Aluminum (Al) was used as absorbing material without k-edge in the energy range of interest.

The tradeoff between a negligible transmission of x-rays with energies higher than the K-edge, that requires thick filters, and a significant transmission of photon up to the K-edge energy (in order to have a measurable flux) that requires thin filters, was achieved with the filter set having the characteristics reported in Table 4.8. Also, a plot of their expected transmission is shown in Fig. 4.29. As it can be seen, all filters have the same transmission for energies smaller that the respective k-edge, with maximum ranging from 0.18 for Zr to 0.29 for Mo. Also, for energies above the K-edge the transmission drops to values smaller than 0.003 up to 24 keV.

This filter set and subtractive analysis previously discussed allow us to extract information about the photon energy distribution of the x-ray beam transmitted by the Al filter $\varphi_{Al}(E)$ in four energy bins (see Table 4.9).

The information that is possible to obtain from the subtraction of fluxes measured with the PIN diode is the energy distribution $\varphi_{Al}(E)$ of the beam filtered with 1.30 mm of Al. In order to estimate the flux of the unfiltered

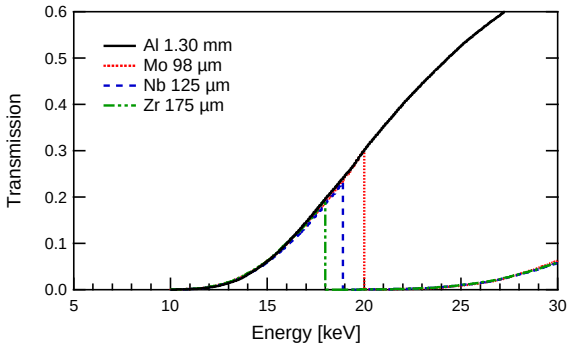

Figure 4.29: Expected transmission as a function of the energy, for the filters listed in Table 4.8. The linear attenuation coefficients $\mu(E)$ are taken from *Xmudat: Photon attenuation data on PC* [87] (database from Boone and Chavez [88]).

Table 4.8: Filters characteristics.

Material	K-edge energy (keV)	Thickness (μm)
Al	no K-edge	1300 $\pm$ 50
Zr	18	175 $\pm$ 2
Nb	19	125 $\pm$ 2
Mo	20	98 $\pm$ 2

Table 4.9: Flux subtractions scheme for energy distribution evaluation.

Energy bin	Flux information	Average energy (keV)
$\varphi_{Al}(< 18$ keV)	φ_{Zr}	17.0
φ_{Al}(18-19 keV)	φ_{Nb} - φ_{Zr}	18.5
φ_{Al}(19-20 keV)	φ_{Mo} - φ_{Nb}	19.5
$\varphi_{Al}(> 20$ keV)	φ_{Al} - φ_{Mo}	21.0

beam, the average energy of each bin is required to allow the calculation of Eq. (4.11). For the central bins (18-19 and 19-20 keV) the halfway energies, namely 18.5 keV and 19.5 keV, were used. For the other two energy bins ($E < 18$ keV and $E > 20$ keV) an *a priori* knowledge of the photon energy distribution is required. In the case of the SL-Thomson source this knowledge is provided by computational simulations and theoretical analysis of the physical process that give an estimation of the expected energy distribution of photons. Instead, in the case of this preliminary test of the technique, the choice of these energies was made taking into account the end-point energy of the spectra due to kilovoltage applied at the x-ray tube and the expected shape of the Al-filtered spectrum, resulting to be 17.0 for $E < 18$ keV region and 21.0 for $E > 20$ keV, as reported in Table 4.9.

Spectra measurement

A sketch of the experimental setup is shown in Fig. 4.30. The test x-ray beam is provided by a W-anode x-ray tube at 22kVp, with a 0.8 mm-thick Be window and an added filtration of 3.10 mm of Al. The x-ray tube power supplier is equipped with capacitors that provide a constant high-voltage. The voltage applied is measured and monitored using a high-voltage divider and a nominal value of the anodic current is provided by the control panel of the system. The spectroscopic detector is an HPGe detector Mod. GLP-25325/10-P (EG&C, ORTEC), with a measured $FWHM$ at 59.54 keV (Am-241) equal to 730 eV. The Ge crystal sensitive volume is 25 mm of diameter and 13 mm-thick, so it is possible to consider the efficiency equal to one in the whole energy range of our interest. This detector was placed at a distance of 156 cm from x-ray tube exit window. Discs of the materials listed in Tab. 4.8 (diameter = 2.5 cm) were mounted on a filter-wheel remotely controlled positioned along the x-ray beam-line. Several stage of collimation provide a circular beam of 3 mm of diameter on the detector. Each spectroscopic measurement was made using a nominal anodic current of 0.2 mA and an acquisition time of 600 s.

Flux measurement

As described in Sec. 4.3, by knowing the energy of the incident photon beam is possible to obtain the flux multiplying the current produced by a calibration coefficient R that can be calculated from a theoretical model of energy absorption in the silicon layer or, alternatively, measured using a monochromatic source with known flux and energy. The photocurrent produced during the exposure was measured by an electrometer Keithley mod. 6517B (Keithley Instruments Inc., Ohio, US). The PIN diode system was placed in the same position of the HPGe detector and, in order to obtain a significant signal, an anodic current of 40 mA and a larger circular

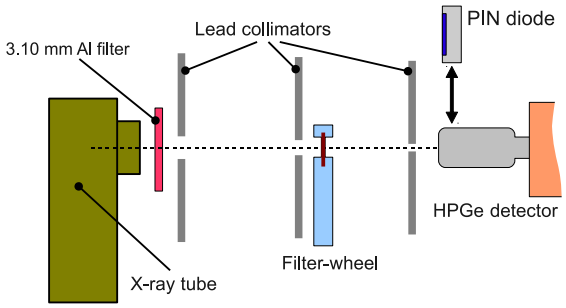

Figure 4.30: Sketch of the experimental setup for the test of the k-edge technique for energy distribution evaluation.

Table 4.10: Calibration coefficient K and corresponding photon average energy used for flux calculation in each energy bin.

Energy bin (keV)	Energy (keV)	K (ph/C)
<18	17	3.28×10^{15}
18-19	18.5	3.70×10^{15}
19-20	19.5	4.01×10^{15}
>20	21	4.53×10^{15}

collimation of the beam ($\phi = 6.2$ mm) were used.

K-edge subtraction

The difference between the diode currents produced by x-ray beams filtered by a couple of K-edge filters is proportional to the flux of the photons that lie in the energy range between the two K-edges energies. Thus, by knowing the calibration factor R at the average energy in this range, it is possible to calculate the photon flux within the energy bin. The energy bins provided by our set of filters, the corresponding average energy used in calculation and the calibration coefficient R are reported in Table 4.10. The coefficients were calculated by interpolating the data of Table 4.4 in Sec. 4.3 measured with monochromatic x-rays at ELETTRA synchrotron facility.

Results of the experimental test

The measured energy spectrum of the beam used for testing the method is reported in Fig. 4.31(a) and the same spectrum, with a further filtration of 1.3 mm of Al is reported in Fig. 4.31(b). In the same figure are also shown the spectra re-binned according to the energy split of Table 4.9. Therefore the re-binned spectrum of Fig. 4.31(a) is the reference for the result that

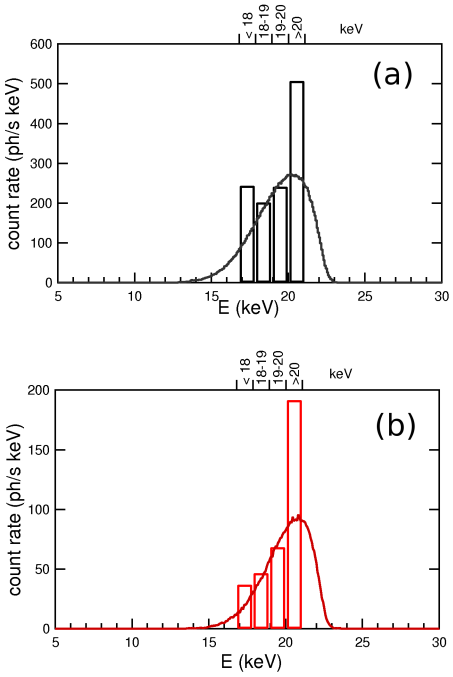

Figure 4.31: (a) X-ray tube spectrum measured with a HPGe detector (W-anode, Be-window, 22 kVp and nominal anodic current of 0.2 mA) with additional 3.10 mm of Al filter, (b) with additional (3.10 + 1.30) mm Al filter. Histograms represent the same spectra re-binned according to the energy split of Table 4.9 (*reported on top axis*).

we should obtain with the method being tested.

Spectra transmitted by the filters of Table 4.10 are shown in Fig. 4.32. As can be seen, the filter transmission for energies lower than the K-edge energy is the same for all the absorber materials, while for energies above the K-edge the transmission is negligible. The counts in the spectra with energies higher than the K-edge are resulting from the spread due to the energy resolution of the spectroscopic system. These results confirm the good selection of the filter set, in fact conditions (4.8) and (4.7) previously described are fulfilled.

The integral of the count rate of spectra of Fig. 4.31 and Fig. 4.32 provide us with the total photon fluxes impinging on the detector (see Table 4.11). Uncertainties are not reported for these data because the relative statistic fluctuation was negligible for the aim of our analysis. Applying the subtraction analysis to this data set we have calculated the photon flux of each energy bin reported in Tab. 4.12.

In Table 4.11 are also reported the photocurrents I_{PD} obtained with the PIN diode system when exposed to the same filtered beams. Applying the subtraction analysis to these current data and multiplying for the

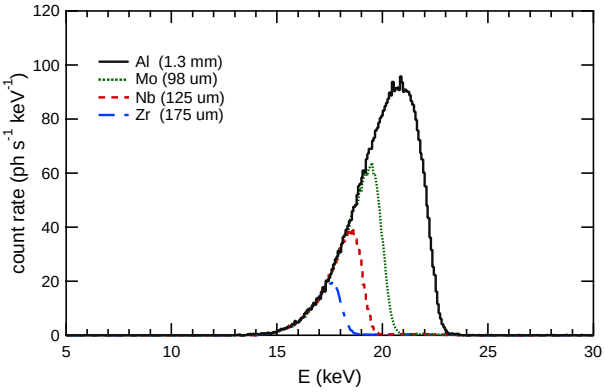

Figure 4.32: X-ray tube spectra measured with a HPGe detector (W-anode, Be-window and additional 3.10 mm Al filter, 22kVp and nominal anodic current of 0.2 mA) with additional filtrations of Al, Zr, Nb and Mo with thicknesses reported in Table 4.8.

Table 4.11: Total photon fluxes φ_{HPGe} obtained by integrating energy spectra of filtered beams which have been measured by using HPGe detector. Photocurrents I_{PD} obtained with PIN diode.

Filtration	φ_{HPGe} (ph/s)	I_{PD} (A)
Zr	35.3	$(8.1 \pm 0.3) \times 10^{-12}$
Nb	79.5	$(17.1 \pm 0.7) \times 10^{-12}$
Mo	144.9	$(29.9 \pm 1.2) \times 10^{-12}$
Al	343.2	$(63.3 \pm 2.5) \times 10^{-12}$
None	1192.3	$(236.0 \pm 9.5) \times 10^{-12}$

appropriate calibration factor K we obtained the fluxes reported in Tab. 4.13.

Differences in the anodic current circulating in the x-ray tube and in the collimation of the beam make the two set of fluxes obtained not directly comparable. The comparison of the normalized energy distributions of the spectra obtained is reported in Table 4.14. As can be seen the data are in good agreement, with a maximum discrepancy not larger than 7%.

Finally the comparison between the unfiltered beam energy distributions measured with the HPGe detector and evaluated with the k-edge subtraction technique is shown in Table 4.15 and in Fig. 4.33, also in this case the maximum discrepancy is less than 7%.

The results of this experimental test show that this k-edge subtraction technique permits to evaluate the energy distribution of an x-ray beam with a precision better than 10%, provided that the beam is limited in the energy band and an approximative knowledge *apriori* of this band is given. Furthermore this technique requires various measurement of the x-ray beam filtered

Table 4.12: Photon fluxes obtained via subtraction method using HPGe detector measurements.

E (keV)	Subtraction of fluxes	φ_{HPGe} (ph/s)	φ_{HPGe} (norm.)
<18	φ_{Zr}	35.3	0.103
18-19	φ_{Nb} - φ_{Zr}	44.3	0.129
19-20	φ_{Mo} - φ_{Nb}	65.4	0.190
>20	φ_{Al} - φ_{Mo}	198.2	0.578
	Total	343.2	1.000

Table 4.13: Photon fluxes obtained via subtraction method using diode current measurements.

E (keV)	I_{PD} subtraction	I_{PD} (A)	K (ph/C)	φ_{PD} (ph/s)	φ_{PD} (norm.)
<18	I_{Zr}	(8.1±0.3)× 10^{-12}	3.28×10^{15}	(2.66±0.19) × 10^4	0.101±0.007
18-19	I_{Nb} - I_{Zr}	(9.0±1.0)× 10^{-12}	3.70×10^{15}	(3.33±0.47)× 10^4	0.127 ±0.018
19-20	I_{Mo} - I_{Nb}	(12.8±1.8)× 10^{-12}	4.01×10^{15}	(5.13±0.9) × 10^4	0.196±0.034
>20	I_{Al} - I_{Mo}	(33.4±3.7)× 10^{-12}	4.53×10^{15}	(1.51±2.1) × 10^5	0.576 ±0.082
			Total	2.62× 10^5	1.000

Table 4.14: Comparison between normalized energy distributions obtained using filtered spectra subtractions φ_{HPGe}(E), PIN diode signal subtractions φ_{PD}(E) and direct measurement with HPGe φ_{Al}(E).

E (keV)	φ_{HPGe}(E)	φ_{PD}(E)	φ_{Al}(E)
<18	0.103	0.101	0.107
18-19	0.129	0.127	0.136
19-20	0.190	0.196	0.199
>20	0.578	0.576	0.558

Table 4.15: Energy distribution of the x-ray tube measured φ(E) and obtained from PIN diode current φ_{PD}(E) (normalized data).

E (keV)	φ(E) (norm.)	φ_{PD}(E) (norm.)
<18	0.204	0.191
18-19	0.169	0.158
19-20	0.202	0.198
>20	0.425	0.451

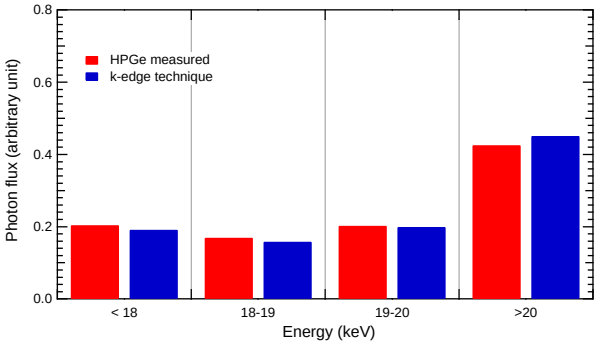

Figure 4.33: Histogram of the unfiltered energy distributions obtained with HPGe spectrum analysis and using the k-edge subtraction technique.

with different materials, for this reason, in the case of a pulsed source, it is needed that the beam spectrum does not change from shot-to-shot but is precisely repeatable. In order to check the repeatability other techniques for single shot energy distribution evaluation, as the one described by Golosio *et al.* [96] of BEATS2 collaboration will be used, as well as complementary methods as proposed by Endrizzi *et al.* [93].

5

ELI-NP-GBS demonstration system

The ELI-NP gamma beam system (GBS) will provide photon beams with continuously adjustable energy ranging from 0.2 to 19.5 MeV and a relative energy bandwidth of 0.3% , obtained by collimating the photons emerging from the Compton interaction region as previously described in Sec. 3.3. A precise energy calibration of the gamma beam and the monitoring of the stability of its parameters as well as a fast feedback on the energy distribution, intensity and shape profile of the beam are essential for the commissioning and development of the machine, as well as a check for proving the fulfillment of the requirements of the tender reported in Sec. 3.2. Furthermore during operation as an experimental user facility, the ELI-NP-GBS will need a monitoring system of these parameters for routine diagnostic of the beam delivered. Given the unprecedented characteristics of the beam, these tasks are extremely challenging. For these reason an apparatus of detectors, named gamma beam demonstration system, has been designed in order to permit the thorough characterization and monitor of the beam produced. This apparatus design is a result of the collaboration of the research unit of INFN sections of Ferrara, Firenze and Catania from Italy, as well as STFC Daresbury (UK) for the engineering part.

In the following a brief overview will be illustrated.

5.1 Demonstration system overview

In order to verify the performance of the gamma beam system and monitor its operation, the gamma beam demonstration system is expected to accurately measure the photon flux and the energy distribution.

According to the beam specifications described in Sec. 3.2, the required resolution on the energy measurement should be compatible with the expected bandwidth of 0.3% within an energy range between 0.2 and 20 MeV. The system must be able to cope with pulses of 2 to 6×10^5 photons with a pulse duration of 1-2 ps, and pulse trains separated by 15 ns.

While in the commissioning and calibration phases destructive measurements can be performed, during the routine operation of the source performance monitoring should have a negligible impact on the beam, to avoid

affecting downstream applications.

Considering the measurement of the gamma energy distribution, the ultra-short duration of a gamma pulse (about 1 ps), makes impossible to easily resolve the response of a single photon to any detector directly exposed to the beam line. The high energy range implies that the K-edge absorption technique based on beam filtration, as previously described (see Sec. 4.4), is not usable in this case due to the limitation of maximum K-edge energy available [96, 97]. A possible solution is to use Compton scattered radiation from a single photon interaction in a thin target to evaluate the energy of incident photons. In fact by measuring precisely the energy and position of the scattered electrons and photons with respect to the primary beam direction it is possible to retrieve the energy of a single interacting photon for each pulse. The advantage of such a technique is the negligible interference with the primary beam, considering that in average only one photon at maximum will interact in the target, making it an ideal tool for beam energy monitoring. Performing a suitably large amount of such measurements, the beam energy distribution can be determined accurately.

A complementary approach to evaluate the beam spectrum consists in performing a measurement of the total beam energy by entirely absorbing the gamma pulses in a longitudinally segmented calorimeter. The advantage of this approach is that the full photon statistics can be exploited and, since fast detectors can be used, a significant measurement can be performed for each single pulse. Though, being a destructive measurement, this technique is not compatible with any downstream application of the beam, but will be fundamental during gamma beam system commissioning and tuning to provide an immediate feedback on the beam energy, intensity and variations within a macro-pulse.

Furthermore, an absolute energy calibration apparatus needs to be included in the characterization system. Using appropriate targets, the detection of resonant scattering condition during a beam energy scan can provide a precise absolute confirmation of the beam energy for several values, providing an accurate calibration for the other detectors and the following experiments.

To summarize, the general concept of the gamma beam demonstration system consists of five basic elements:

- a beam flux monitor to measure and monitor the beam intensity;
- a beam position imager to spot the beam position for alignment and diagnostics purposes;
- a Compton spectrometer, to measure the photon energy spectrum for monitoring purposes;
- a calorimeter for a combined measurement of the beam average energy

and intensity, to be used during machine commissioning and development;

– a resonant scattering spectrometer for absolute beam energy calibration and inter-calibration of the other detector elements.

In Fig. 5.1 a drawing of the complete demonstration system is shown.

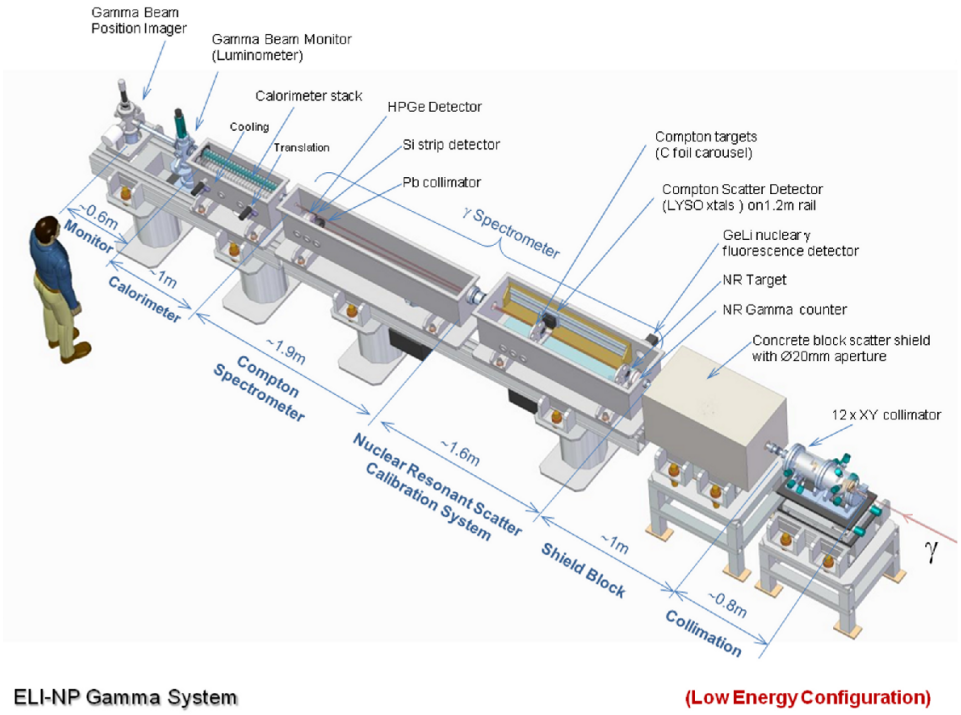

Figure 5.1: Drawing of ELI-NP gamma beam demonstration system. (Courtesy of N. Bliss, STFC-Daresbury)

The ELI-NP gamma beam system is foreseen to have two beamlines for high and low energy range respectively. Thus, two similar beam characterization systems will be realized for the two gamma beam lines, optimized for the different energy ranges. All the characterization system detectors will be contained in specific interaction chambers in vacuum, in direct connection with the gamma beam pipe in order to avoid as much as possible transition windows. In the next sections will be given a brief description of the Compton scattering spectrometer (see Sec. 5.1.1) and the absorption calorimeter (see Sec. 5.1.2), studied by the research unit of INFN Firenze. In Sec. 5.1.3 the nuclear resonant scattering calibration system, studied by the INFN Catania unit is described. Finally in Sec. 5.2 and Sec. 5.3 will describe the flux monitor and the beam profile imager studied by the INFN Ferrara research unit.

5.1.1 Compton scattering spectrometer

The Compton scattering spectrometer is designed to precisely measure the energy and position of single electrons recoiling at small angles from incidents photons scattered by Compton interaction in a thin target. Then, using the position and energy of electron recoiled it is possible to retrieve the energy of the incident photon. At small recoil angles with respect to the beam direction, the electron carries most of the incident photon energy and the sensitivity to polar angle, whose knowledge is limited by the beam size and the multiple scattering inside the target, is minimal. By also detecting in coincidence the scattered photon, whose position and energy can be predicted from the electron measurements, the background on the electron detector produced by possible pair-production and Compton photons, as well as from electrons not fully contained in the detector sensitive volume, can be strongly suppressed. A schematic representation of the spectrometer is illustrated in Fig. 5.2.

The thin target should minimize the relative contribution of pair production, for this reason a low-Z material was chosen, in particular, graphite is a practical solution, since foils of almost any thickness are available on the market.

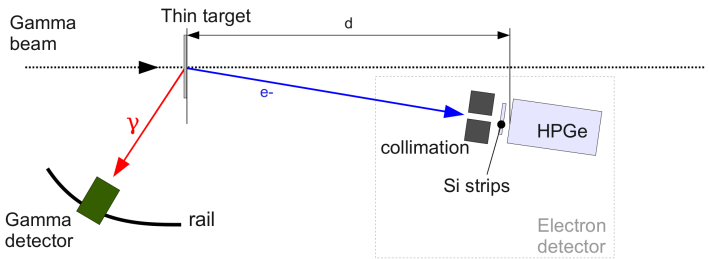

Figure 5.2: Conceptual drawing of the Compton spectrometer configuration.

To obtain the required resolution on the beam energy, the electron must be contained in an high-resolution homogeneous detector, the best solution is to use a high purity germanium (HPGe) or and LaBr crystal as a cost-effective alternative. For both these technologies, the time needed for the measurement is not shorter than the macro-pulse length (about 500 ns) and any pile-up occurring in this time window would spoil the measurement. This implies that the rate of useful measurement cannot be larger than the macro-pulse repetition rate (100 Hz), and the target for Compton scattering must have a very small thickness t in order to keep the number of detected electrons per macro-pulse low (≤ 1), considering the probability of interaction and the number of photons per pulse it results in being $t \sim 2 - 10$ μm.

This is indeed an advantage, since such a micrometric target is almost transparent for the beam, and minimizes the multiple scattering of the emerging electron that is the most limiting effect to the beam energy resolution.

Electrons in the energy range of interest can be contained with good efficiency using an HPGe (or LaBr) cylinder with a radius of 65 mm. To enhance the full energy peak of the measured electrons while reducing pile-up, only particles entering the central part of the detector can be selected using a lead collimator placed in front of the detector. The collimator has an inner hole of radius 30 mm, and a depth of 45 mm to effectively filter out electrons, positrons and photons outside the fiducial region. To measure the electron scattering angle a double-sided silicon microstrip detector, for a precise position measurement, will be placed between the lead collimator and the energy detector. This will also improves the identification of electrons against photon background. We plan to use a ,The angle of the detector axis with respect to the beam direction must be the minimum allowed by the detector size, for several reasons: as already mentioned, the sensitivity of the reconstructed gamma energy on the electron polar angle is minimal, in addition since the electron energy is maximal, the error on the measured angle, due to multiple scattering that is inversely proportional to the electron momentum, it is minimized. Furthermore, though the peak of the distribution of electron recoil angle depends on the incident photon energy (from about 160 to 24 mrad from 2 to 20 MeV), defined as the fraction of signals in the detector that are due to Compton electrons with respect to other radiation entering the detector, is maximal at the lowest possible angle for any energy between 2 and 20 MeV.

Finally, the distance d of the detector from the target along the beam direction is chosen as a compromise between conflicting requirements: a larger distance allows to reduce the polar angle for a fixed detector size, and the error on due to the beam spot size; a smaller distance increases the acceptance, allowing to reduce the target thickness for a given rate, reducing the contribution of multiple scattering. This parameter was optimized computing, as a function of d, the target thickness needed to obtain a fixed rate (20 Hz) of isolated electron signals for 10 MeV gammas, placing the detector at the minimal practically possible angle of 80 mm/d. The results for this optimization lead to the choice of $d = 200$ cm as a compromise between getting a reasonable rate and a good energy resolution taking into account a resolution on the electron energy of 0.1%r.m.s., the uncertainty on the gamma position on the target (1 mm r.m.s. in the transverse directions), the effects of multiple scattering and energy loss of the electron inside the target.

The distribution of the reconstructed beam energy is shown in Fig. 5.3. To evaluate the expected resolution, the energy peak is fitted with a gaussian function. As shown in Fig. 5.3, the fitted mean values are shifted from the true values by about 30 keV, as expected from the average value of energy

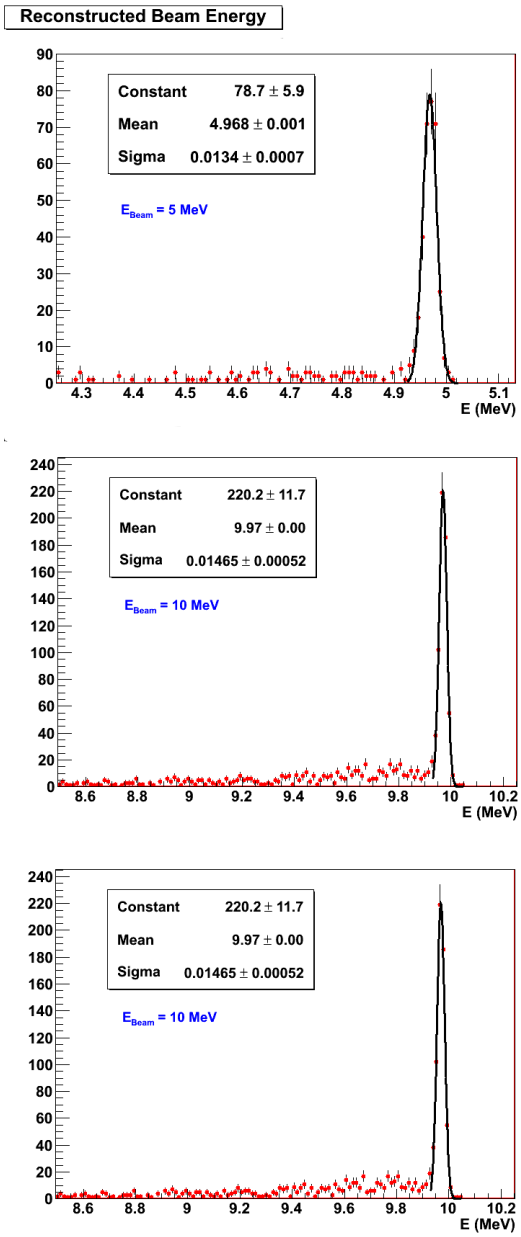

Figure 5.3: Reconstructed beam energy by the Compton spectrometer for a simulated beam energy of 5, 10 and 20 MeV (top to bottom).

lost in the passive materials. The resulting resolution varies from 0.15 to 0.2 % from 5 to 20 MeV. The residual tails in the beam energy reconstruction can be further suppressed using the information from the impact position of the recoil gamma. In conclusion, the simulations show that a clean sample of well reconstructed Compton interactions can be selected using the Compton Spectrometer, providing the beam energy with a resolution between 0.15 and 0.2 %. The expected number of useful signals per incident photons corresponds, for the nominal beam flux, to a rate of a few Hz for the whole range of beam energy. The spectrometer will be able to provide a continuous monitoring of the beam energy during the routine operations of the ELI-NP facility with the required accuracy. The resolution function obtained from the simulations with a fixed beam energy, that can be verified using sources of monochromatic gammas, then can be deconvolved from the measured distribution. Therefore, after an adequate number of measurements, an accurate reconstruction of the time integrated energy spectrum of the ELI-NP gamma beam can be achieved.

5.1.2 Absorption calorimeter

The absorption calorimeter, studied and desinged by the research unit of INFN Firenze, will measure the energy distribution and the total number of photons for each beam pulse. In the energy range of interest for ELI-NP, for low atomic number materials, the total cross section for the interaction of gamma radiation decrease with energy. The average longitudinal position of photons scattering inside a calorimeter made of a low-Z material is thus expected to increase as the energy increase. Moreover the average depth of the resulting electromagnetic showers in the detector also tends to increase with energy. So, the idea for this detector is to parameterize, using detailed simulations, the expected profile of the energy release in a longitudinally segmented calorimeter as a function of energy of incident photons. The average energy of the beam (and, with less sensitivity, its bandwidth) can be measured by fitting the measured longitudinal profile against the parameterized distributions. Once the photon energy is known it is possible to obtain the number of impinging photons from the total energy release, taking account also for the expected leakage that can be obtained from simulations. Organic scintillators are natural candidates for being low-Z absorber and active detectors at the same time, also having the advantage of fast response time allowing to resolve pulses within a macro-pulse. However, the absorption of the very intense and collimated gamma pulses requires the detectors to be radiation hard. Our simulations suggest that, at 20 MeV gamma energy, doses up to 10^{-9} Gray per incident photon are released in the central area of 1 mm^2 around the beam direction. For any practical plastic scintillator, the performance is quickly degraded after about 10-100 Gray, so considering a fluence of the order of 10^9 ph/mm^2, it would correspond to less than

10 hour of operation according to the beam specifications. Therefore, the scheme of a sampling device was adopted, where a passive plastic absorber is interleaved with thin detector layers, made of a radiation-hard and fast technology. For this purpose silicon pixel planes were chosen. The sampling scheme is not expected to degrade too much the achievable resolution, since, due to the high beam intensity, the quantum fluctuations on the measured signals are not expected to be larger than the longitudinal fluctuations of the primary particle distribution.

An optimization study, performed using GEANT4 simulations, was made for the size and the number of component of the detector, analyzing the distribution of the released energy and its fluctuation as a function of the longitudinal and transverse position of detection. This resulted in the absorber length to be 75 cm, and the transverse size to be 6×6 cm^2 in a layout consisting in a stack of 25 identical detector elements, each one consisting of 3 cm of plastic absorber and a 0.2 mm Si plane. A drawing of the concept for the detector is shown in Fig. 5.4.

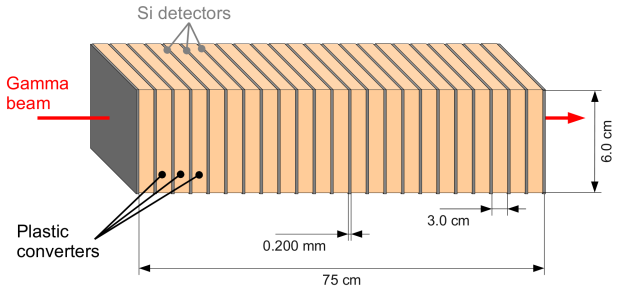

Figure 5.4: Drawing of a schematic representation of the stack calorimeter detector.

The response has been studied simulating monochromatic photon pulses with energy between 2 and 20 MeV in steps of 0.1 MeV. For each energy value, the number of simulated events is 10^7 (corresponding approximately to the total number of photons in a macro-pulse). The fraction of deposited energy in each layer with respect to the sum of the 25 signals is then parameterized as a function of energy, as well as the fraction of sampled energy with respect to the total beam energy. Using this parameterization, the beam energy and its intensity are simultaneously obtained from a fit to the longitudinal energy profile. The energy resolution obtained with this method is shown in Fig. 5.5 as a function of the incident beam energy for a single gamma beam pulse of 10^5 photons. The expected resolution is in the range between 1.6 % and 3.2% in the energy interval of interest. The intensity is measured with similar precision, since the error on the beam energy is the main limitation to its accuracy. The statistical error on the energy mea-

surement can be decreased below 0.1% after integrating over a few seconds, and, assuming the macro-pulse reproducibility on this time scale, a detailed time profile of the macro-pulse can be obtained.

To reach this level of accuracy this system will need an experimental calibration and verification that can be provided by the joint use with the resonant scattering calibration system that will provide very accurately the beam energy for several reference values, for which the measured profiles can be tuned to the shape expected from the simulation.

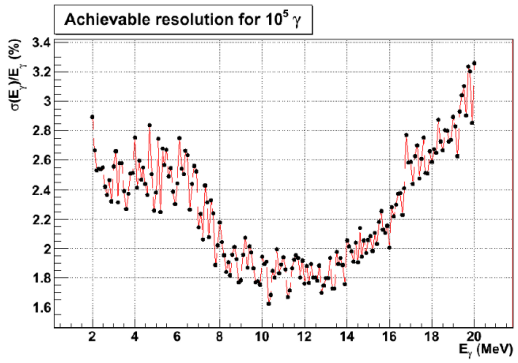

Figure 5.5: Resolution of the calorimetric measurement of the beam energy expected from 10^5 photons. Only the statistical errors due to the fluctuations of longitudinal profiles are taken into account in this plot [45].

5.1.3 Nuclear resonant scattering calibration system

The measurement of the beam energy distribution using the Compton scattering spectrometer and the absorption calorimeter previously described (see Sec. 5.1.1 and 5.1.2) requires an absolute calibration of the energy value with an accuracy better than 0.1%. In order to reach this level of precision, the research unit of INFN section of Catania proposed and study the feasibility of a resonant scattering calibration system. The basic idea of this system to detect the gamma decays of properly selected nuclear levels of some suitable targets, when resonant conditions with the beam energy are achieved. Nuclear resonant scattering is a process consisting in the absorption of a gamma photon by a nucleus, followed by its de-excitation with the emission of one or more photons, according to the decay sequence of the nuclear level. While scanning continuously a beam energy range, the reaching of a known resonant energy can be precisely identified through the detection of the corresponding decay photons. Resonance lines are usually very narrow allowing for an extremely precise calibration. Resonances in typical nuclei are narrow (widths of order 10^{-3} to 10^{3} eV). The resonance energy corresponds to isotope-specific energy differences between the final state and excited states of the target nuclei, with generally small corrections accounting for nuclear

recoil.

Measurement of nuclear resonant scattering can be performed by measuring gamma-beam intensity attenuation at the resonant energies or detecting disexcitation photon emission. Considering the expected ELI-NP-GBS energy bandwidth (about 1-10 keV) compared to the typical resonances width (10^{-3}-10 keV), it is clear that an attenuation measurement it would be very difficult to implement due to the small variations of intensity. Furthermore, this measurement should be used as a calibration so it is expected to operate simultaneously with the Compton spectrometer or the absorption calorimeter, then a photon fluence detector would actually interfere with the primary beam spoiling the calibration.

For this reason a resonance monitor aimed to detect the photons emitted by de-excitation at large angles will be used. This detector will unambiguously determine the establishment of resonance condition of the gamma beam with some properly selected nuclear levels. In resonance condition the gamma beam energy is known with a resolution simply given by the energy spread of the beam ($\sim 0.3\%$ in the case of ELI-NP), since the intrinsic level width as well as the error of its energy value is usually negligible in comparison.

In figure 5.6 a schematic representation of the resonant scattering system is shown. As it can be noticed, the device is composed by two different detectors. The first is a high-efficiency and fast-response gamma counter, that covers emission in the backward direction, while the second is a gamma spectrometer placed around the perpendicular direction.The gamma counter allows for a fast beam energy scan, giving prompt information about the establishment of resonance condition, while the gamma spectrometer, which is a slower detector allows the precise identification of the resonant level through the measurement of the energy of the emitted de-excitation photon. Several thin target, made of different materials to explore the entire energy interval of interest, will be mounted on sample holder remote controlled.

The resonant gamma counter will have a 20 mm diameter hole to allow beam crossing, and will be segmented in eight sectors housing the gamma counters. The eight gamma counters will be a stack of lead converters alternated with fast plastic scintillators. For the low energy gamma beam line a possible utilization of lead-loaded plastic scintillator will be studied.

The resonant gamma spectrometer detector is aimed to clearly identify resonant excited levels, in particular when a complex decay pattern is expected. A good energy resolution and an anti-Compton shield for background rejection are necessary to distinguish the peaks in the pattern. For the low-energy line the resonant gamma spectrometer would be a Ge(Li) detector, 30 mm diameter and 45 mm length, positioned just outside the vacuum chamber, at about 20 cm from the target. For the high-energy line a much larger detector is needed, while nuclei with lower density of levels will be used. So a less demanding energy resolution is needed and a NaI

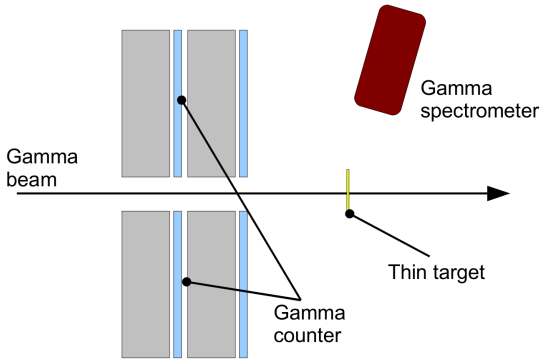

Figure 5.6: Drawing of a schematic representation of the resonant scattering system.

detector, 80 mm diameter and 150 mm long, will be fit for this purpose.

5.2 Gamma beam flux monitor

The tasks of the gamma beam flux monitoring system are:

- to provide a prompt information for a real-time check of the apparatus proper operation that is fundamental in the commissioning phase of the source, in particular during the alignment and synchronization of collisions;

- to monitor the repeatability of the source and to provide the information about the delivered gamma flux during experiments after the commissioning phase, when the GBS will be working for the user facility.

This device is intended as a monitor of the flux, hence a relative evaluation of the flux is made measuring the energy released in the detector that is proportional to the number of photons and their energy distribution. In order to perform an absolute measurement of gamma beam flux, the efficiency of the detector and the incident beam energy distribution must be known very accurately. Even if a preliminary estimation can be done by means of Monte Carlo simulations, an experimental calibration will also be needed, using a gamma source of known flux and energy distribution. For this reason an absolute flux measurement includes the characterization of the gamma beam performed by dedicated systems, such as the absorption calorimeter and Compton spectrometer described in Sec. 5.1.1 and 5.1.2.

The required features for this flux monitor are:

- *Time resolution*, this depends on the information needed. Whether the average intensity of a macro-pulse is needed, the detector should operate at a frequency of 100 Hz; otherwise, if the information on the intensity of each pulse is needed, the detector must be faster and suitable to follow a signal with pulses time separation shorter than 15 ns (67 MHz);
- *Stability*, the stability of the detector response must be good so as to allow to check the repeatability of the source over a sufficiently long period of time (at least as long as an experimental session);
- *Radiation hardness*, the radiation hardness of the device should be compatible with a user-facility routine utilization, in order to guarantee an adequate lifetime of the monitoring system;
- *No contamination of gamma beam*, the interaction of gamma beam with the monitor should not produce secondary radiation along the primary beam direction to avoid to interfere with downstream applications.

5.2.1 Design

Due to the peculiar time structure of the ELI-NP gamma beam (described in detail in Sec. 3.3), two different flux monitors have been studied to be realized:

- a *fast monitor* with a single-pulse time resolution (2 ps-long pulses every 16 ns, corresponding about 67 MHz);
- a *slow monitor* for integral (and more accurate) measurement of macro-pulses, that are made up of 36 of the pulses previously described, with a repetition rate of 100 Hz.

The two distinct monitor systems must be switchable and removable from the beam, for this reason they have to be installed on a remotely controlled shifting frame. The choice to realize two distinct monitor was made to allow a prompt verification of the time structure and shot-to-shot repeatability with the fast monitor oriented to the apparatus diagnostic and characterization, while a more accurate measurement of the integral macro-pulse signal will be needed in the final application as a user experimental facility.

Slow monitor

The system is based on the coupling of a relatively slow scintillator material to an off-axis light detector placed in the transverse plane with respect to the beam direction of propagation. The coupling between the scintillator

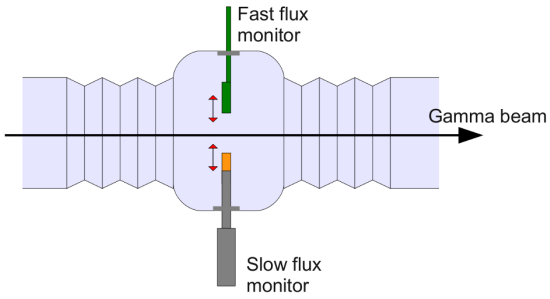

Figure 5.7: A schematic representation of the gamma beam flux monitoring system.

Table 5.1: ZnSe(Te) scintillator parameters [98].

Material	ZnSe(Te,O) - Zinc Selenide
Decay time τ (μs)	1-3(fast), 30-70(slow)
Density (g/cm^3)	5.4
Effective atomic number Z	33
Emission maximum λ_{max} at 300 K (nm)	610
Afterglow (after 10 ms) (%)	<0.05
Attenuation coefficient at λ_{max} (cm^{-1})	0.1-0.3
Melting point, C	1773 - 1793
Refractive index at λ_{max}	2.58 - 2.61
Hygroscopic	No
Light yield [γ/MeV]	8.0 x 10^4
Radiation stability (rad)	10^8

(in vacuum) and the light detector (in air) will be made using a plastic light guide that is used also for the transition between vacuum and air using a ring gasket. The requirements for the light detector and reading electronics are not particularly demanding: the system should have a good response stability and signal processing time compatible with a source frequency of 100 Hz. Either a photomultiplier or a diode commercially available can be used. The scintillator must have a good light output with a wavelength matched with the light detector sensitivity and a slow decay time (longer than 500 ns), moreover it should have a good radiation stability to be compatible with routine use in the facility. Various scintillator have been considered and the choice was made for a crystal of ZnSe(Te,O). This scintillator presents all the characteristics required; in particular its radiation stability is 1 or 2 order of magnitude better than more common crystal like CsI.

ZnSe(Te) also exhibits a relatively high light output at longer wavelengths (red) with no afterglow and high thermal stability, a summary of its characteristics is reported in Table 5.1.

The unique not optimal feature of this crystal is the poor transparency to the scintillation light wavelength, implying that the transverse crystal size

should be not larger than a few centimeters, to avoid an excessive light self-absorption. Considering the beam size a square crystal of size 1.0×1.0 mm^2 will be used. The detection efficiency of the monitor should be relatively low (few per cent) in order to interfere as less as possible with the primary beam and high enough to generate a significant signal. For this reason Monte Carlo simulations have been performed in order to evaluate the thickness of scintillator that is the best compromise. The result is that the optimal thickness should be of 1.0 mm, as discussed in more detail in Sec. 5.2.2.

Fast monitor

The fast monitor should measure a quantity proportional to the number of photons in each pulse (2 ps pulse duration and 16 ns of pulse-to-pulse separation, corresponding to 67 MHz). A system made of a fast plastic scintillator coupled to a fast detector such as a photomultiplier can be used. The major issue of this device is the poor radiation hardness of plastic scintillator that start to degrade after an absorbed dose exceeding 10-100 Gy (few hours of irradiation with the ELI-NP gamma beam system). For this reason an alternative suitable solution, like a semiconductor detector, has been considered. A silicon detector has the required features such as low efficiency, low scatter production, radiation hardness and short time of signal formation and read-out. In particular due to the similar purpose and characteristics, this flux monitor will be made with the same silicon detectors that will be used in the absorption calorimeter described in Sec. 5.1.2 in collaboration with the project research unit of INFN-Firenze.

Summarizing, the silicon detector for the fast monitor should have the following main characteristics:

- to be radiation-hard, in order to avoid a significant degradation of the response after several weeks of data taking, corresponding to doses of at least 50 KGy;
- the signal production and acquisition should be fast enough to permit a clear separation between the various pulses within the macro-pulse.
- they should allow a good signal-to-noise ratio.

Silicon sensors are the best candidates for this task. In fact, the technologies developed in the last 15 years for the LHC tracking systems allow to realize radiation-hard detectors that can safely sustain irradiation up to 10^{14} MeV neutron/cm^2 and up to 100 KGy [99]. The thickness of the sensors and the bias voltage applied can be chosen to have collection times on the electrodes of the order of 2-3 ns, allowing the measurement of the signal produced by a single gamma pulse. The detector will be made of a 6x6 cm^2, 200 μm-thick silicon sensors (n-type bulk), with a proper implantation pattern (p-type implants) of 16 pads on a 4x4 matrix. This configuration is

Table 5.2: Expected signals in the slow beam flux monitor

E (MeV)	dose/ph (Gy)	E/ph (keV)	E tot (keV)	Scint. γ per macropulse
1	2.76E-013	1.14E+001	4.56E+007	3.65E+009
5	3.03E-013	1.25E+001	5.01E+007	4.01E+009
10	2.99E-013	1.24E+001	4.94E+007	3.95E+009
20	3.32E-013	1.37E+001	5.48E+007	4.39E+009

due to the use of the same detector for the segmented calorimeter, anyway in this case, having no needs to obtain a transverse spatial information, the readout will be made with only one electronic channel, bonding all the pads together. A summary of the expected performances of this detector will be given in Sec.5.2.2.

5.2.2 Expected performances

Slow monitor signal production

In order to evaluate the light output and the dose absorbed by the crystals, the energy released in the scintillators was calculated performing Monte Carlo simulations using EGSnrc code [100]. A parallel monochromatic gamma beam was simulated with energy ranging from 1 to 20 MeV, impinging on a cylindrical ZnSe crystal with a radius of 2 cm and various thicknesses ranging from 0.1 to 5 mm. The beam has circular cross section with a radius of 0.5 mm, corresponding to a 25 μrad semi-divergence at 20 m from the interaction point.

The optimal thickness was found to be 1.0 mm to have an optimal compromise between the fraction of photon interacting (a few percent) and the signal produced, considering also the optical light collection efficiency that depends on the scintillator thickness. A summary of the results in the energy range 1-20 MeV, in the case of a scintillator 1.0 mm-thick, is shown in Table 5.2, where the dose per incident photon on the ZnSe slab, the energy released per photon and the total energy released per macro-pulse are reported. We have considered each macro-pulse made of 40 pulses, each one of 10^5 photons and a light conversion efficiency of 80 photons per keV absorbed. Considering the loss of light due to geometrical factors, internal reflection and optical coupling the final collection efficiency can be roughly estimated to be about 5%, resulting in 10^7 photons reaching the detector per macro-pulse with a time scale corresponding to the scintillation time of the detector that is of the order of 10-100 μs. This number of photon is compatible with the generation of a significant signal in a suitable low-gain photomultiplier or state of the art silicon diode system.

Considering a repetition rate of 100 Hz of macropulses of $4x10^6$ photon each, the mean dose rate released on the crystal cross section intercepting the gamma beam is about 700 Gy/hour. Radiation stability of ZnSe has been

verified up to 1 MGy [98] corresponding to about 1400 hours of continuous irradiation.

In order to evaluate the production of scattered particles produced by the interaction of the primary beam with the scintillator crystal, a Monte Carlo simulation was performed and the scattered particles energy, position and direction were scored at the exit of scintillator layer. Using EGSnrc code a parallel monochromatic gamma beam was simulated with energy ranging from 1 to 20 MeV, impinging on a cylindrical ZnSe crystal with a radius of 2 cm and a thickness of 1 mm. The beam has a circular cross section with a radius equal to 0.5 mm, corresponding to a 25 μrad semi-divergence at 20 m from the interaction point. Figure 5.8 and Figure 5.9 show the energy distributions of the scattered particle. The number of scattered particle divided by the total number of histories generated (10^6) is plotted as a function of the energy, both for charged particles (electron and positrons) and photons for incident energies respectively of 1 MeV and 20 MeV.

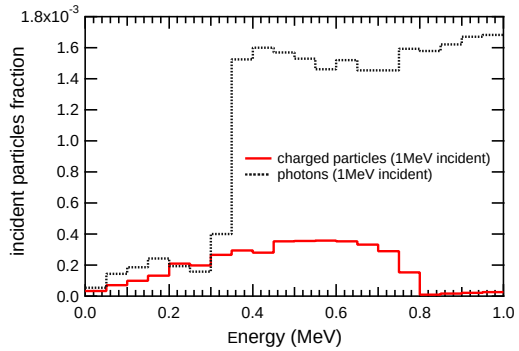

Figure 5.8: Fraction of scattered photon and charged particles after the scintillator layer for incident energy of 1 MeV.

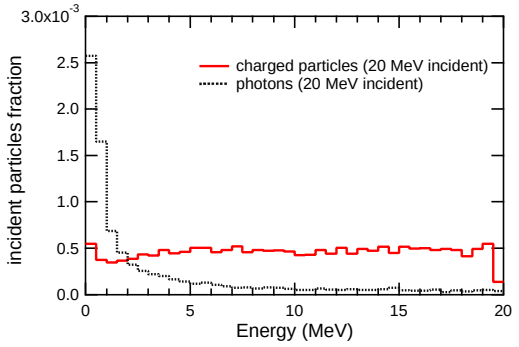

Figure 5.9: Fraction of scattered photon and charged particles after the scintillator layer for incident energy of 20 MeV.

The total fraction of particles produced with any energy and direction

is reported in Table 15.

A plot of the fraction of scattered particle with respect to the propagation direction expressed as the direction cosine of the z-axis w, where z is the direction of propagation of the primary beam, is shown in Fig.5.10.

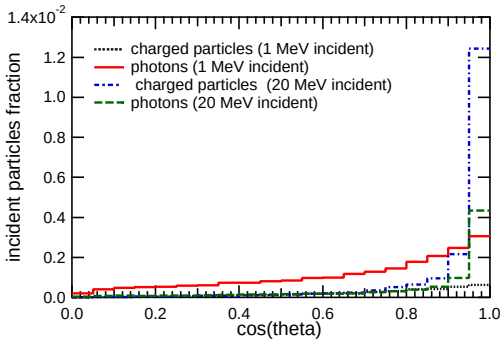

Figure 5.10: Plot of the fraction of scattered photon and electrons after the scintillator layer as a function of the direction of propagation, for incident photon energies of 1 MeV and 20 MeV.

In conclusion a non negligible fraction of particle are scattered close to the forward direction, especially in the high energy range. This implies that depending on the final distance of the experimental user area from the monitor and the final shielding apparatus that will be realized, a collimation system might be needed after the monitor scintillator.

Fast monitor

In order to evaluate the energy released and the resulting charge produced in a 200 mm-thick layer of silicon a Monte Carlo simulation using EGSnrc code has been performed. The simulation was made considering a parallel monochromatic photon beam with energy ranging from 1 MeV to 20 MeV with a circular cross section of 1 mm of diameter. The beam impinges on a silicon slab 200 μm-thick and with a diameter of 2.0 cm. A summary of the results of this simulation is shown in Table 5.3, where the incident photon beam energies, the dose per incident photon on the silicon slab, the energy released per photon and the energy released by a pulse made of 10^5 photons are reported. Moreover, the number of electron-hole pairs produced and the corresponding charge were calculated, dividing the total energy by the average energy required to produce a pair (3.6 eV [81]).

The values of charge produced in the silicon detector per gamma pulse are ranging from 0.27 pC to 1.02 pC, depending on the incident energy. This charge represents a significant signal that can be read with specifically designed read-out electronics. To cope with such signals, a fast spectroscopy shaping amplifier with reduced gain will be developed in collaboration with

Table 5.3: Expected signals in the fast monitor silicon slab.

E (MeV)	dose/ph (Gy)	E/ph (keV)	E/pulse (keV)	e- in Si/pulse	Charge in Si (C)
1	6.28E-014	2.30E-001	2.30E+004	6.38E+006	1.02E-012
5	1.97E-014	7.20E-002	7.20E+003	2.00E+006	3.20E-013
10	1.65E-014	6.02E-002	6.02E+003	1.67E+006	2.68E-013
20	1.73E-014	6.31E-002	6.31E+003	1.75E+006	2.80E-013l

the INFN Firenze unit.

5.3 Gamma beam profile imager

The task of the beam profile imager is to provide an image of the gamma spatial distribution to display the location and uniformity of the beam. This image is crucial in giving informations on the alignment of the collimation system and on the right positioning of other detectors, as well as to control the size and uniformity of the field at the exit of the collimation system. Considering a beam divergence of 25-250 μrad and an approximative distance from the interaction point of 20 m, the typical size of the beam cross section is expected to vary between 1 mm to 10 mm of diameter, for which the spatial resolution of the system will have reasonably to be at least between 0.05 mm and 0.10 mm.

In Figure 5.11 the conceptual drawing of the imager is shown: it is basically composed of a tilted scintillator screen crossing the gamma beam, a lens system to focus the scintillator light distribution on a CCD camera, a frame grabber and an acquisition system. The system will be enclosed in a light tight vacuum chamber, except for the CCD camera that can be placed in air and collect the light signal through a suitable glass view-port.

The scintillator screen considered for this detector is a commercially available scintillator screen *Kodak Lanex Fast* (Kodak, New York, US), composed of terbium-doped gadolinium oxysulphide phosphor (Gd_2O_2S:Tb) with a 133 mg/cm^2 mass thickness. The imaging detector considered is a standard cooled CCD camera, having a pixel size of 20×20 μm, a typical dark current $<$ 1 e-/pixel/s and a readout noise in the range of 20-30 e-/pixel. The CCD size is considered to be larger than 2048×2048 pixels, corresponding to about 40 ×40 mm^2.

The performances of the imager have been evaluated estimating the signal produced by the light sensor of the device. The average number of electrons produced in the CCD per incident gamma photon for the setup described can be calculated as:

$$n_{CCD}^{e-} = \frac{E_\gamma \delta_a \delta_i \delta_t \delta_C \beta}{\epsilon_k} \tag{5.1}$$

where:

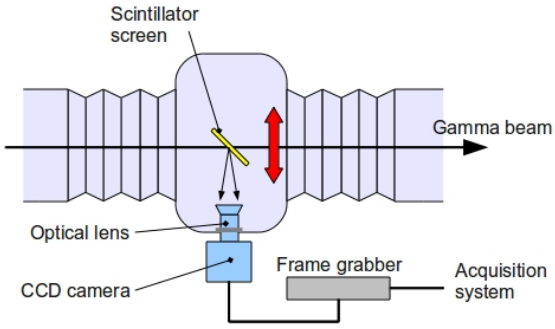

Figure 5.11: A schematic representation of the beam profile imager.

- E_γ is the energy of incident photons;
- δ_a is the fraction of incident photon energy absorbed by the phosphor calculated using a Monte Carlo simulation;
- δ_i is the intrinsic gamma-ray to light energy conversion efficiency (0.15 for Gd_2O_2S:Tb);
- δ_t is the fraction of light that escape from phosphor (0.4 for Gd_2O_2S:Tb);
- δ_C is the lens system collection efficiency defined as:

$$\delta_C = T\frac{1}{1+4f^2(1+m)^2}, \tag{5.2}$$

  where T is the lens system light transmittance, m is the magnification factor and f is the relative aperture of lens system;
- β is the CCD quantum efficiency (typically in the range between 30% and 50%);
- ε_k is the mean energy of light photons created by phosphor (ε_k= 2.4 eV).

The fraction of incident photon energy absorbed by the scintillator δ_a has been evaluated using a Monte Carlo simulation with EGSnrc code. The Monte Carlo was carried out with beams having energies of 1, 5, 10, 15 and 20 MeV impinging on a gadolinium oxysulphide slab with a 133 mg/cm^2 mass thickness to simulate the Lanex scintillator. The results for the fraction of incident photon energy absorbed δ_a are reported in Table 5.4 as a function of the beam energy. A magnification factor $m = 1$ for the lens system with a relative aperture $f = 1.2$ and transmission factor $T = 0.7$ were considered. The average number of electrons produced in the CCD per incident photon impinging on the scintillator, calculated using eq. (5.1) is reported in Table

Table 5.4: Total number of electrons produced in the CCD by single macro-pulse as a function of the beam energy.

Beam Energy (MeV)	1.0	10.0	15.0	20.0
Fraction of energy released δ_a	2.725×10^{-3}	1.870×10^{-4}	1.320×10^{-4}	1.070×10^{-4}
Electrons per photon	7.439×10^{-1}	5.105×10^{-1}	5.405×10^{-1}	5.842×10^{-1}
Electrons per macropulse	2.98×10^{6}	2.04×10^{6}	2.16×10^{6}	2.34×10^{6}

Table 5.5: Average number of electrons per CCD pixel per macro-pulse for two different beam divergence

Beam Energy (MeV)	1.0	10.0	15.0	20.0
Average signal per pixel 25μrad (electrons)	8.50×10^{2}	5.83×10^{2}	6.18×10^{2}	6.68×10^{2}
Average signal per pixel 250μrad (electrons)	8.50	5.83	6.18	6.68

5.4. In the same table also the average number of electrons produced in the CCD per incident macro-pulse is reported as a function of the gamma beam energy.

Starting from these results, it is possible to estimate the average number of electron per pixel that is a function of the image size and the CCD pixel size. If the CCD pixel size is 20 μm as mentioned, considering the beam size at 20 m from the interaction point, the dimensions of the images are in the range 50×50 - 500×500 pixels with magnification factor $m = 1$, while the average signal (number of electrons) per macro-pulse is given in Table 5.5.

As previously mentioned, for a standard cooled CCD camera the typical dark current is less than 1 e-/pixel/s, while the readout noise is in the range 20-30 e-/pixel: from these data the average signal for macro-pulse is larger than the readout noise signal for 25 μrad beam divergence, while it is lower than readout noise for 250 μrad beam divergence. To increase the lower signal it is possible to use the CCD binning modality that increases the pixel size summing the signal of neighbor pixels, otherwise it is possible to integrate the signal produced by several macro-pulses. Besides, in this case, considering the large number of pixels involved it would be possible to decrease the magnification factor in order to increase the signal per pixel.

Conclusions

The activities described in this work concern the study of devices and techniques for the characterization of inverse Compton - Thomson sources, in particular as part of two major projects BEATS2 experiment at SPARC-LAB LNF and ELI-NP-GBS proposal of E-Gammas collaboration. An overview of the basic physics of inverse Compton interaction was made to illustrate the main features of these sources. After a brief overview of the two projects and the description of the expected characteristics of the radiation produced by SL-Thomson and ELI-NP-Gamma Beam System, a detailed description of the activities carried out has been made.

Concerning BEATS2 experiment, SL-Thomson source is expected to produce a beam with energy ranging from 16 to 21 keV in pulses containing about 10^9 photons each. The duration of pulses will be 5-15 ps and the repetition rate 1-10 Hz.

The main tasks have included the realization of the hardware for collimation and filtration of the x-ray beam and the realization of devices and techniques for its characterization, in particular:

- design and realization of an x-ray flux on-line monitoring system;
- design and realization of a device for accurate flux measurement;
- implementation of a techniques for the evaluation of the x-rays energy distribution.

The x-ray experimental beamline, comprising a collimation and filtering system, a free-air ionization chamber for on-line beam monitoring and an optical table for samples and detectors, has been assembled and installed on SL-Thomson at SPARC-LAB.

A free-air, parallel plate, ionization chamber was designed and realized as on-line monitor of the beam flux. The chamber was tested for background analysis and its response was evaluated for irradiation with traditional x-ray tubes and monochromatic synchrotron radiation in the energy range 16-24 keV. This detector has shown linear response for fluxes from 10^7 to 10^{10} ph/s in continuous irradiation, whereas in case of pulsed irradiation the chamber can detect signal produced by pulses down to 10^7 photons. The loss of linearity due to recombination effect has been evaluated, the collection efficiency decreases as the number of photons per pulse increases. In the case of the SL-Thomson application, considering 2.3 nC as the charge expected to be produced by each pulse, the resulting collection efficiency is about 0.5. In conclusion this chamber is suitable for a relative monitoring of the x-ray flux, permitting to check the shot-to-shot repeatability of the source and to evaluate small fluctuations of the source photon yield.

In order to perform an absolute x-ray flux measurement, a device based on a silicon PIN diode was realized. A precise knowledge of the response

function of this detector is fundamental to perform the accurate flux evaluation of radiation beams with a known energy distribution. For this reason the device has been tested and calibrated with monochromatic beams for several energies in the range 16-24 keV. Its response was compared to that expected from a theoretical response model showing good agreement, thus ensuring the possibility to interpolate the measured response function in the entire energy range of interest. In a continuous irradiation regime the response was verified to be linear for fluxes ranging from about 10^5 to 10^{10} ph/s.

Considering the actual application to SL-Thomson, the irradiation of the diode with such an ultra-fast intense source will produce an instantaneous charge density extremely high, possibly leading to charge recombination and partial collection of charge, resulting in an underestimation of the real number of interacting photons. To evaluate the relevance of this effect an experimental test has been made irradiating the diode with intense pulsed laser light. The result of this tests showed that this device allows to detect a very small number of photons per pulse, namely 10^3-10^4, considering x-rays with energy of about 20 keV, and maintains a linear response only up to 10^5-10^6 ph/pulse. Therefore, this PIN diode device could be not reliable for direct flux measurements on the fully commissioned SL-Thomson source where each pulse will be made of 10^9 photons. However, it is going to be very useful during the source commissioning, especially in the initial stage of synchronization and collision alignment, when the yield of photon can be very low, but is detection is a fundamental signature of correct operation.

To overcome this limitation, an alternative system for the photon flux evaluation that permit to avoid the non-linearity effect has been realized and calibrated. Instead of using the direct interaction of radiation in the diode active layer, a high-efficiency, slow scintillator (2 mm-thick CsI:Tl crystal) was optically coupled with the active surface of a silicon PIN diode. In this way, the signal is produced only by the scintillation light produced and not by direct interaction in the diode active volume. The crystal CsI:Tl was used to increase the duration of charge production process in the silicon diode. This crystal, in fact, shows a relatively slow scintillation decay (about 1 μs) and no evidence for linearity loss at high dose-rates. The response of the diode-crystal system has been calibrated at Larix laboratories of Ferrara University using quasi-monochromatic x-ray beams in the energy range 16-24 keV. The result of this calibration showed that the response of this device, comparable with that of the PIN diode system with no scintillator, is compatible with the application for the measurement of x-ray flux of the fully commissioned SL-Thomson source.

The last part of the activity regarding BEATS2 experiment concerns the evaluation of the energy distribution of the x-ray beam produced by SL-Thomson source, that is crucial for the study and development of its applications. Moreover, the energy spectrum of emitted photons is also

an important signature of the correct operation of the apparatus, showing that the energy and focusing of the electron and laser beam are properly set, as well as the alignment of the collision. The application of traditional spectroscopic techniques based on single-photon detection is very difficult because of the extremely high instantaneous flux produced by the source. For this reason a technique for the evaluation of the energy distribution was developed and experimentally tested using an x-ray beam with a spectrum comparable to that expected for BEATS2. This technique is based on photon-flux measurements of the beam filtered with several different K-edge materials suitably selected for the energy range of interest. From these measured fluxes it is possible to retrieve an evaluation of the energy distribution of the incident beam. The results of the experimental test have shown that this technique allows to measure the energy distribution of an x-ray beam with a precision better than 10% and an energy resolution of about 1 keV, provided that the beam has a limited energy band and an approximative *a priori* knowledge of this interval is given. In the case of the SL-Thomson source this knowledge is obtained by computational simulations and theoretical analysis of the physical process, that give an estimation of the expected energy distribution of photons. Another limitation of this technique is the necessity of various measurements on the x-ray beam filtered with different materials, that requires a repeatable shot-to-shot energy distribution. In order to check the repeatability other techniques for single-shot energy distribution evaluation, as the one described by Golosio *et al.* [96] of BEATS2 collaboration, will be used, as well as complementary methods such as the one proposed by Endrizzi *et al.* [93].

ELI-NP Gamma Beam System of the proposal of E-Gammas collaboration is expected to produce radiation with energy ranging from 0.2 to 20 MeV in pulses containing approximatively 10^5 photons each. The temporal structure will consist in macro-pulse with a repetition rate of 100 Hz, each made up of 32 pulses of 1 ps of duration with a time separation of 16 ns. Within E-Gammas collaboration, the research unit of Ferrara section of INFN has been involved in the design of the collimation, characterization and monitoring system of the gamma beam. In particular, the main activity has concerned the realization of the preliminary design and the evaluation of the expected performance of two flux monitor devices.

The first, having fast signal production and acquisition, is aimed to provide information on the pulsed temporal structure of the photon beam. This detector, that will be realized in collaboration with INFN-Firenze research unit, is based on the direct interaction of the gamma beam in a fast silicon detector. A preliminary design and the size scaling of the detector was performed via Monte Carlo simulations to evaluate the energy released in silicon by the expected beam. A detector 200 μm-thick suitably polarized resulted compatible with the fast signal production and acquisition required, as well as with a significant signal generation by the direct interaction with

the gamma beam.

The second device designed is based on scintillator crystal for a slower and more accurate evaluation and monitoring of the source photon yield. This system is based on radiation-hard, slow scintillator, crystal coupled to a light detector. Monte Carlo simulations for the evaluation of the optimal scintillator and its size were performed, resulting in the choice of a 1 mm-thick ZnSe(Te).

Moreover, the design and the evaluation of the expected performances of an imaging system for the high-energy gamma beam was carried out. This detector is composed of a tilted scintillator screen crossing the gamma beam, an optical system to focus the scintillator light distribution on a CCD camera, a frame grabber and an acquisition system. The scintillator considered is *Kodak Lanex Fast* (Gd_2O_2S:Tb) with a 133 mg/cm^2 mass thickness. Also in this case a Monte Carlo simulation was performed in order to select the scintillator screen that could provide a significant signal on a typical commercial CCD camera. A suitable resolution is required to provide a diagnostic tool for the beam profile shape, position, collimation and alignment. Considering the beam divergence and the distance from the interaction point, the typical size of the beam cross-section is expected to vary between 1 mm to 10 mm of diameter. The detector designed allows to obtain a significant image for short exposure times (> 1 s), with an expected spatial resolution between 0.05 mm and 0.10 mm, suitable to obtain an image of the beam satisfactory for diagnostic applications.

Bibliography

[1] Wayne A. Hendrickson. Synchrotron crystallography. *Trends in Biochemical Sciences*, 25(12):637 – 643, 2000.

[2] Ian Gentle. Applications of synchrotron science to chemistry. *Australian Journal of Chemistry*, 65(3):203, 2012.

[3] Carolyn Therese Dillon. Synchrotron Radiation Spectroscopic Techniques as Tools for the Medicinal Chemist: Microprobe X-Ray Fluorescence Imaging, X-Ray Absorption Spectroscopy, and Infrared Microspectroscopy. *Australian Journal of Chemistry*, 65(3):204, 2012.

[4] G. Calas, W.A. Bassett, J. Petiau, M. Steinberg, D. Tchoubar, and A. Zarka. Some mineralogical applications of synchrotron radiation. *Physics and Chemistry of Minerals*, 11:17–36, 1984.

[5] Gordon E. Brown and Neil C. Sturchio. An overview of synchrotron radiation applications to low temperature geochemistry and environmental science. *Reviews in Mineralogy and Geochemistry*, 49(1):1–115, 2002.

[6] Vivian Stojanoff, Paul Northrup, Ruth Pietri, and Zhong Zhong. Synchrotron radiation in life sciences. *Protein and Peptide Letters*, 19(7):761–769, 2012.

[7] Frank E Carroll. Tunable monochromatic X rays: a new paradigm in medicine. *AJR. American journal of roentgenology*, 179(3):583–90, September 2002.

[8] R Lewis. Medical applications of synchrotron radiation x-rays. *Physics in Medicine and Biology*, 42(7):1213, 1997.

[9] Lighsources of the World. `http://www.lightsources.org`.

[10] Frank E Carroll, Marcus H Mendenhall, Robert H Traeger, Charles Brau, and James W Waters. Pulsed tunable monochromatic X-ray beams from a compact source: new opportunities. *AJR. American journal of roentgenology*, 181(5):1197–202, November 2003.

[11] E. Burattini, M. Gambaccini, M. Marziani, O. Rimondi, P. L. Indovina, M. Pocek, G. Simonetti, M. Benassi, C. Tirelli, and R. Passariello. X-ray mammography with synchrotron radiation. *Review of Scientific Instruments*, 63(1):638 –640, jan 1992.

[12] F. Arfelli, A. Bravin, G. Barbiellini, G. Cantatore, E. Castelli, M. Di Michiel, P. Poropat, R. Rosei, M. Sessa, A. Vacchi, L. Dalla Palma, R. Longo, S. Bernstorff, A. Savoia, and G. Tromba. Digital mammography with synchrotron radiation. *Review of Scientific Instruments*, 66(2):1325 –1328, feb 1995.

[13] E. Castelli, F. Arfelli, D. Dreossi, R. Longo, T. Rokvic, M.A. Cova, E. Quaia, M. Tonutti, F. Zanconati, A. Abrami, V. Chenda, R.H. Menk, E. Quai, G. Tromba, P. Bregant, and F. de Guarrini. Clinical mammography at the syrmep beam line. *Nuclear Instruments and Methods in Physics Research Section A: Accelerators, Spectrometers, Detectors and Associated Equipment*, 572(1):237 – 240, 2007.

[14] E Castelli, M Tonutti, F Arfelli, and Renata Longo. Mammography with synchrotron radiation: first clinical experience with phase-detection technique. *radiology*, 259(3), 2011.

[15] H Elleaume, S Fiedler, F Estve, B Bertrand, A M Charvet, P Berkvens, G Berruyer, T Brochard, G Le Duc, C Nemoz, M Renier, P Suortti, W Thomlinson, and J F Le Bas. First human transvenous coronary angiography at the european synchrotron radiation facility. *Physics in Medicine and Biology*, 45(9):L39, 2000.

[16] R A Lewis. Medical phase contrast x-ray imaging: current status and future prospects. *Physics in Medicine and Biology*, 49(16):3573, 2004.

[17] P. Oliva, M. Carpinelli, B. Golosio, P. Delogu, M. Endrizzi, J. Park, I. Pogorelsky, V. Yakimenko, O. Williams, and J. Rosenzweig. Quantitative evaluation of single-shot inline phase contrast imaging using an inverse compton x-ray source. *Applied Physics Letters*, 97(13):134104, 2010.

[18] KJ Kim. Characteristics of synchrotron radiation. *X-ray Data Booklet*, LNL/PUB-940(Rev. 3):1782–1789, 2009.

[19] The ELI-Nuclear Physics working groups. The white book of eli nuclear physics. `www.eli-np.ro/documents/ELI-NP-WhiteBook.pdf`, 2010.

[20] Henry R. Weller, Mohammad W. Ahmed, Haiyan Gao, Werner Tornow, Ying K. Wu, Moshe Gai, and Rory Miskimen. Research opportunities at the upgraded HIγS facility. *Progress in Particle and Nuclear Physics*, 62(1):257–303, 2009.

[21] European Synchrotron Facility ESRF. `http://www.lightsources.org`.

[22] ID15 High Energy Diffraction and Scattering Beamlines at ESRF. `http://www.esrf.eu/UsersAndScience/Experiments/StructMaterials/ID15`.

[23] Spring8 synchrotron radiation facility. `http://www.spring8.or.jp`.

[24] Diamond Light Source UK national synchrotron science facility. `http://www.diamond.ac.uk`.

[25] Richard H. Milburn. Electron scattering by an intense polarized photon field. *Phys. Rev. Lett.*, 10:75–77, Feb 1963.

[26] F.R. Arutyunian and V.A. Tumanian. The compton effect on relativistic electrons and the possibility of obtaining high energy beams. *Physics Letters*, 4(3):176 – 178, 1963.

[27] O.F Kulikov, Y.Y Telnov, E.I Filippov, and M.N Yakimenko. Compton effect on moving electrons. *Physics Letters*, 13(4):344 – 346, 1964.

[28] Carlo Bemporad, Richard H. Milburn, Nobuyuki Tanaka, and Mircea Fotino. High-energy photons from compton scattering of light on 6.0-gev electrons. *Phys. Rev.*, 138:B1546–B1549, Jun 1965.

[29] J. Ballam, G. B. Chadwick, R. Gearhart, Z. G. T. Guiragossian, P. R. Klein, A. Levy, M. Menke, J. J. Murray, P. Seyboth, G. Wolf, C. K. Sinclair, H. H. Bingham, W. B. Fretter, K. C. Moffeit, W. J. Podolsky, M. S. Rabin, A. H. Rosenfeld, and R. Windmolders. Total and partial photoproduction cross sections at 1.44, 2.8, and 4.7 gev. *Phys. Rev. Lett.*, 23:498–501, Sep 1969.

[30] L. Federici, G. Giordano, G. Matone, G. Pasquariello, P.G. Picozza, R. Caloi, L. Casano, M.P. Pascale, M. Mattioli, E. Poldi, C. Schaerf, M. Vanni, P. Pelfer, D. Prosperi, S. Frullani, and B. Girolami. Backward compton scattering of laser light against high-energy electrons: the ladon photon beam at frascati. *Il Nuovo Cimento B Series 11*, 59:247–256, 1980.

[31] M. Preger, B. Spataro, R. Bernabei, M.P. de Pascale, and C. Schaerf. Monochromatic and polarized tagged ladon gamma ray beams. *Nuclear Instruments and Methods in Physics Research Section A: Accelerators, Spectrometers, Detectors and Associated Equipment*, 249(23):299 – 305, 1986.

[32] G. Matone, P. Picozza, D. Prosperi, A. Tranquilli, R. Caloi, C. Schaerf, S. Frullani, and C. Strangio. A monochromatic and polarized photon beam for photonuclear reactions. the ladon project at frascati. In Sergio Costa and Carlo Schaerf, editors, *Photonuclear Reactions II*, volume 62 of *Lecture Notes in Physics*, pages 149–164. Springer Berlin Heidelberg, 1977.

[33] Shigeru Kashiwagi, Ryunosuke Kuroda, Takashi Oshima, Fumio Nagasawa, Tomoaki Kobuki, Daisuke Ueyama, Yoshimasa Hama, Masakazu

Washio, Kiminori Ushida, Hitoshi Hayano, and Junji Urakawa. Compact soft x-ray source using thomson scattering. *Journal of Applied Physics*, 98(12):123302, 2005.

[34] E.G. Bessonov, M.V. Gorbunkov, P.V. Kostryukov, Yu.Ya. Maslova, V.G. Tunkin, A.A. Postnov, A.A. Mikhailichenko, V.I. Shvedunov, B.S. Ishkhanov, and A.V. Vinogradov. Design study of compact thomson x-ray sources for material and life sciences applications. In C. L. S. Lewis and D. Riley, editors, *X-Ray Lasers 2008*, volume 130 of *Springer Proceedings in Physics*, pages 521–535. 2009.

[35] O. Williams, G. Andonian, M. Babzien, E. Hemsing, K. Kusche, J. Park, I. Pogorelsky, G. Priebe, J. Rosenzweig, and V. Yakimenko. Characterization results of the BNL ATF Compton X-ray source using K-edge absorbing foils. *Nuclear Instruments and Methods in Physics Research Section A: Accelerators, Spectrometers, Detectors and Associated Equipment*, 608(1):S18–S22, September 2009.

[36] G. Priebe, D. Laundy, P. J. Phillips, D. M. Graham, S. P. Jamison, S. Vassilev, E. a. Seddon, J. B. Rosenzweig, G. a. Krafft, T. Heinzl, D. Filippetto, O. Williams, K. M. Spohr, S. Ter-Avetisyan, U. Schramm, Y. M. Saveliev, L. B. Jones, and S. L. Smith. First results from the Daresbury Compton backscattering x-ray source (COBALD). In *Proc. of SPIE Vol. 7805*, volume 7805, pages 780513–780513–14, 2010.

[37] A.S. Chauchat, V. Le Flanchec, J.P. Nègre, A. Binet, P. Balleyguier, J.P. Brasile, and J.M. Ortega. Instrumentation developments for production and characterisation of Inverse Compton Scattering X-rays and first results with a 17MeV electron beam. *Nuclear Instruments and Methods in Physics Research Section A: Accelerators, Spectrometers, Detectors and Associated Equipment*, 622(1):129–135, October 2010.

[38] R. Kuroda, H. Toyokawa, M. Yasumoto, H. Ikeura-Sekiguchi, M. Koike, K. Yamada, T. Yanagida, T. Nakajyo, F Sakai, and K. Mori. Quasi-monochromatic hard X-ray source via laser Compton scattering and its application. *Nuclear Instruments and Methods in Physics Research Section A: Accelerators, Spectrometers, Detectors and Associated Equipment*, 637(1):S183–S186, May 2011.

[39] W. Luo, W. Xu, Q. Y. Pan, X. Z. Cai, J. G. Chen, Y. Z. Chen, G. T. Fan, G. W. Fan, W. Guo, Y. J. Li, W. H. Liu, G. Q. Lin, Y. G. Ma, W. Q. Shen, X. C. Shi, B. J. Xu, J. Q. Xu, Y. Xu, H. O. Zhang, Z. Yan, L. F. Yang, and M. H. Zhao. A laser-Compton scattering prototype

experiment at 100 MeV linac of Shanghai Institute of Applied Physics. *The Review of scientific instruments*, 81(1):013304, January 2010.

[40] F. Sakamoto, M. Uesaka, Y. Taniguchi, T. Natsui, E. Hashimoto, L.K. Woo, T. Yamamoto, J. Urakawa, M. Yoshida, and T. Higo. Compton scattering monochromatic X-ray source based on X-band multi-bunch linac at the University of Tokyo. *Nuclear Instruments and Methods in Physics Research Section A: Accelerators, Spectrometers, Detectors and Associated Equipment*, 608(1):S36–S40, September 2009.

[41] K Sakaue, T Gowa, H Hayano, Y Kamiya, S Kashiwagi, R Kuroda, a Masuda, R Moriyama, J Urakawa, and K Ushida. Recent progress of a soft X-ray generation system based on inverse Compton scattering at Waseda University. *Radiation Physics and Chemistry*, 77(10-12):1136–1141, October 2008.

[42] W. Brown and F. Hartemann. Three-dimensional time and frequency-domain theory of femtosecond x-ray pulse generation through thomson scattering. *Physical Review Special Topics Accelerators and Beams*, 7(6):1–20, 2004.

[43] E. Feenberg and H. Primakoff. Interaction of cosmic-ray primaries with sunlight and starlight. *Phys. Rev.*, 73:449–469, Mar 1948.

[44] V. Petrillo, a. Bacci, R. Ben Alì Zinati, I. Chaikovska, C. Curatolo, M. Ferrario, C. Maroli, C. Ronsivalle, a.R. Rossi, L. Serafini, P. Tomassini, C. Vaccarezza, and a. Variola. Photon flux and spectrum of Compton sources. *Nuclear Instruments and Methods in Physics Research Section A: Accelerators, Spectrometers, Detectors and Associated Equipment*, 693:109–116, nov 2012.

[45] L. Serafini et al. Technical design report of the e-gammas proposal for the eli-np gamma beam system, 2013.

[46] E. Esarey, S.K. Ride, and P. Sprangle. Nonlinear thomson scattering of intense laser pulses from beams and plasmas. *Physical Review E*, 48(4), 1993.

[47] P Tomassini, A Bacci, J Cary, M Ferrario, A Giulietti, D Giulietti, L A Gizzi, L Labate, L Serafini, V Petrillo, and C Vaccarezza. Linear and Nonlinear Thomson Scattering for Advanced X-ray Sources in PLASMONX. *Plasma Science, IEEE Transactions on*, 36(4):1782–1789, 2008.

[48] S.G. Anderson, C.P.J. Barty, S.M. Betts, W.J. Brown, J.K. Crane, R R Cross, D.N. Fittinghoff, D.J. Gibson, F.V. Hartemann, J. Kuba, G.P. LeSage, J.B. Rosenzweig, D.R. Slaughter, P.T. Springer, and

a.M. Tremaine. Short-pulse, high-brightness X-ray production with the PLEIADES Thomson-scattering source. *Applied Physics B: Lasers and Optics*, 78(7-8):891–894, May 2004.

[49] Istituto Nazionale di Fisica Nucleare. `http://www.infn.it/`.

[50] Laboratori Nazionali di Frascati. `http://www.lnf.infn.it/`.

[51] M. Ferrario, D. Alesini, A. Bacci, M. Bellaveglia, R. Boni, M. Boscolo, M. Castellano, L. Catani, E. Chiadroni, S. Cialdi, A. Cianchi, A. Clozza, L. Cultrera, G. Di Pirro, A. Drago, A. Esposito, L. Ficcadenti, D. Filippetto, V. Fusco, A. Gallo, G. Gatti, A. Ghigo, L. Giannessi, C. Ligi, M. Mattioli, M. Migliorati, A. Mostacci, P. Musumeci, E. Pace, L. Palumbo, L. Pellegrino, M. Petrarca, M. Quattromini, R. Ricci, C. Ronsivalle, J. Rosenzweig, A. R. Rossi, C. Sanelli, L. Serafini, M. Serio, F. Sgamma, B. Spataro, F. Tazzioli, S. Tomassini, C. Vaccarezza, M. Vescovi, and C. Vicario. Direct measurement of the double emittance minimum in the beam dynamics of the sparc high-brightness photoinjector. *Phys. Rev. Lett.*, 99:234801, Dec 2007.

[52] M. Ferrario, D. Alesini, A. Bacci, M. Bellaveglia, R. Boni, M. Boscolo, M. Castellano, E. Chiadroni, A. Cianchi, L. Cultrera, G. Di Pirro, L. Ficcadenti, D. Filippetto, V. Fusco, A. Gallo, G. Gatti, L. Giannessi, M. Labat, B. Marchetti, C. Marrelli, M. Migliorati, A. Mostacci, E. Pace, L. Palumbo, M. Quattromini, C. Ronsivalle, A. R. Rossi, J. Rosenzweig, L. Serafini, M. Serluca, B. Spataro, C. Vaccarezza, and C. Vicario. Experimental demonstration of emittance compensation with velocity bunching. *Phys. Rev. Lett.*, 104:054801, Feb 2010.

[53] L. A. Gizzi, A. Bacci, S. Betti, C. A. Cecchetti, M. Ferrario, A. Gamucci, A. Giulietti, D. Giulietti, P. Koester, L. Labate, T. Levato, V. Petrillo, L. Serafini, P. Tomassini, and C. Vaccarezza. An integrated approach to ultraintense laser sciences: The plasmon-x project. *The European Physical Journal Special Topics*, 175:3–10, 2009.

[54] SPARC. `http://www.lnf.infn.it/acceleratori/sparc`.

[55] L. Palumbo, J. Rosenzweig, et al. Technical design report for the sparc advanced project. Jan 2004.

[56] P. Oliva, a. Bacci, U. Bottigli, M Carpinelli, P. Delogu, M. Ferrario, D. Giulietti, B. Golosio, V. Petrillo, and L. Serafini. Start-to-end simulation of a Thomson source for mammography. *Nuclear Instruments and Methods in Physics Research Section A: Accelerators, Spectrometers, Detectors and Associated Equipment*, 615(1):93–99, March 2010.

[57] A. Bacci, F. Broggi, C. DeMartinis, D. Giove, C. Maroli, V. Petrillo, A.R. Rossi, L. Serafini, P. Tomassini, and L. Cultrera. Status of Thomson source at SPARC/PLASMONX. *Nuclear Instruments and Methods in Physics Research Section A: Accelerators, Spectrometers, Detectors and Associated Equipment*, 608(1):S90–S93, September 2009.

[58] A. Bacci, M. Bellaveglia, A. Clozza, G Di Pirro, et al. BEATS. *LNF Internal Report*, 2012.

[59] M. Gambaccini, A. Taibi, A. Del Guerra, F. Frontera, and M. Marziani. Narrow energy band x-rays via mosaic crystal for mammography application. *Nuclear Instruments and Methods in Physics Research Section A: Accelerators, Spectrometers, Detectors and Associated Equipment*, 365(1):248 – 254, 1995.

[60] Loewen.R. J. A compact light source: Design and technical feasibility study of a laser-electron storage ring x-ray source. *SLAC Report*, 632, June 2003.

[61] A. Bacci, C. Maroli, V. Petrillo, A. Rossi, and L. Serafini. Maximizing the brightness of an electron beam by means of a genetic algorithm. *Nuclear Instruments and Methods in Physics Research Section B: Beam Interactions with Materials and Atoms*, 263(2):488 – 496, 2007.

[62] European Project Extreme Light Infrastructure ELI. `http://www.extreme-light-infrastructure.eu/`.

[63] Horia Hulubei National Institute of Physics and Nuclear Engineering IFIN HH. Bucharest Magurele. `http://www.nipne.ro/`.

[64] Henry R. Weller, Ahmed, and Mohammad W. The higs facility: A free-electron laser generated gamma-ray beam for research in nuclear physics. *Modern Physics Letters A*, 18(23):1569–1590, 2003.

[65] Extreme Light Infrastructure Nuclear Physics ELI-NP. `http://www.eli-np.ro/`.

[66] European Collaboration for the proposal of a Gamma-Beam System to the ELI-NP Project EGAMMAS. `http://www.e-gammas.com/`, 2013.

[67] M. Gambaccini, P. Cardarelli, A. Taibi, A. Franconieri, G.Di Domenico, M. Marziani, R.C. Barn, L. Auditore, E. Morgana, D. Loria, A. Trifir, and M. Trimarchi. Measurement of focal spot size in a 5.5 mev linac. *Nuclear Instruments and Methods in Physics Research Section B: Beam Interactions with Materials and Atoms*, 269(10):1157 – 1165, 2011.

[68] FLUKA 2011.2.17 Tool for calculations of particle transport and interactions with matter. http://www.fluka.org/, 2012.

[69] B. Golosio, P. Delogu, I. Zanette, P. Oliva, A. Stefanini, G. Stegel, and M. Carpinelli. Visibility of tumor-like details in inline phase contrast mammography using quasimonochromatic x-ray sources. *Nuclear Instruments and Methods in Physics Research Section A: Accelerators, Spectrometers, Detectors and Associated Equipment*, 608(1, Supplement):S66 – S69, 2009.

[70] Bruno Golosio, Pasquale Delogu, Irene Zanette, Massimo Carpinelli, Giovanni Luca Masala, Piernicola Oliva, Arnaldo Stefanini, and Simone Stumbo. Phase contrast imaging simulation and measurements using polychromatic sources with small source-object distances. *Journal of Applied Physics*, 104(9):093102, 2008.

[71] M. Endrizzi, M. Carpinelli, P. Delogu, P. Oliva, B. Golosio, T. E. Gureyev, U. Bottigli, and A. Stefanini. X-ray phase-contrast imaging with an inverse compton scattering source. *AIP Conference Proceedings*, 1266(1):39–41, 2010.

[72] Martin Bech. *X-ray imaging with a grating interferometer*. PhD thesis, University of Copenhagen, 2009.

[73] Liberato De Caro, Cinzia Giannini, Alessia Cedola, Daniele Pelliccia, Stefano Lagomarsino, and Werner Jark. Phase retrieval in x-ray coherent fresnel projection-geometry diffraction. *Applied Physics Letters*, 90(4):041105, 2007.

[74] Liberato De Caro, Francesco Scattarella, Sabina Tangaro, Daniele Pelliccia, Cinzia Giannini, Ubaldo Bottigli, and Roberto Bellotti. Deconvolution by finite-size-source effects of x-ray phase-contrast images. *Medical Physics*, 38(4):1951–1961, 2011.

[75] R. C. Chen, H. L. Xie, L. Rigon, R. Longo, E. Castelli, and T. Q. Xiao. Phase retrieval in quantitative x-ray microtomography with a single sample-to-detector distance. *Opt. Lett.*, 36(9):1719–1721, May 2011.

[76] Marco Endrizzi. *X-ray imaging applications of a Thomson Scattering source*. Phd thesys, Università di Siena, 2011.

[77] http://www.nist.gov/pml/data/xraycoef/index.cfm. NIST, X-ray and gamma ray data.

[78] Stephen M. Seltzer. Calculation of photon mass energy-transfer and mass energy-absorption coefficients. *Radiation Research*, 136(2):pp. 147–170, 1993.

[79] H. E. Johns. *Physics of Radiology, Fourth Edition.* Charles C. Thomas Pub, Springfield, Illinois, USA, 1983.

[80] J.W. Boag. Ionization measurements at very high intensities. pulsed radiation beams. *British J Radiology*, 23:601–611, 1950.

[81] G. Lutz. *Semiconductor Radiation Detectors, II ed.* Springer-verlach, Berlin, Germany, 2007.

[82] Robin L Owen, James M Holton, Clemens Schulze-Briese, and Elspeth F Garman. Determination of x-ray flux using silicon pin diodes. *J. of synchrotron radiation*, 16(Pt 2), 2009.

[83] Michael Krumrey. Comments on Determination of X-ray flux using silicon pin diodes by R. L. Owen et al. (2009). J. Synchrotron Rad. 16, 143-151. *Journal of synchrotron radiation*, 16(Pt 5):690; author reply 690–1, 2009.

[84] Hamamatsu mod. s358409 datasheet (HAMAMATSU,Japan). `http://jp.hamamatsu.com/products/sensor-ssd/pd041/pd054/pd058/S3584-08/index_en.html`.

[85] NIST. Xcom: Photon cross sections database. `http://www.nist.gov/pml/data/xcom/index.cfm`.

[86] SYRMEP. `http://www.elettra.trieste.it/it/lightsources/elettra/elettra-beamlines/syrmep/syrmep.html`.

[87] R Nowotny. Xmudat: Photon attenuation data on pc. `http://www-mds.iaea.or.at/reports/mds-195.htm`. IAEA- NDS-195, International Atomic Energy Agency, Vienna, Austria (1998).

[88] John M. Boone and Andres E. Chavez. Comparison of x-ray cross sections for diagnostic and therapeutic medical physics. *Medical Physics*, 23(12):1997–2005, 1996.

[89] INO. Istituto nazionale di ottica, sez. pisa. `http://www.ino.it/?p2=sedi&p=pisa`.

[90] P Baldelli, A Taibi, A Tuffanelli, M C Gilardoni, and M. Gambaccini. A prototype of a quasi-monochromatic system for mammography applications. *Physics in medicine and biology*, 50(10):2225–40, May 2005.

[91] L. Abbene, G. Gerardi, F. Principato, S. Del Sordo, R. Ienzi, and G. Raso. High-rate x-ray spectroscopy in mammography with a cdte detector: A digital pulse processing approach. *Medical Physics*, 37(12):6147, 2010.

[92] S. Aiello, U. Bottigli, F. Fauci, B. Golosio, D. Lo Presti, G.L. Masala, P. Oliva, G. Raso, S. Stumbo, and S. Tangaro. Fluxen portable equipment for direct x-ray spectra measurements. *Nuclear Instruments and Methods in Physics Research Section A: Accelerators, Spectrometers, Detectors and Associated Equipment*, 518(1-2), 2004.

[93] Marco Endrizzi, Pasquale Delogu, and Arnaldo Stefanini. X-ray spectra reconstruction from analysis of attenuation data: A Back Scattering Thomson source application. *Nuclear Instruments and Methods in Physics Research Section A: Accelerators, Spectrometers, Detectors and Associated Equipment*, 608(1):S78–S82, September 2009.

[94] Emil Y. Sidky, Lifeng Yu, Xiaochuan Pan, Yu Zou, and Michael Vannier. A robust method of x-ray source spectrum estimation from transmission measurements: Demonstrated on computer simulated, scatter-free transmission data. *Journal of Applied Physics*, 97(12):124701, 2005.

[95] K. Chu and A. Fenster. Determination of x-ray spectral distribution from transmission measurements using K-edge filters. *Medical physics*, 10:772, 1983.

[96] Bruno Golosio, Marco Endrizzi, Piernicola Oliva, Pasquale Delogu, Massimo Carpinelli, Igor Pogorelsky, and Vitaly Yakimenko. Measurement of an inverse compton scattering source local spectrum using k-edge filters. *Applied Physics Letters*, 100(16):164104, 2012.

[97] Paolo Cardarelli, Giovanni Di Domenico, Michele Marziani, Irena Muçollari, Gaia Pupillo, Francesco Sisini, Angelo Taibi, and Mauro Gambaccini. Energy distribution measurement of narrow-band ultrashort x-ray beams via k-edge filters subtraction. *J App Physics*, 112(7):074908, 2012.

[98] V Ryzhikov, G Tamulaitis, N Starzhinskiy, L Galchinetskii, A Novickovas, and K Kazlauskas. Luminescence dynamics in znse(te) scintillators. *Journal of Luminescence*, 101(12):45 – 53, 2003.

[99] S. Braibant et al. Investigation of design parameters for radiation hard silicon microstrip detectors. *Nuclear Instrum. Meth. A*, 485(3):343 – 361, 2002.

[100] Electron Gamma Shower National Research Council Canda (EGSnrc). `http://irs.inms.nrc.ca/software/egsnrc/`.